Design and Development of Desktop Fiber and Fabric Manufacturing System for Advanced Materials

by

David Donghyun Kim

BASc., University of Waterloo (2013)
S.M., Massachusetts Institute of Technology (2015)

Submitted to the Department of Mechanical Engineering
in partial fulfillment of the requirements for the degree of

Doctor of Philosophy in Mechanical Engineering

at the

MASSACHUSETTS INSTITUTE OF TECHNOLOGY

May 2020

Author .....
Department of Mechanical Engineering
May 15, 2020

Certified by .....
Brian Anthony
Principal Research Scientist
Thesis Supervisor

Accepted by .....
Nicolas Hadjiconstantinou
Chairman, Department Committee on Graduate Theses

Design and Development of Desktop Fiber and Fabric Manufacturing System for Advanced Materials

by

David Donghyun Kim

Submitted to the Department of Mechanical Engineering
on May 15, 2020, in partial fulfillment of the
requirements for the degree of
Doctor of Philosophy in Mechanical Engineering

Abstract

This thesis presents two novel desktop fiber manufacturing systems and a desktop fabric manufacturing system. The desktop fiber manufacturing system achieved two goals. The first goal was the use of the system to teach smart manufacturing fundamentals. The second goal was to develop a low-cost platform for prototyping the fiber for biological and neurological research applications. The educational system was deployed in multiple classes, which proved to be a useful tool for teaching smart manufacturing. The advanced fiber manufacturing system was able to produce a variety of fibers using different preform materials. The preform materials included fibers with Polycarbonate(PC) core and Polymethyl Methacrylate (PMMA), hollow fibers with PC and PMMA, and 3 layer fiber with Polystyrene (PS) cladding, Polycaprolactone (PCL) layer, and PS core. These fibers were used for neural probing and cell scaffold. Finally, a generalized approach to designing a desktop fiber prototyping system is introduced.

For the fabric manufacturing system, a novel knitting process was invented. Nitinol (NiTi) wires exhibit either shape memory properties or super-elastic properties. There has been extensive research progress on using conventional knitting machines to produced knitted fabric with shape memory Nitinol wires. However, there has not been any development with knitting the fabric using super-elastic Nitinol wires without preprocessing. With the new system, the super-elastic Nitinol wires can be directly knitted without preprocessing the wire to loop shapes. The new system significantly reduces the processing steps to make knitted super-elastic fabric. The resulting fabric showed large strain capabilities at low stress. This thesis will describe in detail the design and fabrication of the fabric knitting system. It will also discuss the property of the knitted fabric produced from the system. The model was introduced to characterize the stress and strain relationship of the fabric. The model was also validated with the experimental data. The generalized approach in designing the super-elastic fabric system is also introduced. The relationship between the resulting fabric properties and the design parameters are discussed.

Thesis Supervisor: Brian Anthony
Title: Principal Research Scientist

Acknowledgments

I would like to thank my advisor Dr. Brian Anthony for all the help he as provided me. He was an amazing advisor who guided me through my long journey through my Ph.D. and I appreciate him very much for all the effort he took. He was also the great role model for me to develop my insight as researcher and entrepreneur. My last half-decade of career changed my life and it was all thanks to Dr. Brian Anthony.

I want to also thank my committee members Professor Hosoi and Professor Kim. They were always very supportive and helpful during my committee meetings. I really appreciated their advices and time they devoted to make this thesis possible.

I also would like to thank my lab members especially, Sangwoon Kim and Shirley Lu who were assigned to the same project as me. I also would like to thank Athena Huang, Dr. Xian Du, Ian Lee, Katie Hahm, Samantha Young and others in our lab for their support. In addition to my lab members, I would like to mention my close friends Hank Yang, Muyuan Lin, Prof. Seongjun Park, Dr. Youzhi Liang, Leixin Ma, Dr. Qifang Bao, Dr. Lei Zhou, Yajing Zhao and others for their support as well.

Special thanks to my friend Dr. Juner Zhu for his help with modeling the fabric and simulating the stress and strain curve. Also special thanks to Yuwei Li for checking my fabric model.

Last but not the least, I would like to thank my parents and family who were always supportive when my journey was in turmoil.

Thank you so much everyone. I would not have been able to finish this work without you all.

Contents

List of Figures

List of Tables

Chapter 1

Introduction

The fiber and fabric manufacturing has been an integral part of human history since ancient times. From ancient times, weaving clothes and producing fibers from cotton and animal furs led to the evolution of the economy, maintain health, and eventually, the industrial revolution. In modern days, the fiber has positioned itself as high-value material by being used as optical communication transmission material used globally to connect the entire world. Although both fiber and fabric technology existed for such a long time, there are still needs for innovation in both areas. This thesis will discuss the innovations that were made in the fiber drawing process for smart manufacturing and fabric knitting process for advanced materials.

1.1 Background

1.1.1 Optical Fiber Drawing Process

Optical fiber drawing has been a crucial process that supported significant communication innovations with the spread of the Internet around the world. The typical fiber draw tower is shown in Fig. 1-1. The typical optical fiber drawing process fundamentally follows from the preform feed into the radiative heater. Then the heated preform is pulled with the controlled velocity at the capstan assembly. Fig. 1-2 show the different sub-systems on the industrial optical fiber draw tower. The preform is

Figure 1-1: The example an industrial optical fiber draw tower [1]

fed into the heater by a linear stage. The preform is fixed with a three-jaw chuck, such as shown in Fig. 1-2a. As the preform is translated, it enters the heater. The radiative heater is shown in Fig. 1-2b. The fiber then goes into the capstan system shown in Fig. 1-2c. The capstan will change the velocity to control the diameter of the fiber. The system used multiple sensor systems to control the quality of the fiber. The first sensor system is the temperature sensor. The temperature sensors and controllers are shown in Fig. 1-2d. It can be noted that three screens and three yellow wires indicate 3 zones for the heater. The heater zones are separated along the path of the fiber, and different zones can be seen in the radiative heater as well

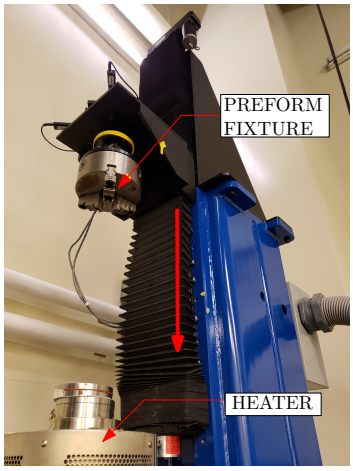

(a) The preform feed mechanism

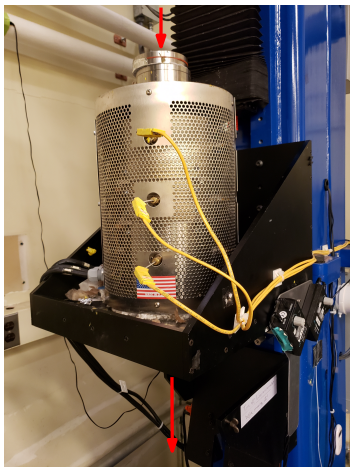

(b) The radiative heater

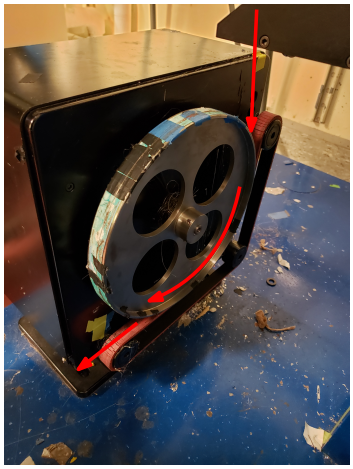

(c) The capstan mechanism

(d) The temperature controller

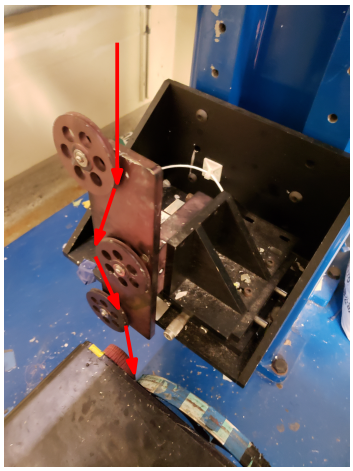

(e) The tension sensor

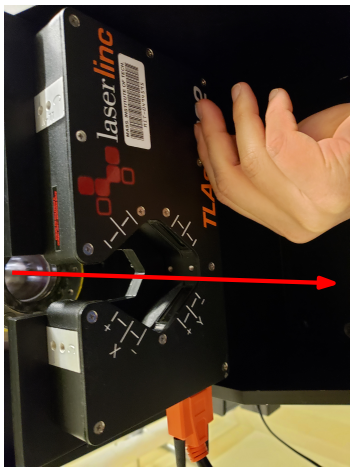

(f) The laser micrometer

Figure 1-2: Industrial fiber tower sub-systems

with three yellow wires. For industrial optical fiber drawing, the tension of the fiber is also monitored. Fig. 1-2e shows the tension sensor and how the fiber goes through the sensor. The fiber will contact 3 pulley wheels. The middle pulley has a load cell that measures the force applied on the pulley wheel. The last sensor that the industrial tower has is the laser micrometer—the laser micrometer displayed in Fig. 1-2f has 2 perpendicular measurement capabilities. This can detect the eccentricity of the fiber. Depending on the different brands and models of the tower, there may be other sensors and actuators, but the essential components were shown in Fig. 1-2.

The optical fiber drawing process is complex and challenging to control. Considerable research effort has taken place to improve the fiber drawing process. As early as the 1970s, the efforts were taken to model the optical fiber drawing process. The initial models focused on the neck-down shape and the temperature distribution, and the model was verified experimentally [2]. This initial model was further developed into different solutions for non-isothermal conditions [3]. In addition, the modern approach using iterative methods to improve the model was introduced by Choudhury et al. . [4]. The modeling methods were better improved by identifying the critical parameters to the process of optical fiber drawing and including the practical aspects of the drawing process such as gas flow and iris opening sizes [5, 6]. From the developed models, work was done to simplify the model [7], along with work to enable high-speed production as well [8,9]. The optical fiber drawing process was further perfected with research involving the implantation of stochastic characteristics on the numerical simulation model [10] and investigating which parameters on fiber drawing stabilizes the fiber diameter [11]. These improvements in the models led to the development of better control methods with the optical fiber drawing process.

In addition to the numerical modeling, controlling the diameter of the optical fiber was extensively researched in the past. The conventional optical manufacturing process is using the thermal drawing process. The optical fiber draw process heats the large diameter glass rod (preform), which then is pulled axially out of the furnace to generate a thin cross-section [2]. From the main principle, multiple control methods to maintain the steady diameter output of the fiber were developed. In the early

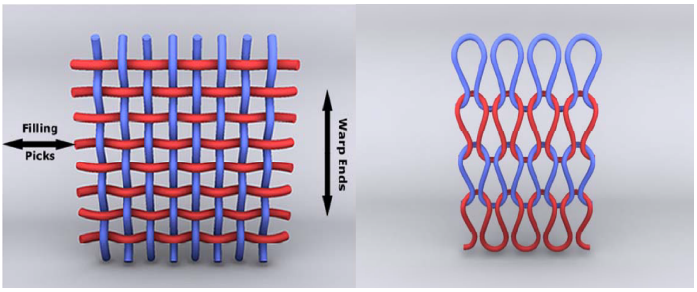

Figure 1-3: The example of weaved (Left) and knitted (Right) fabric [18]

1990s, Mulpur and Thompson developed a modal diameter control method based on the simulation approach [12]. They made assumptions on isothermal and utilized the modal control method. Mulpur and Thompson then expanded their research into applying nonlinear control on the optical fiber diameter [13]. Afterward, state-space modeling of the optical fiber drawing process and using the state-space model with Linear Quadratic Gaussian optimal controllers was investigated [14, 15]. The better modeling of the neck-down profile and controlling the process using draw tension allowed high-speed production [16]. The research was further developed to produce a reduced-order model that can be utilized with robust control methods [17]. As a result, there is clear evidence of an in-depth investigation of controlling the optical fiber manufacturing process. All the research mentioned above focuses on developing a better model and control strategies to maintain the diameter at a set point. As mentioned in [14], as setpoints vary, the new state model has to come from CFD in conventional control architecture. If a research effort was to target for the development of fiber with varying diameter along the length of the fiber, both hardware that reduces the cost of prototype and software that can control the varying diameter are required. This thesis focuses on the hardware development to prototyping such innovative fiber.

1.1.2 Fabric Manufacturing Process

The fabric production existed for thousands of years around the world. It was also the main process that led to the first industrial revolution. The process can be generally classified into two methods: weaving and knitting. The produced fabrics from weaving

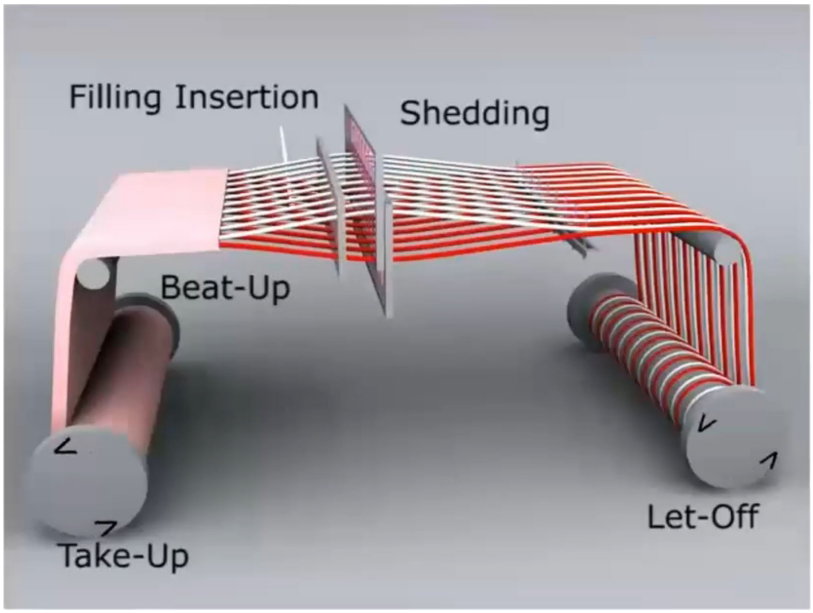

Figure 1-4: The weaving method to produce fabric [19]

and knitting are shown in Fig. 1-3. The weaving method and knitting methods are very different in both the production stage and the resulting fabric properties.

The weaving produces a fabric with more rigid properties. The typical weaving machine is shown in Fig. 1-4. The weaving process is done by shedding the fibers using the two frames. The two frames slide up and down in Fig. 1-4 separating the fiber rows in up and down locations indicated as red and white fibers in the figure. For each shedding motion, a filling is inserted. The filling is another strand of fiber that is inserted to create a new filled row each time. After the filling, the newly created row is beat-up into the final fabric and gets collected into take-up roll, as shown in Fig. 1-4. The weaving process existed over thousands of years, and the improvements to actuators and precision machine design made the system faster, but the fundamental method stayed the same.

The modern knitting was first introduced in the patent from the 1800s [20]. The typical knitting machine is shown in Fig. 1-5. The knitting machines use multiple latch needles. An example of the latch needle is shown in Fig. 1-6. The details of the knitting machine mechanism and operation are explained in Section 4.1.1. The knitting machines utilize multiple knitting needles to form many knits with one-

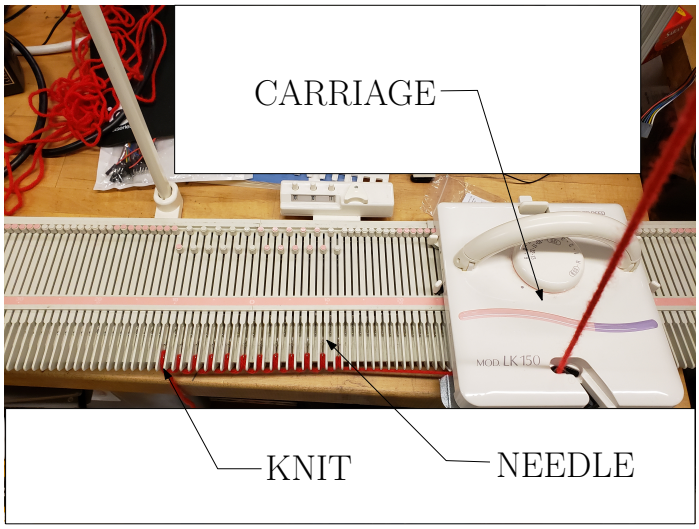

Figure 1-5: The conventional manual knitting machine

directional travel of the carriage quickly. The carriage contains a cam surface that pushes and pulls the needles in a coordinated manner so each needle will grab the fiber feed correctly to form the knits. This highly organized mechanism did not change since the industrial revolution time but improved efficiency with new actuators over time.

1.1.3 Smart Manufacturing

Smart manufacturing was introduced with the growing applications on Big Data and the Internet of Things (IoT). Before, the acquisition, storage, and processing of the large data were too expensive. However, with recent innovations with storage solutions and the Graphics Processing Unit (GPU), the concept of 'Big Data' became popular. The cost reduction of communication modules and sensors led to the wide applications of IoT. The use of IoT to get the big data for manufacturing purposes would define what the Smart Manufacturing is.

In recent years, the development and implementation of smart manufacturing and smart factories have gained momentum. Manufacturing systems must become easier to reconfigure, and "smarter," in order to follow the customers' increasing demands for high quality and customizations [21]. The smart manufacturing system will be key to economic value by enabling more types of product and more product variations [22].

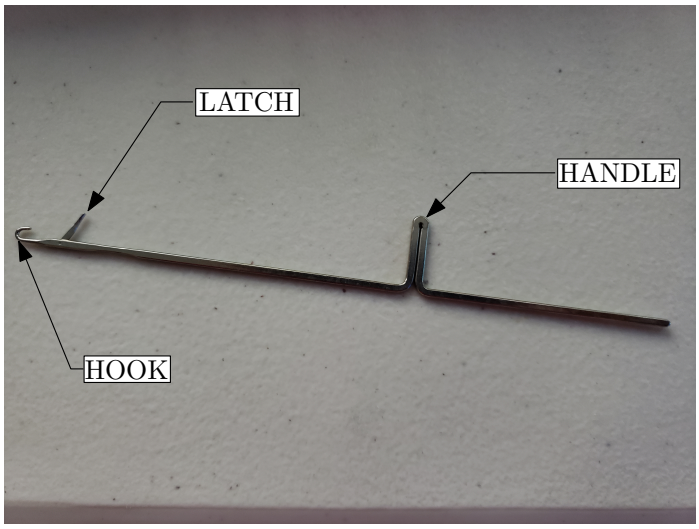

Figure 1-6: A knitting needle used in knitting machine

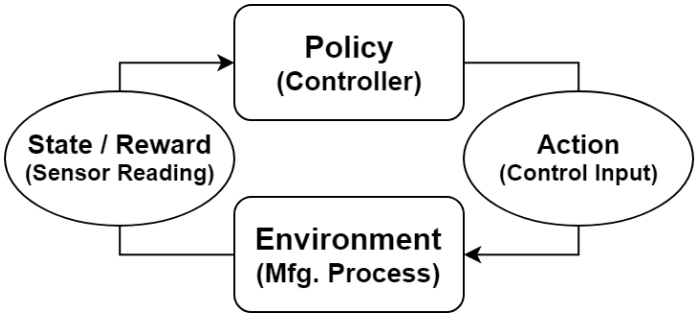

Figure 1-7: General schematic of how machine learning interacts with fiber system [26]

In the past, smart manufacturing solutions would have a high cost associated with the collection and storage of the data. Data-enabled smart manufacturing systems are made possible through the evolution of capabilities in the Internet of Things (IoT) and Big Data [23, 24] infrastructure as the demand for smart manufacturing systems increase, the need for training and education increases as well. Workforce education on smart manufacturing systems is one of the ten priority actions for smart manufacturing [25]. This thesis discusses an instrumented, controlled, and a data-enabled scale version of an optical fiber drawing system. This system is used to teach the foundational knowledge about the smart manufacturing system.

1.2 Data Analytics and Process Control Education

With the growing demand for smart manufacturing, educating people with smart manufacturing has become a paramount need. The system that was developed for this thesis has been widely used in MIT classes. The classes ranged from on-line [27, 28] and MIT's class [29] offered to students. The principles of smart manufacturing come from data analytics and process control. It costs a lot to acquire big data and test new process control methods in the manufacturing setting. It is impractical to use industrial equipment to teach smart manufacturing. In addition to education, the recent rise of interest in artificial intelligence also needs equipment like the system developed in this thesis. The foundational research in artificial intelligence (AI), especially in machine learning technique called Deep Reinforcement Learning (DRL), has allowed AI to play complex games like Go [30] and Atari [31] better than human. The recent development in DRL and machine learning, in general, focuses a lot on simulation environments [32–34] or highly determinant environments [35, 36]. There still is an opportunity to research more about how machine learning techniques can help improve the real environment and real process control with stochasticity. The fiber manufacturing system described in this thesis allows the machine learning researchers to acquire data at significantly less cost (financial and time spent). The researchers can also implement new algorithms and control methods to see if the process improves. The added stochasticity of the system allows the researchers to focus on the robustness of their algorithms. This robustness will allow the researchers to develop machine learning algorithms that can be applied to solve real-world problems quicker. The described machine learning algorithm would interact with the developed fiber system, as shown in Fig. 1-7. An example of the use of the fiber system for the development and testing of the machine learning algorithm was presented [26].

1.3 Advanced Fiber in Biological and Neurological Applications

Despite the fiber manufacturing technology being a stable process, and having a long history, multiple research topics in biological and neurological studies have relied on fiber manufacturing technologies. For example, there was a research that looked at the placement of microstructures inside the optical fiber [37]. The work was further developed with modeling the hollow fiber drawing process [38]. The condition that influenced the optical property of these fibers were also investigated [39]. Embedding the micro-structure into the optical fiber was significant improvement broadening the sensing and transmission capabilities in the optical fiber, but it was limited to optical communications purposes.

The use of multi-material inside the optical fiber has revolutionized the capabilities of fiber to be used in different applications. The general use of semiconductor cores in thermally drawn fiber was summarized before [40]. The semiconductor core thermally drawn fibers were demonstrated to be used as optical sensors [41], fiber as a radially emitting laser source [42], and using the fiber as thermal sensor [43]. In addition to the multi-material fiber, biological application fibers were researched as well—the use of fiber for optical spinal cord probing [44]. Probing neural activity and neuromodulation through waveguide [45,46], and fiber that combines waveguide, electrodes, and microfluidic channels to interact with brain circuits [47]. In addition to interacting with brain and neuron activity, the fiber research has also been focused on connecting the severed nerve using the fiber. The research proved that porous fiber could be thermally drawn to grow nerve cells in the direction guided by the fiber [48, 49]. These fibers are called neural scaffolds, and it is known to accelerate the neuron cell connection process.

The examples of the use of multi-material fibers and their biological and neurological applications are significant. The industrial optical fiber manufacturing equipment is not low cost [50]. Most of the above mentioned thermally drawn fiber examples require long prototype steps and difficult to tune the parameter to create different

prototypes in short terms. This thesis will introduce a system that is low-cost compared to the industrial optical fiber manufacturing system. The system presented in this thesis will also allow small volume fabrication of the fiber samples, which will allow the researchers to try different parameters of the sample fiber in short terms.

1.4 Knitting Advanced Fibers

There has been considerable research progress with advanced knitting fibers. Such examples come from knitting the shape memory alloy (SMA) Nitinol (NiTi) fibers. The NiTi was first invented in Naval Ordnance Laboratory [51, 52]. NiTi has two unique properties that distinguish itself from other metals. Depending on the set austenite temperature, the NiTi can be an SMA or super-elastic. The SMA effect of NiTi comes from solid-state phase transformation, also called as martensitic transition [52]. When NiTi is heated, it assumes the austenite phase. At low temperatures, NiTi changes to martensite. The physical deformation changes the martensite NiTi to be detwinned. Heating the detwinned NiTi would transform the NiTi to the austenite phase, which is returning the material to its programed shape [53]. When the material is cooled, it returns to the martensite phase but the twinned arrangement. The temperature in which solid phase transition happens can be controlled with the composition of Nickel and Titanium in NiTi. When the austenite transformation finish temperature is lower than room temperature, the NiTi will display the super-elastic properties at room temperature.

The SMA NiTi fiber has been used extensively in fabric research. The foundational research that allowed the SMA fiber to be knitted as active fabric started in 2013 [54]. The 2013 paper by Abel et al. . [54] introduced how different knit loops can provide different actuation characteristics. This work was further developed with more generalization and experimental verification [55]. The article [55] also relates the knit fabric's geometric property to the performance of the knitted actuator. After the classification and modeling effort, the knitted SMA fabrics were made as self-fitting wearables [56]. The introduction of self-fitting wearable with SMA led to many

research developments. There more efforts on performance modeling [57], verifying the performance experimentally [58] and improvement on self-fitting wearables [59]. The research efforts led to some novel application of using SMA fabric for maintaining air pocket in clothing for fire-fighter protections [60]. The constant effort in improving the use of SMA in fabric shows that there is strong demand for producing a fabric with advanced materials.

Despite considerable research effort in the use of NiTi fiber for knitting fabric, there is an opportunity for development for knitting fabric with super-elastic NiTi. The super-elastic NiTi is used widely for medical devices such as guidewires and cardiovascular stents [53]. The typical manufacturing approach using super-elastic NiTi is limited to machining, laser cutting, and manual forming. An improvement of manual forming was presented in an article before [61]. Koon et al. showed that super-elastic NiTi could be knitted with fixture and baking and conventional knitting machine. This work had a high impact because it allowed highly dense knitted fabric. Fabric with higher density allowed better load capabilities. The limitation of this fabric fabrication method is that it has too many processing steps. For different loop geometries, new fixtures would have to be made. After that, the wire had to be formed into a loop shape with the fixture. The formed fiber is then put into the oven for 15 minutes in $400°C$. Finally, the thermal processed NiTi fiber can be manually knitted with a conventional knitting machine. If there is a need to continue knitting extended length, this method is impossible to continue as fabric in the knitting machine cannot be reattached back to the fixture for manual forming. The new fabric system presented in this thesis will solve this problem by directly knitting the super-elastic fiber without thermal processing.

1.5 Summary and Overview of the Thesis

This thesis introduces 3 different machines that were developed: a fiber system for education, a fiber system for advanced fiber prototyping, and a fabric knitting system for advanced fiber. For the fiber system for education, the mechanical design of

each component of the system is discussed. After the process of fiber, drawing is modeled, and open-loop data was acquired to design the closed-loop controller for the process. Finally, the fiber drawing experiments with a designed closed-loop controller was performed, and the results were analyzed. For the fiber system for advanced fiber, more focus on the resulting fiber types were emphasized. The chapter still starts with a discussion of the mechanical design of the components as the system was revised significantly. Moreover, the revised controller design is discussed. After the system development discussion, the experimental section is presented. In the experimental section, details about different types of fiber preform preparations and different fiber that were prototyped are presented. In the next chapter, fabric knitting system development is discussed. The conventional knitting method is investigated in limitations on knitting super-elastic fiber is identified. With the limitations in mind, a new knitting process was designed. The mechanical design of the components to implement the new process is then presented after the presentation of the system. The resulting super-elastic knit fabric's stress and strain property is modeled and compared to the experimental data. This thesis ends with the conclusions which discussed the future application of the three systems and further research that lies ahead for the projects.

Chapter 2

Desktop Fiber Manufacturing System for Education

This section discusses the desktop fiber manufacturing system that was built for educational purposes. The initial hardware that was developed for the educational purpose was presented in a conference [62]. The hardware was improved for better performance and reliability since then. Some key functional requirements for the education fiber system were safety and data-richness of the system. The system introduced in this chapter models the optical fiber manufacturing process. The preform material (glue stick) is heated and then pulled with controlled velocity to achieve the desired diameter. Multiple sensors and actuators are used to introduce various sensor types and applications to the students using this system. This system and its data were deployed in multiple educational settings to teach smart manufacturing.

2.1 Mechanical Design

The system that was built for educational purposes is shown in Figure 2-1. The educational fiber system has to be safe to operate in the classroom environment. Also, the system had to produce enough data to be used for data analytics and process control classes. For safety, the system was designed to use glue sticks, which are non-toxic for the fiber drawing process. Various sensors were deployed to produce rich

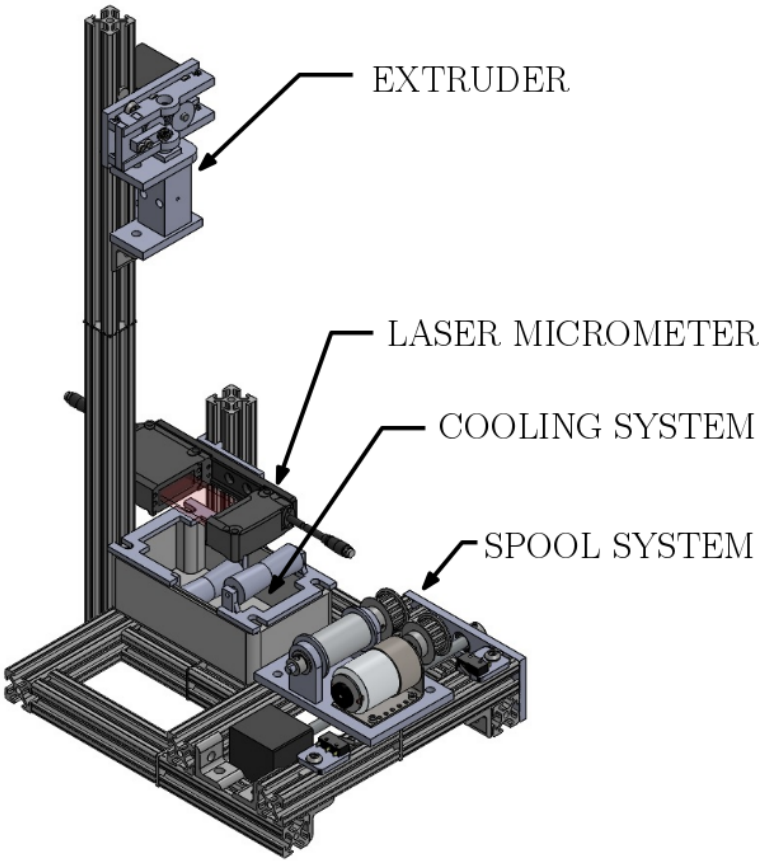

Figure 2-1: The Desktop Fiber Manufacturing System for Education

data for educational purposes. On top of the sensor systems, the different mechanical systems are designed. In this section, details about each system are discussed.

2.1.1 Extruder System

The main function of the extruder system is to feed the preform material into the heating chamber. The extruder system is shown in Figure 2-2. The design is similar to the industrial optical fiber tower. This system can be divided into a feeder system and a heating chamber.

The feeder system was composed of a stepper motor with driven gears and the idler gears. The gears were used to provide better grip to the preform material, and the stepper motor drove the preform material into the heating chamber at the desired velocity. NEMA 17 stepper motor with $38mm$ length was used as the actuator. The

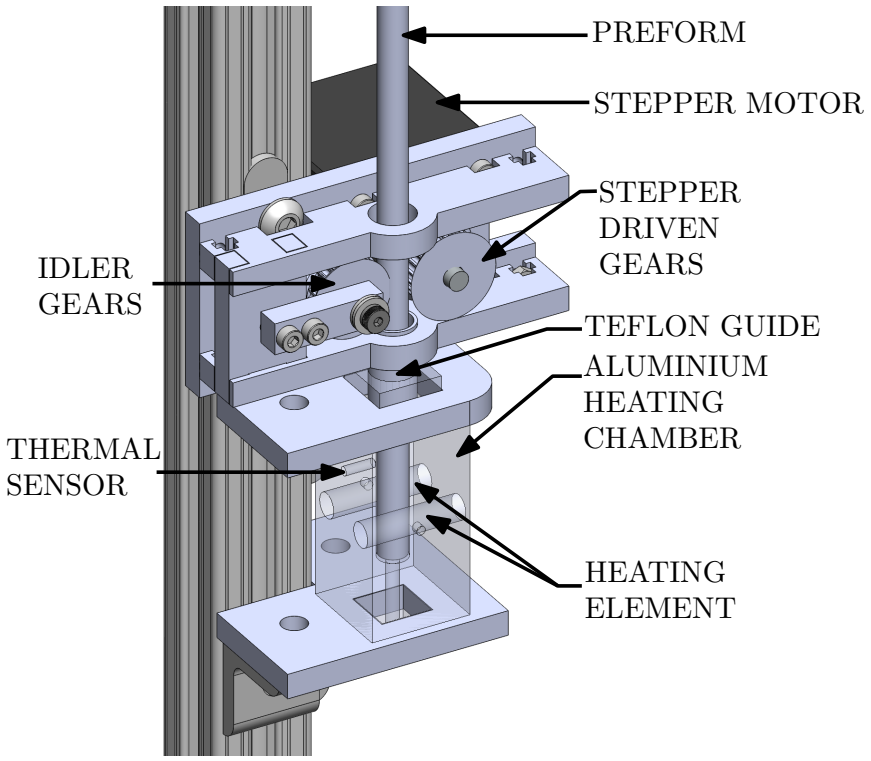

Figure 2-2: The Extruder System Composed of Feeder and Heating Chamber

stepper motor driver board DRV8825 actuated the motors. With the design described, the feeder system was able to feed the preform material to the heating chamber at a controlled rate.

The heating chamber is composed of a heating chamber, cartridge heater, and resistance temperature detector (RTD). The educational system had 2 of the $40W$ cartridge heaters. Each heater was $6.35mm$ in diameter and $20mm$ in length. Set screws were used to fix the heater inside the heating chamber. The RTD was used to detect the temperature of the heating chamber. The 3-wire PT100 RTD was used with Adafruit's RTD sensor amplifier - MAX31865 was used. The sensor amplifier communicates with the microcontroller through serial communication to send the temperature information to the micro-controller.

2.1.2 Cooling System

The cooling system is shown in Figure 2-3. The cooling system cools down the fiber that comes out from the extruder system and also guides it to the spool system.

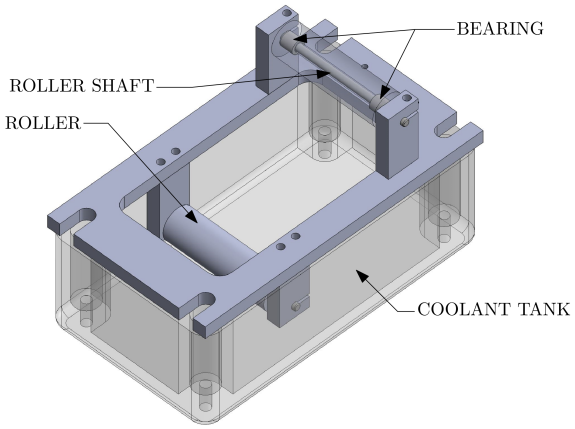

Figure 2-3: The Cooling System

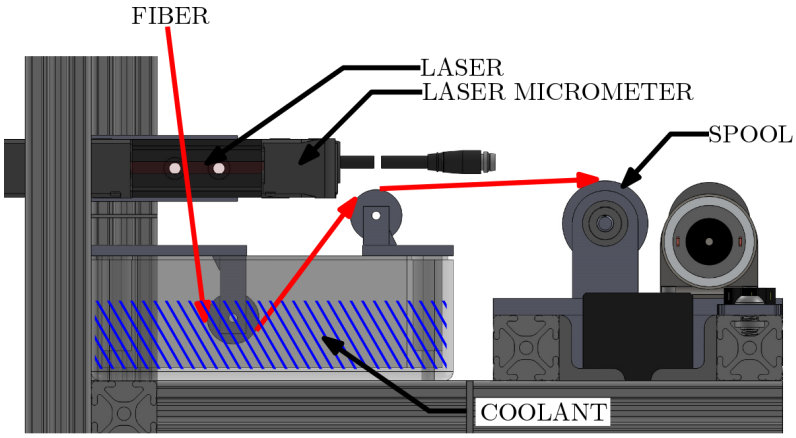

Figure 2-4: The Fiber Production Process in Educational Fiber System

The coolant thank is filled with room temperature coolant, which was water for the educational system. The coolant ensured that the glue-fiber is cooled enough, so it does not adhere to rollers or other surfaces. The fiber that came out from the extruder system goes through the two rollers in the coolant system, as shown in Figure 2-4. The roller in the coolant system guided the fiber into the water after going through the laser micrometer. The fiber then exits the water, and the second roller ensures that the fiber enters the spool system without touching other elements in the system.

2.1.3 Spooling System

The spooling system is shown in Figure 2-5. The spooling system collects the fiber and also controls the diameter of the fiber that is being produced. The spooling

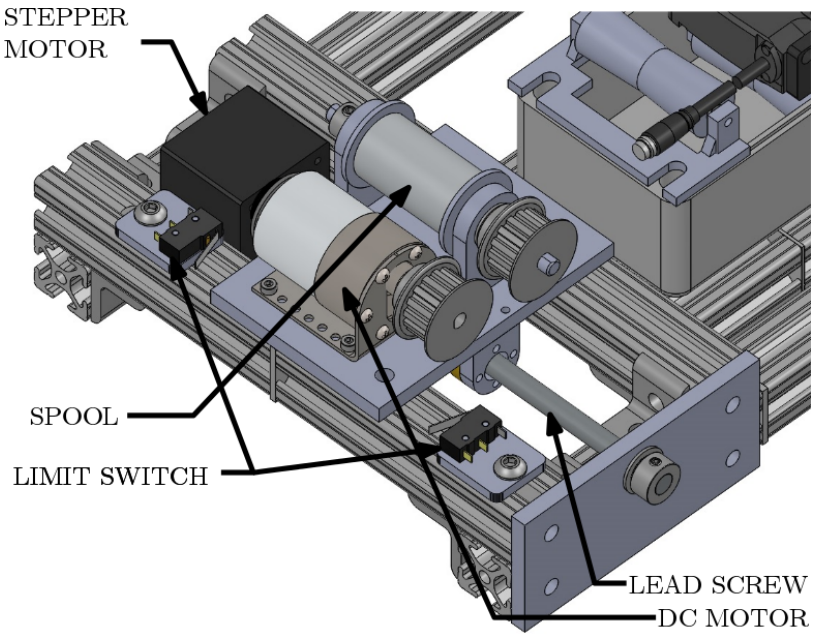

Figure 2-5: The Spooling System

system has two actuators. The DC motor with encoder spins the spool at the desired velocity. Timing belt was used to couple the DC motor's output rotation to the spool's rotation. The rotational velocity will control the diameter of the fiber that is being produced. Stepper motor with a lead screw was used to move the spool. The spool will collect the fiber, and the diameter of the spool will gradually increase. In order to allow the fiber to accumulate in the entire length of the spool, the stepper motor with lead screw translated the spool. The limit switches were used to set the limit of how far the spool will move. The switches ensured that the fiber does not go off the spool when the collection is happening.

2.1.4 Sensor System

Multiple types of sensors were used for this system. The use of different types of sensors exposed the students with the experience to interact with different types of communication methods and converting the sensor signals to the values of interest. The first sensor that was present in the system is the limit switch. The limit switch is one of the simplest sensors that can be used. The sensor provides an on or off signal to the microcontroller based on the switch's contact. The limit switches were installed,

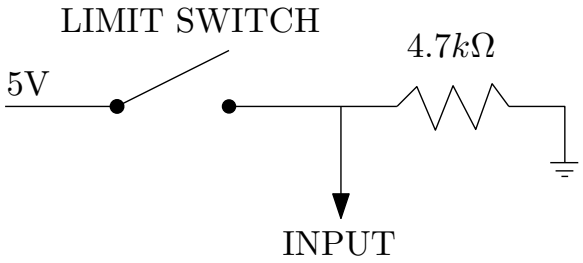

Figure 2-6: The circuit of limit switch implementation

as presented in Fig. 2-5. As the stage contacts the limit switch at the stage end, the limit switch closes and provides a positive voltage to the microcontroller. The circuit design of how the limit switches are implemented is shown in Fig. 2-6. The $5V$ supply from the microcontroller is connected to the one terminal of the limit switch. The normally open side of the limit switch was connected. The other terminal of the limit switch was then connected to the desired input port of the microcontroller. It is important to connect the resister of high value ($4.7k\Omega$) on the input side and connect to the ground of the microcontroller. This resister will protect the microcontroller from drawing a larger current when the switch is closed.

The other sensor that was used is the resistance temperature detector (RTD). The model of the RTD that was installed is PT100 from Adafruit. The RTD was selected because it can measure high temperatures, reaching up to $550°C$ [63]. The RTD sensor changes the resistance according to the change in temperature. The Wheatstone bridge circuit can be used to measure the change in resistance, as presented in literature before [64]. From the initial trials, the Wheatstone bridge produced significant noise in the reading. Later in the development of the system, the amplifier circuit MAX31865 was used to alleviate the noise issues.

Finally, the laser micrometer was used for sensing the diameter of the fiber in real-time. The Keyence IG-028 sensor head unit paired with the IG-1000 amplifier unit was installed on the mounting bracket (Keyence IG-TB02). Initially, the amplifier unit's output wires were directly connected to the microcontroller's input channels. The amplifier was able to send the diameter measurement is translated into linear voltage. This was later changed to the serial communication method because the signal was

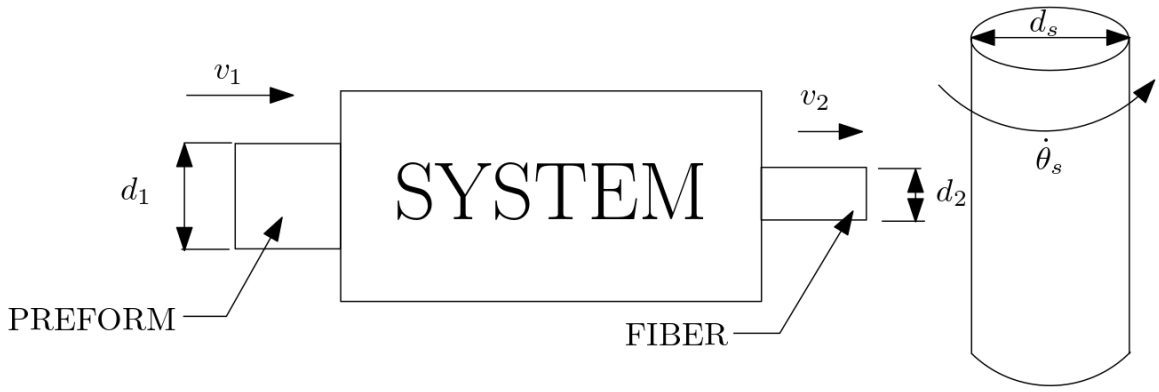

Figure 2-7: The conservation of mass model of the desktop fiber system [66]

noisy, and the limited resolution on the microcontroller's input channels made the laser micrometer lose the best resolution it can provide. The laser micrometer can provide a high-speed sampling rate, but the default setting of averaging 16 data points with a sampling rate of $18.62ms$ was used [65].

2.2 Data Analytics and Controller Design

This section discusses moving from a simple model of the process to analyzing the data for closed-loop controller design. It was discussed in the introduction that modeling of the optical fiber drawing was investigated deeply. It is challenging to apply the findings on silica rod drawing to glue stick drawing. The simple mass conservation model was developed of the desktop fiber drawing system. The desktop fiber system will then operate with an open-loop controller. The collected diameter and sensor readings are analyzed to find any patterns. After the patterns are recognized, the closed-loop feedback controller was designed to control the diameter of the glue fiber. The acquired data is included in Appendix A.

2.2.1 Modeling the process

A simple conservation model of the desktop fiber system can be proposed [62, 66]. Fig. 2-7 describes the overview of the fiber system. The simple mass conservation

equation is written as:

$$v_1 \cdot (d_1/2)^2 \cdot \pi = v_2 \cdot (d_2/2)^2 \cdot \pi \tag{2.1}$$

From Equation 2.1, the v_1 and v_2 represents the velocity of the preform and output fiber respectively. The d_1 and d_2 represents the diameter of the preform and the produced fiber. The equation's left side represents the mass flow into the system (Preform). In contrast, the right-hand side represents the mass flow out of the system (produced fiber) The stepper motor's velocity at the extruder was controlled by setting the pulse rate. The Pulse Width Modulation (PWM) wave from the microcontroller was sent to the stepper motor drive DRV8825. The DRV8825 moves the stepper motor single step with a rising edge of the PWM wave [67]. From the step information, the v_1 can be calculated with the following equation:

$$v_1 = \frac{P_D}{2} \cdot \frac{2\pi}{200 \cdot 16} \cdot \frac{1}{t_p} \tag{2.2}$$

From Equation 2.2, P_D represents the pitch diameter of the gear that drives the preform in Fig. 2-2. t_p represents the period between the pulse waves being sent to the stepper driver DRV8825. In order to control the diameter of the fiber (d_2), the spool velocity has to change. The spool is represented in the mass conservation model on the right side of the Fig 2-7. d_s is the spool diameter and $\dot{\theta}_s$ represents the rotational velocity of the spool. The following equation can be written to relate the rotational velocity of the spool to v_2 in the mass conservation model.

$$v_2 = \frac{\dot{\theta}_s \cdot d_s}{2} \tag{2.3}$$

The Equations 2.1 and 2.3 can be combined as following:

$$d_2 = \sqrt{\frac{\pi \cdot P_D \cdot d_1^2}{1600 \cdot \dot{\theta}_s \cdot d_s \cdot t_p}} \tag{2.4}$$

Parameter	Value
P_D	8.98mm
d_1	0.28"
d_s	25.4mm

Table 2.1: Desktop fiber machine parameters for model

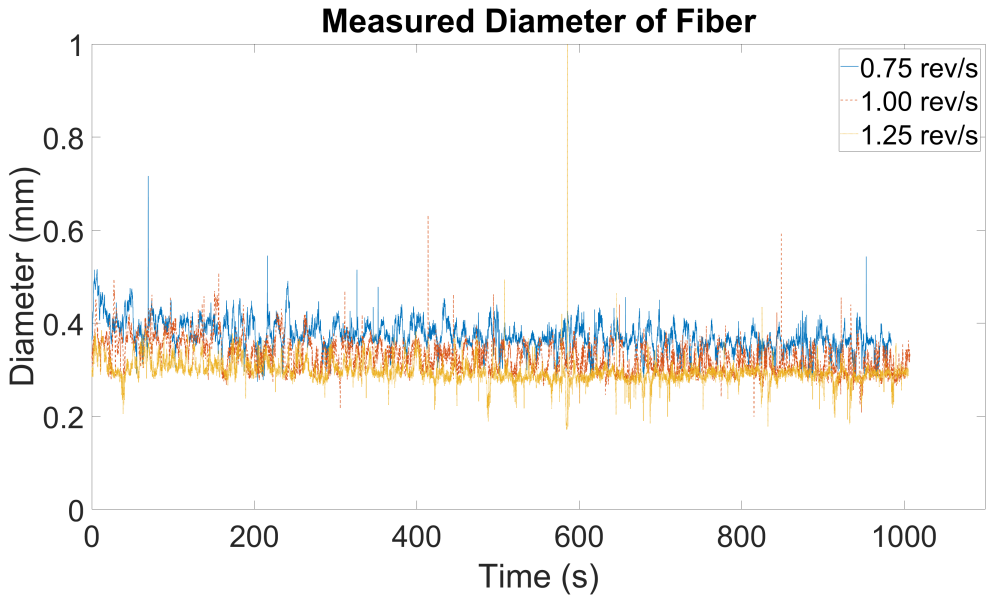

Figure 2-8: The raw diameter data from open-loop experiments [66]

The Equation 2.4 can estimate the diameter of the produced fiber from the control inputs to extruder and spool velocity. This model assumes the values in Table 2.1 as fixed parameters coming from the machine.

2.2.2 Analysis of the Open-loop Data

In order to verify the model, initial experiments took place to acquire open-loop data. The open-loop experiments used a heating chamber at $80^{\circ}C$. The data were sampled at 10Hz. The stage was set to translate at $1.25mm/s$ over approximately $37mm$ travel in each direction. The spool velocity varied for the different experiments. The spool velocities of $0.75rev/s$, $1.00rev/s$ and $1.25rev/s$ were used. The extruder was set to step 10Hz with 1/16 step distance per step. The NEMA 17 motor that was used for extruder has standard 200 steps per step, but with a 1/16 step setting, it can have finer resolution. The Equation 2.2 already included this 1/16 step division.

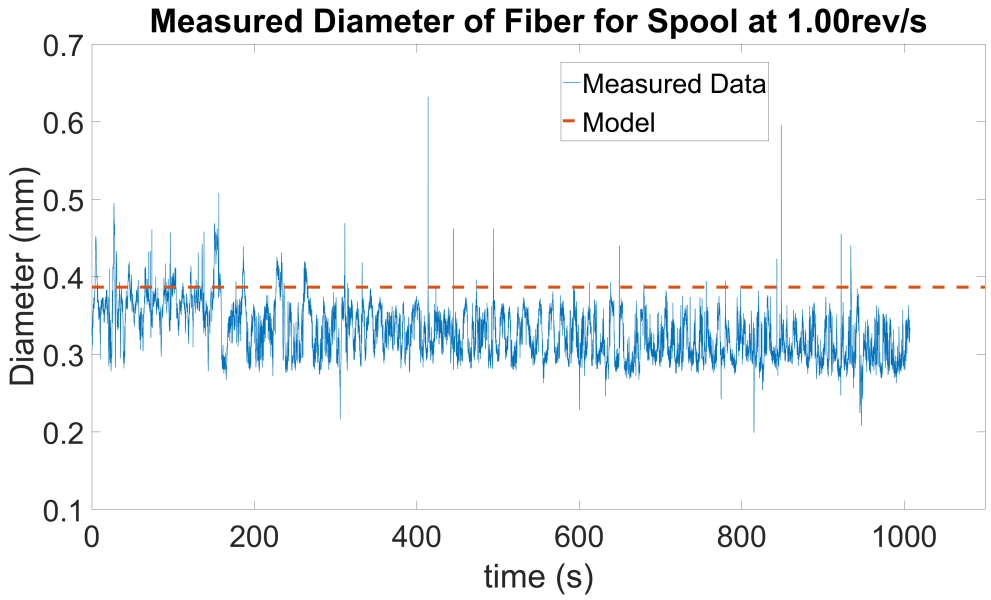

Figure 2-9: The raw diameter data from open-loop experiment with spool velocity of $1.00 rev/s$

The acquired data from this experiment is shown in Fig. 2-8.

From Fig. 2-8 three main characteristics of the system can be observed. The first observation was that with the higher spool velocity, the fiber diameter was smaller. This observation agrees with the Equation 2.4. Faster spool would mean that $\dot{\theta}_s$ is large, so d_2 would decrease with faster spool velocity. The second observation was that despite the different spool velocities, all the diameters tend to decrease over time. The second observation is easier to notice with Fig. 2-9. The mass conservation model creates a horizontal line in the graph that does not change over time. Nevertheless, the diameter measurement tends to decrease over time. Fig. 2-9 only shows one spool velocity, but different velocities show a similar trend. The third observation is that all the signal looks extremely noisy or oscillatory. The data has to be further analyzed to identify what is causing these distinct characteristics and whether these characteristics can be controlled.

Simple statistical analysis and statistical process control charts were used to identify if there were any distinct variations in the data. For the initial statistical analysis, the histogram was created, as shown in Fig. 2-10. It is observed that the mean diameter value is not in the center of the histogram's maximum value. Also, the

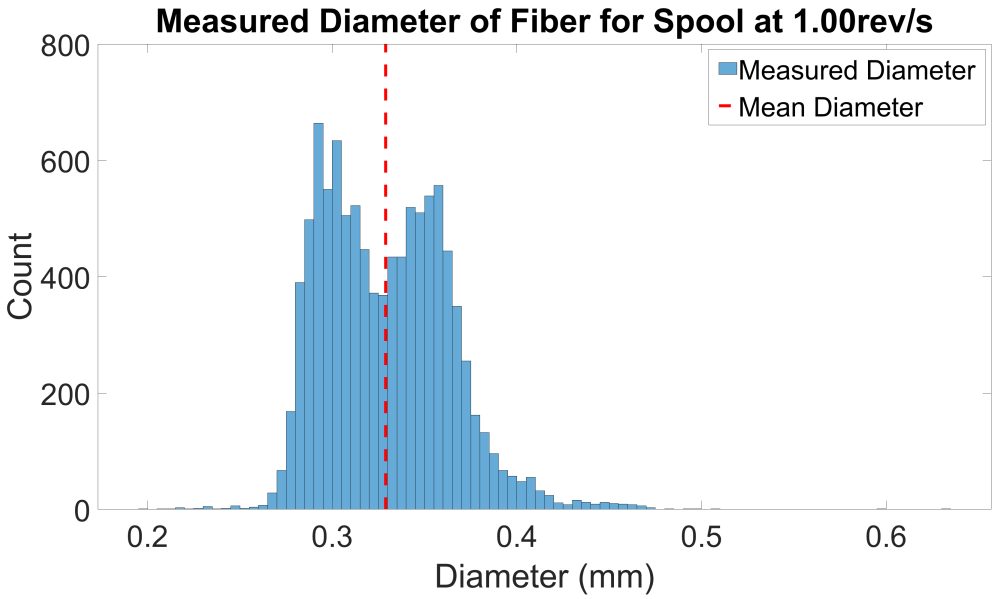

Figure 2-10: The histogram of raw diameter data from open-loop experiment with spool velocity of $1.00 rev/s$

histogram has two peaks, which means that the diameter measurement is not normally distributed. The histogram shows the statistical properties of the system. The distribution is observed to be right-skewed, which is from the increase in the diameter of the spool overtime. In order to look at the time dependency of the statistical properties, we create Statistical Process Control (SPC) charts. The Fig. 2-11 shows the SPC chart from the spool velocity of $1.00 rev/s$. The SPC chart show common process problem where data points are outside of the Upper and Lower Control Limit (UCL and LCL). However, from the raw data, it is hard to identify whether the noise from the data acquisition is causing the outliers. It can be inferred that polymer fiber being drawn cannot change the diameter with a large difference over 0.1 seconds; moving average can be used to introduced filtering concepts and to reduce the influence of noise.

In Fig. 2-12, the SPC chart for diameter data filtered with a moving average of 100 samples is presented. The number of data points outside the LCL or UCL has decreased significantly. It is observed that there is a significant number of consecutive data points on one side of the mean line. This is likely to be caused by the spool continuously collecting the fiber. The collected fiber increases the effective diameter

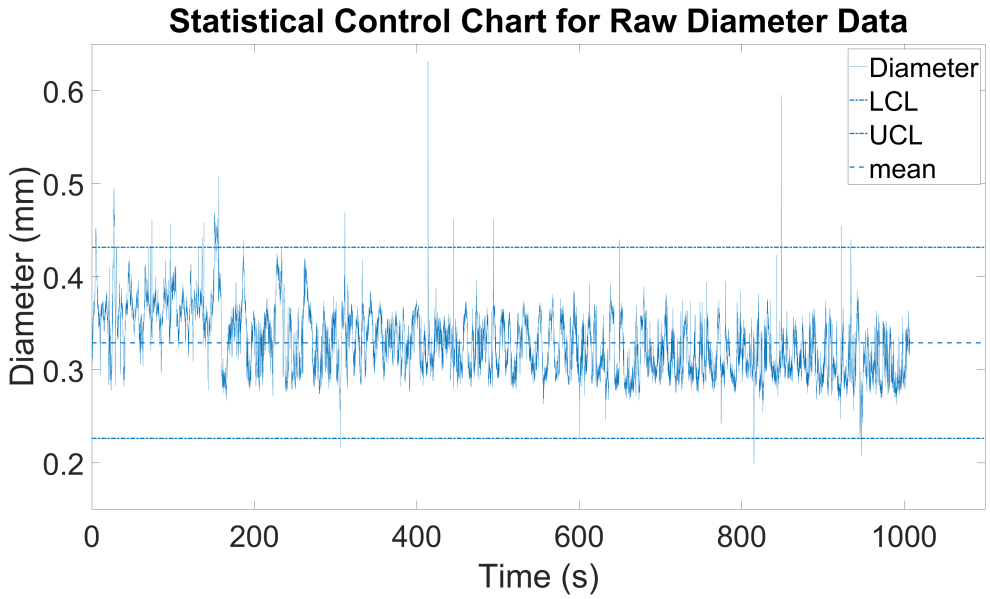

Figure 2-11: The SPC of raw diameter data from open-loop experiment with spool velocity of $1.00 rev/s$

of the spool (d_s), which from the mass conservation model, will decrease the resulting fiber diameter (d_2). The opportunity for further feedback control is introduced to prevent the diameter drift throughout the spool collection.

Finally, the oscillatory property of the diameter data in Fig. 2-8 was investigated. The diameter data may be showing the influence of the environmental or data acquisition noise. If the oscillatory signal property is coming from the environment or data acquisition noise, the moving average will help alleviate the influence. The moving average would reduce the high-frequency noise in the system [68]. It was shown in Fig. 2-12 that even with the moving average, the data still shows strong oscillation. The spectrum analysis was applied to investigate the sources of the oscillation. The Fig. 2-13 shows the result of the power spectrum analysis about the diameter minus the mean of the diameter after moving average was applied. The mean value of the diameter was subtracted from the original measurement to reduce the influence of the DC values. Fig. 2-13 was cropped to show only the major peak frequencies. There is the highest peak near $0Hz$ frequency because of the slow reduction of the fiber's diameter due to the spool's diameter getting large from fiber collection. The fiber collection and decrease in the diameter itself is a low-frequency component of the

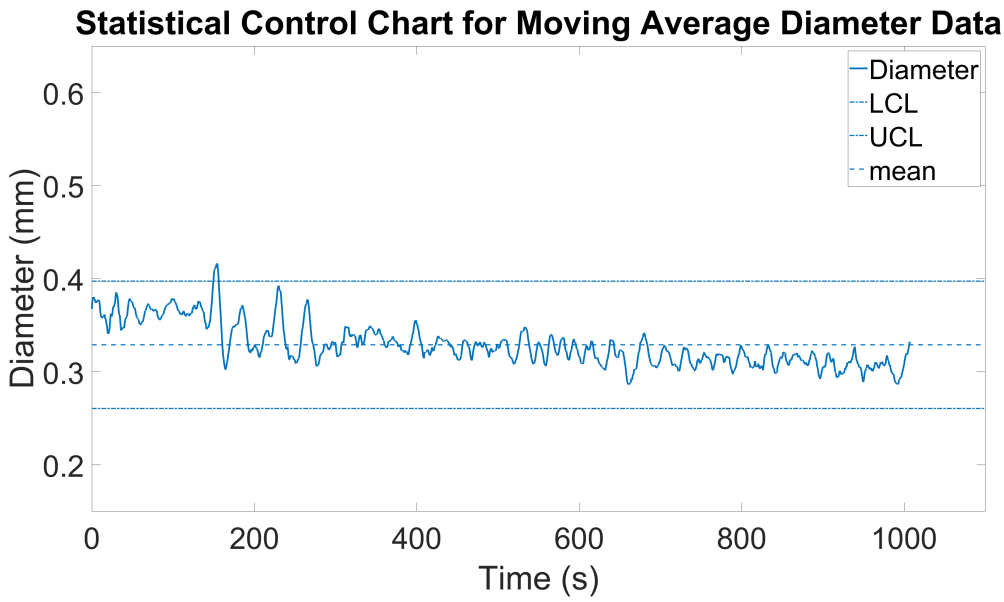

Figure 2-12: The SPC of filtered diameter data from open-loop experiment with spool velocity of $1.00 rev/s$

diameter change. Excluding the near $0Hz$ frequency components, two main frequencies showed high power in the spectrum graph. The first frequency indicated by the circle on the left side of Fig. 2-13 is located at $0.024Hz$. The cause of this frequency component was coming from the temperature fluctuations in the extruder system. Fig. 2-14 shows the spectrum analysis result of the temperature measured during the open-loop testing of spool velocity at $1.00rev/s$. From Fig. 2-14, the peak is observed at $0.019Hz$. This peak frequency is close to $0.024Hz$ in the diameter spectrum analysis result. It can be estimated that the temperature has a strong influence on the diameter oscillation—also, the second peak frequency in Fig. 2-13, indicated by a circle on the right side of the figure, is located at $0.037Hz$. This frequency is equivalent to the period of 27.23 seconds. The stage in the open-loop experiments is moving at the velocity of $1.25mm/s$ over approximately the $37mm$ length. It would take about 29.6 seconds for the stage to travel one way. This time matches the other significant frequency of the diameter. It can be concluded that the oscillations of the measured diameter are coming from the combination of the temperature fluctuations and the stage motion.

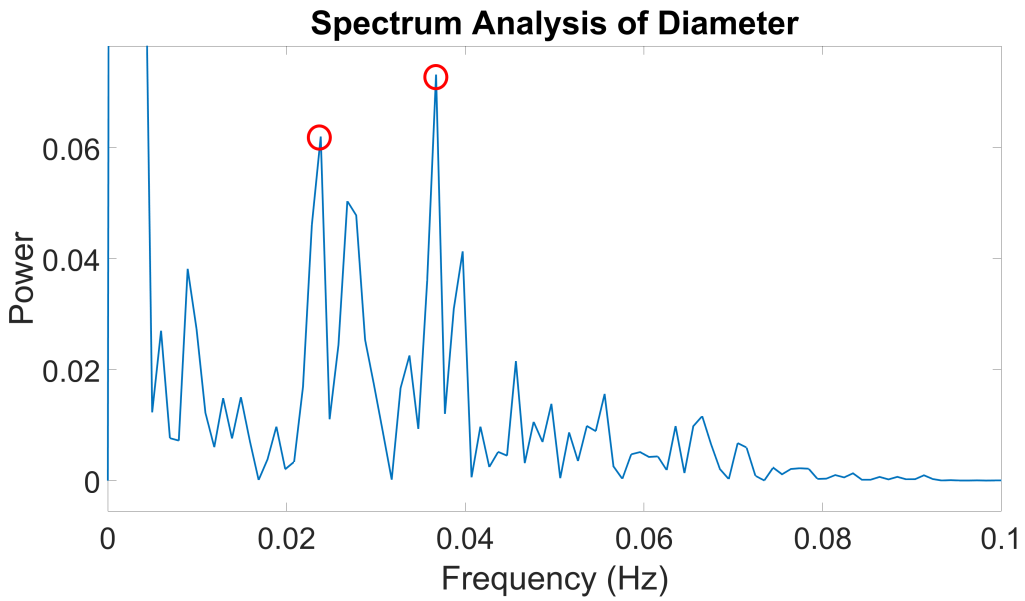

Figure 2-13: The spectrum analysis of filtered diameter data from open-loop experiment with spool velocity of $1.00 rev/s$

2.2.3 Closed-Loop Controller Design

After the open-loop analysis, Fig. 2-15 presents the block diagram of the new closed-loop controller to control the process. It was found that the open-loop data is not in statistical control. The closed-loop system will try to control the system so that the final result is within the statistical control limits. As shown in Fig. 2-15a, the proportional controller (P controller), is used to control the spool's rotational velocity. The output of the spool motor is the rotational velocity of the spool($\dot{\theta}_s$). This output is sent back as the inner feedback loop to the P controller. Encoder attached to the spool's DC motor was used to acquire the rotational velocity. The proportional-integral controller (PI Controller) was used to generate the command velocity into the spool's motor control loop. The output of the PI controller is based on the error of the diameter measurement to the target diameter. The details of how the closed-loop block diagram is implemented into the microcontroller are shown in Fig. 2-15b.

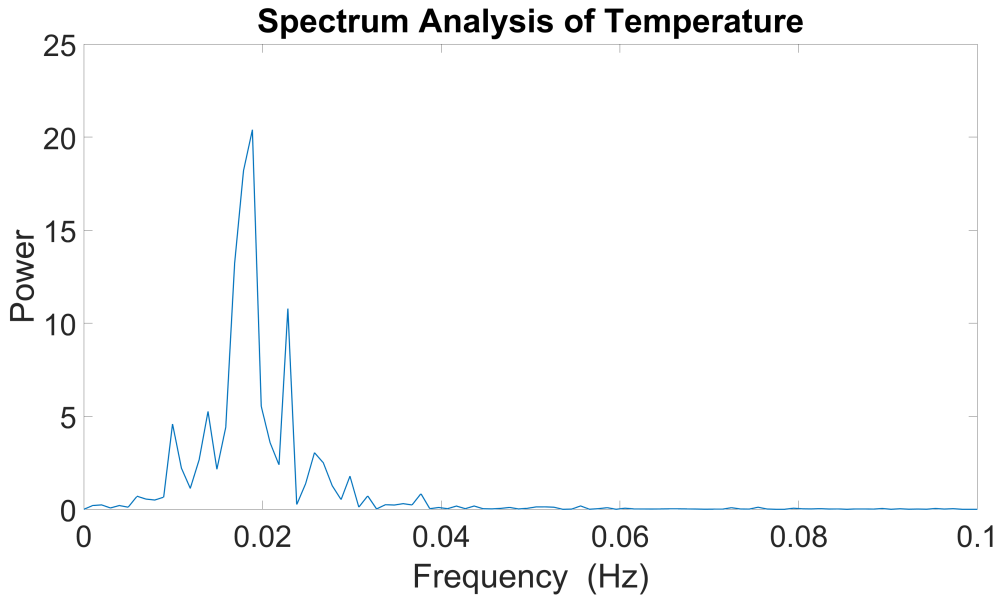

Figure 2-14: The spectrum analysis of temperature data from open-loop experiment with spool velocity of $1.00 rev/s$

2.2.4 Closed-loop Experimental Data Analysis and Results

The closed-loop experiment was performed, and the data from the experiment were analyzed. The acquired data is included in Appendix A. The closed-loop displayed in Figure 2-15 was implemented into the microcontroller. The experiments ran with a target diameter set to be $350\mu m$. The result of the experiment is shown in Fig. 2-16. The significant improvement that can be observed is that the decay of diameter over time is now missing. To verify that the closed-loop system is statistically under control, the same approach that was taken for open-loop results analysis were deployed. Figure 2-17 shows the histogram of the diameter measurement from the closed-loop experiment. The closed-loop diameter measurement follows a normal distribution. The standard deviation of the measured diameter was calculated to be $0.0274mm$. This standard deviation is significantly small compared to the $0.061mm$ standard deviation from the original educational machine introduced in the conference before [62]. In addition to the histogram, the SPC chart was created. Fig.2-18 presents the unfiltered diameter values. The number of data points outside the UCL or LCL has decreased significantly compared to the open-loop experimental results.

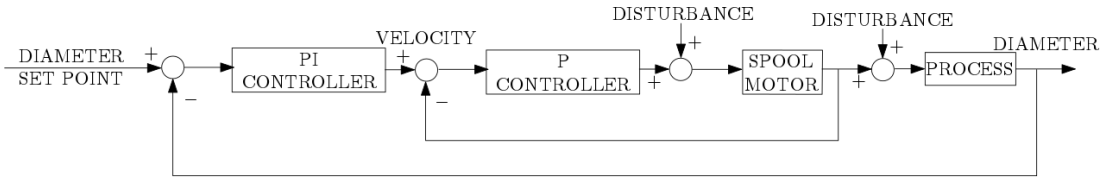

(a) The feedback control diagram of the fiber manufacturing system

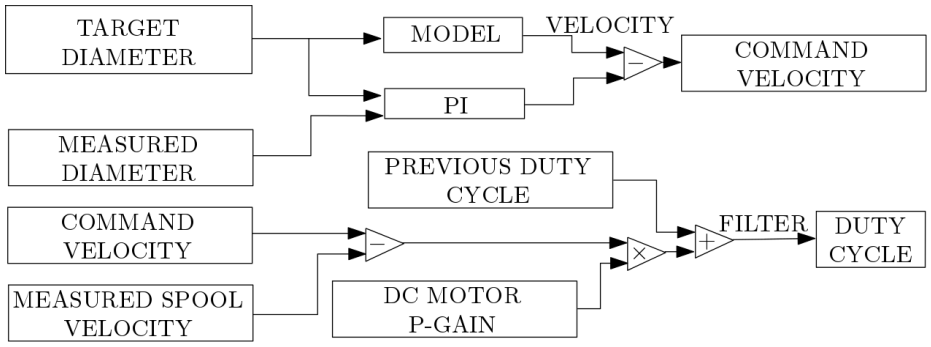

(b) The implemented block diagram of the fiber manufacturing system feedback controller

Figure 2-15: Fiber manufacturing system's feedback controller

The moving average filtering was applied again to clarify if there is any strong trend. The result of the moving average filter is shown in Fig. 2-19. The moving average sampling of 100 points was applied. The data points after filtering are observed to fluctuate between the upper and lower side of the average value. This pattern indicates that the variations in the data were caused by random error. Finally, it is clear to observe that the diameter decay from the open-loop experiments is now gone with closed-loop control implementation.

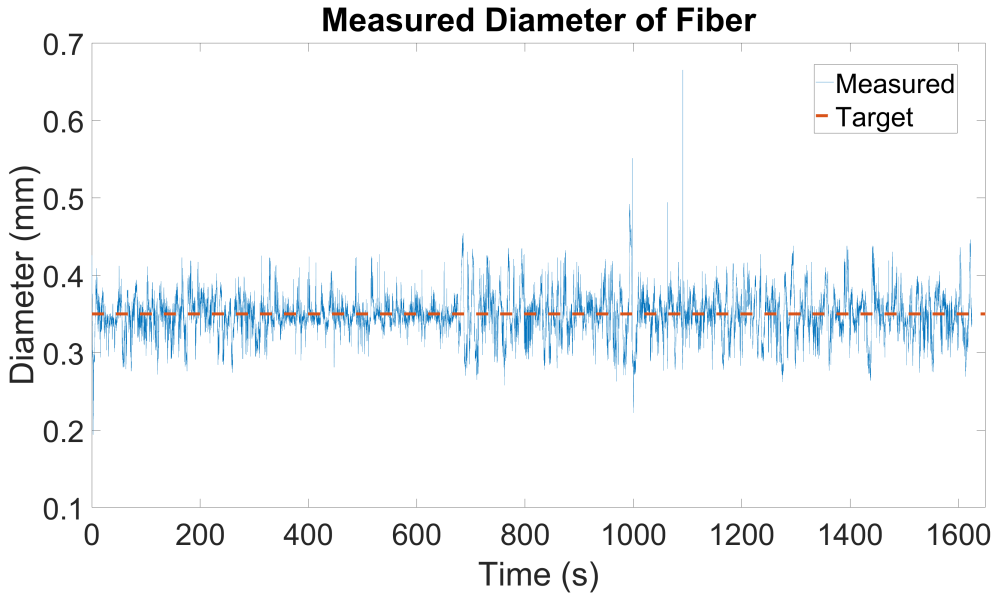

Figure 2-16: The diameter data from closed-loop experiment with target diameter of $350\mu m$

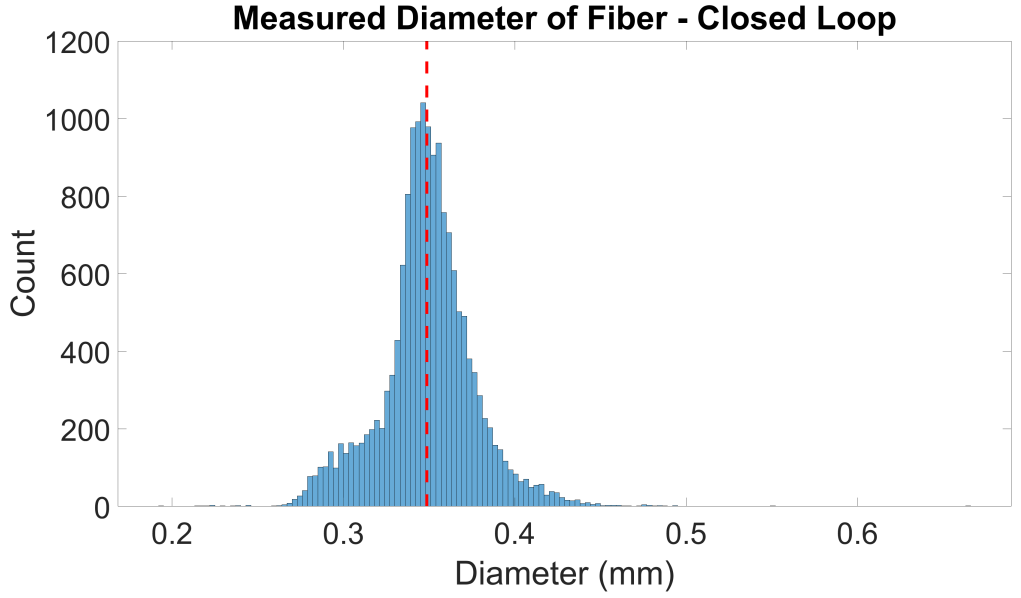

Figure 2-17: The histogram of diameter data from closed-loop experiment with target diameter of $350\mu m$

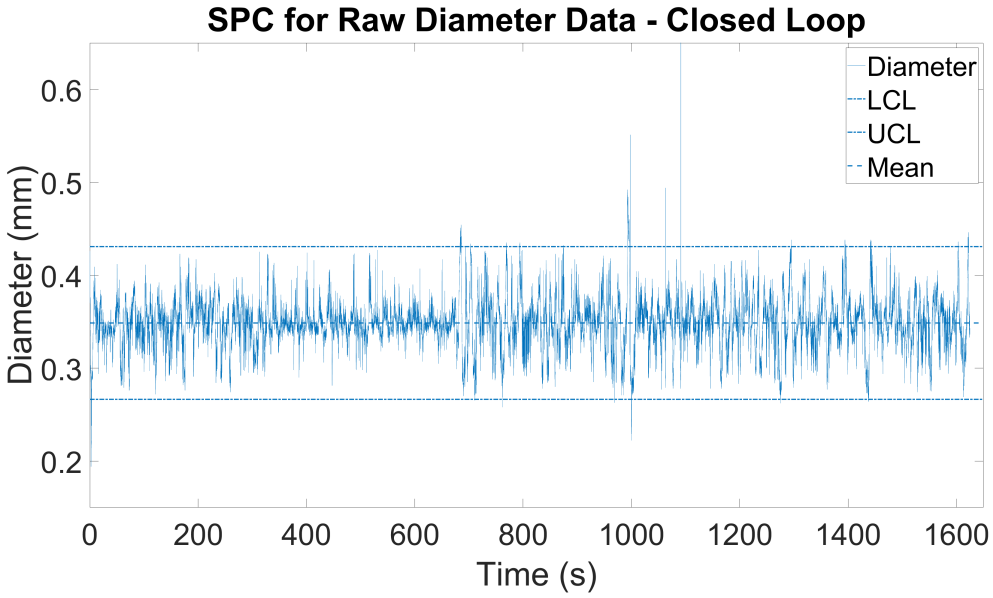

Figure 2-18: The SPC chart of diameter data from closed-loop experiment with target diameter of $350\mu m$

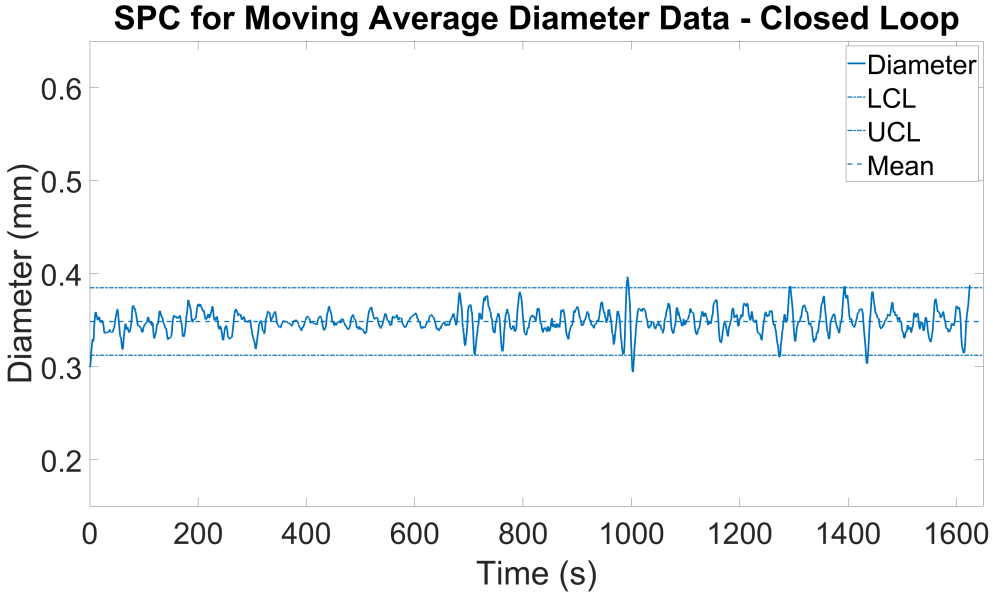

Figure 2-19: The filtered SPC chart of diameter data from closed-loop experiment with target diameter of $350\mu m$

Chapter 3

Desktop Fiber Manufacturing System for Advanced Fiber

This chapter introduces the improved desktop fiber manufacturing system for advanced fiber fabrication. For advanced fiber manufacturing, the consistent quality of the product was considered an essential aspect of the design. Multiple aspects of the machine from the educational version was improved. Also, the improved heating chamber implementation achieved a higher temperature. The advanced fiber manufacturing system produced fibers with different preform materials and different preform structures.

3.1 Mechanical Design

The mechanical design of the system has improved a lot from the educational version of the machine discussed in the previous chapter. The revised system for advanced fiber prototyping is shown in Fig. 3-1. The advanced fiber system consists of less number of sub-systems. The system removed the spooling mechanism to directly control and output the resulting fiber instead of collecting the fiber while controlling the diameter. This simplification reduces the number of variables that would have to be considered during the closed-loop control of the process. Further details of the sub-systems are discussed.

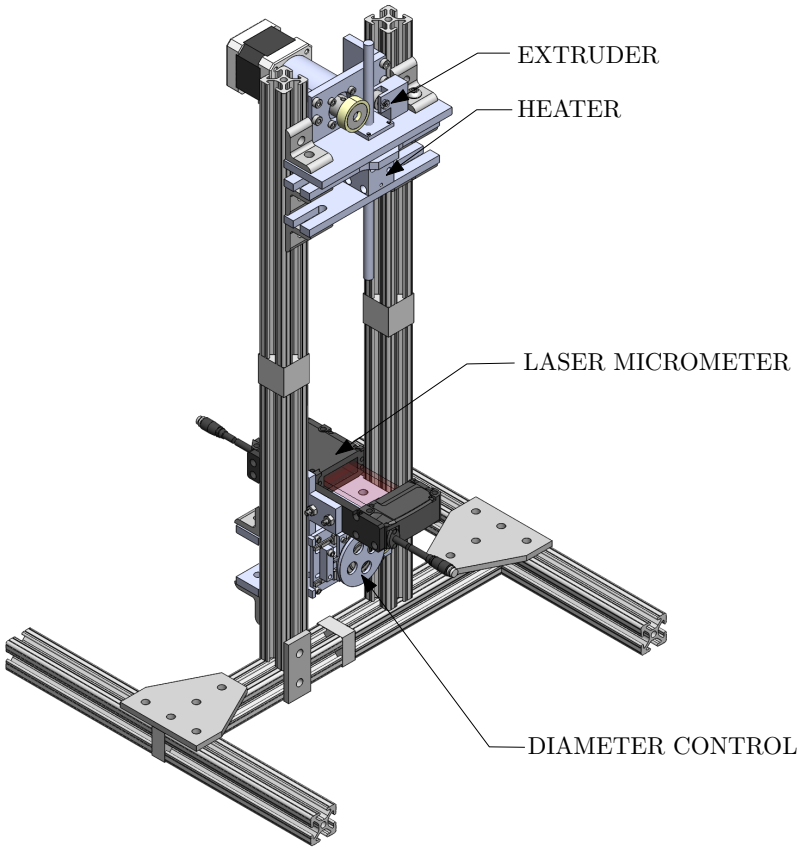

Figure 3-1: The desktop fiber manufacturing system for advanced fiber prototyping

3.1.1 Extruder System

Fig. 3-2 presents the extruder system. The extruder system was re-designed entirely from the educational fiber system. The new extruder system used a stepper motor with a gearbox to turn the roller. The roller with idler roller pinches the preform material. The material was pushed into the heating chamber at a controlled rate. The stepper motor is a typical NEMA 17 motor. The typical NEMA 17 motor has a step angle of 1.8°. The diameter of the roller used for this system is $25mm$. If the roller is directly mounted to the stepper motor's output shaft, each step will result in the linear displacement of about $0.39mm$, which is considerable. The stepper motor controller can be used to half step, but in order to allow for smooth motion of the preform, a gearbox attached stepper motor was chosen. The gearbox ratio is 1:100 output speed reduction. The considerable reduction in speed allows preform to move at a slow rate with smaller step displacement. This speed reduction ensured that

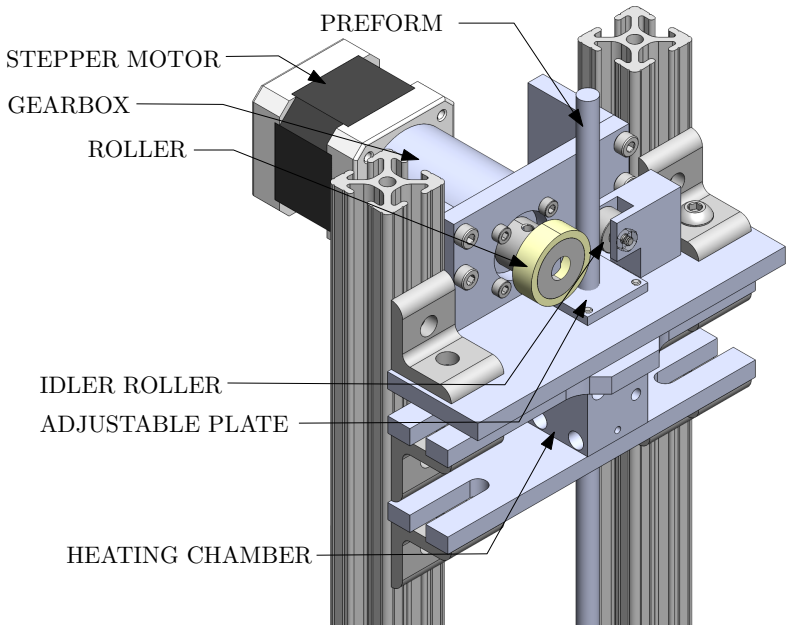

Figure 3-2: The extruder system for advanced fiber manufacturing system

the preform is fed with smooth linear velocity. In order to better guide the preform material, the adjustable plate was placed at the exit of the stepper motor assembly. The adjustable plate has a hole that can match the diameter of the preform. This plate helps guide the preform into the heating chamber without misalignment.

The extruder system also includes a new heating chamber. The new heating chamber is shown in Fig. 3-3. The heating chamber was CNC milled from the aluminum block. The new heating chamber has 4 holes where the cartridge heaters can be placed. The holes were drilled with a 0.25" drill. Each hole for the heater has a perpendicular threaded hole for the set screws to be installed. The set screws will ensure the cartridge heater to maintain contact with the heating chamber body to make the heater more efficient. The set screws also prevent the heater from sliding out of the heating chamber body. For this thesis, 2 of Omega's 150W cartridge heaters were used (model: HDC00005) [69]. There was a hole with a diameter value of 0.125". This hole was used to install the RTD sensor. The RTD sensor was also fixed to the heating chamber with a set screw. The Teflon shield was placed on the top of the heating chamber where the preform was fed. This shield helped to prevent the preform material from overflowing in the reverse direction when the material is

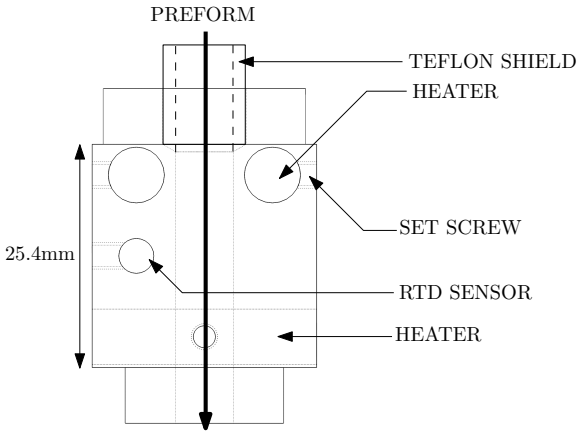

Figure 3-3: The heating chamber for advanced fiber manufacturing system

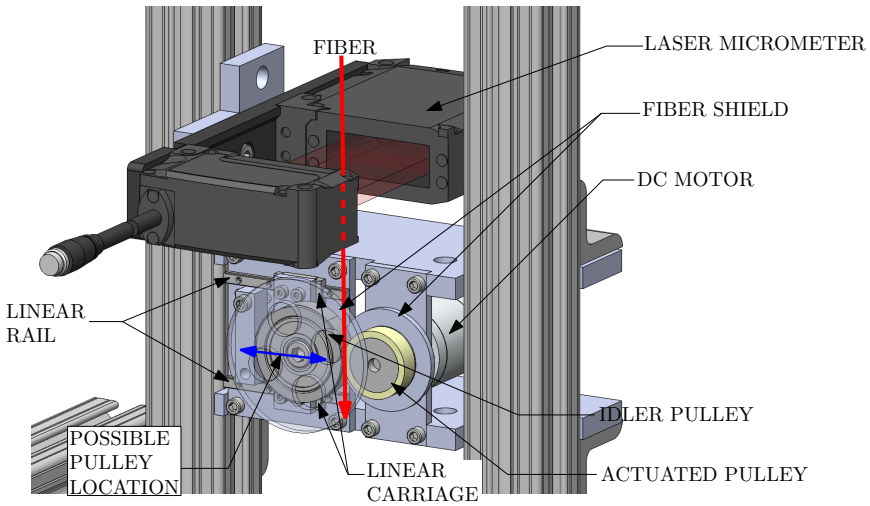

Figure 3-4: The diameter control system for advanced fiber manufacturing system

fed too fast.

3.1.2 Diameter Control System

The diameter control system assembly is shown in Fig. 3-4. Instead of the spooling system in the educational fiber system, the diameter control system pulls the fiber in controlled velocity to control the diameter of the fiber. The diameter control system pinches the fiber with two pulleys and changes the velocity of the pulley to control the diameter. Right above the diameter control system's fiber path, there is a laser micrometer. The idler pulley was mounted on an aluminum plate that is fixed to the linear carriage on the linear rail. This plate is spring-loaded to push the idler

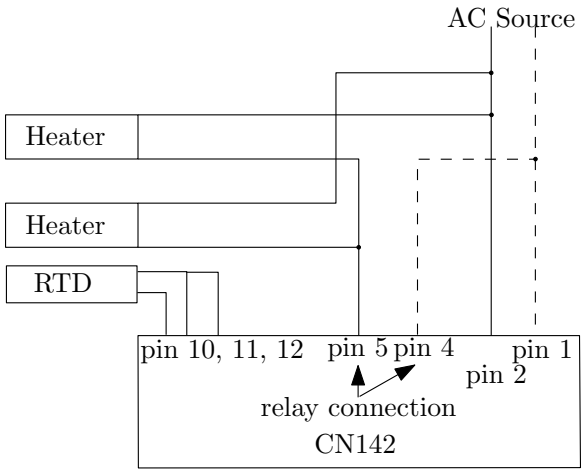

Figure 3-5: The circuit diagram of the heater control for advanced fiber manufacturing system [70]

pulley on the actuated pulley at all times. This spring loading allows the diameter control system to always grab the fiber even with a varying diameter of the fiber. The actuated pulley was rotated with a DC motor. The two fiver shields are attached to both pulleys. These shields prevented the fiber from moving out of the pulleys. The benefit of this diameter control system over the educational fiber system is that the machine does not have to be stopped every time spool is full. Theoretically, as long as the preform is continuously supplied in the extruder system, the fiber can be produced infinite length. The lack of a spool system also removes a variable in the control system design, as discussed in the previous chapter.

3.1.3 Sensors and Electronic Control Systems

The advanced fiber system had a similar sensor and electronic control system as the educational system. For the extruder, the stepper motor was controlled with the controller board from Pololu (Model: Tic T249). This controller board has a USB interface to software on a desktop PC. This controller allowed easily limiting the current on the stepper motor and has gain control feature to smooth the motion of the stepper motor even with slow speed [71].

For the heating chamber, both the sensor and electronic control system was installed to control the temperature. The RTD sensor was used, as discussed in the

above section. However, with the RTD sensor and cartridge heater, the relay-based heater controller was used (Omega CN142-R1-DC2-C4). The circuit diagram of the heating chamber control implementation is shown in Fig. 3-5. The Omega controller allowed the user to set the desired temperature and used a PID controller to maintain the set temperature inside the heating chamber.

In the diameter control system, multiple sensors were deployed. The laser micrometer was installed (Keyence IG-028 and IG-1000) to measure the diameter of the fiber. The laser micrometer used the Keyence DL-RS1A unit to allow the laser micrometer data to be transferred to the computer via serial communication. After the fiber passes the laser micrometer, the diameter control pulleys will rotate at the desired velocity. The desired velocity is monitored with the encoder that is attached to the DC motor. The encoder is a quadrature encoder measuring the output rotational velocity of the DC motor.

3.2 System Control Implementation

The advanced fiber system had a similar control method as the educational system. For the diameter control, the similar block diagram as the one presented in Fig. 2-15. Instead of the output duty cycle being sent to the spool motor, it was sent to the diameter control DC motor in 3-4. Although it will be discussed in the next section, it was found that open-loop control of the system was an effective method when controlling the diameter for various materials. As a result, using the stepper motor controller described in 3.1.1 was set to a fixed velocity. While monitoring the diameter of the fiber being produced, the operator would change the set velocity of the DC motor in the diameter control system.

3.3 Experiments and Results

This section presents the different experimental results from various types of materials that this system is capable of drawing. Initially, when the machine was built,

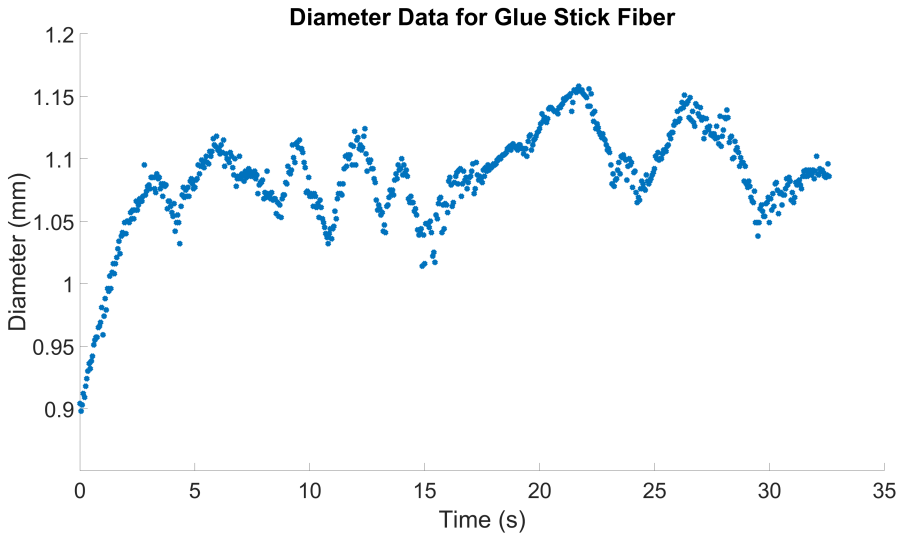

Figure 3-6: The glue stick fiber diameter measurement from advanced fiber system

	mm
Average	1.094
Standard Deviation	0.0282
Maximum	1.158
Minimum	1.014

Table 3.1: Glue stick fiber diameter statistics summary for advanced fiber system

the capability of the machine was verified using the glue stick. The same glue stick that was used for the educational fiber system was used. After verifying the system's functionalities, different preforms composed of different materials were used. It was demonstrated that neural probing fibers and the cell scaffolding fibers could be produced from this system.

3.3.1 Initial Glue Stick Experimental Result

The glue stick fiber drawing used the feedback control system described in the above section. The result of the experiment is shown in Fig. 3-6. From the data, the standard statistical values were calculated. The summary of statistics is shown in Table 3.1. From the result, the standard deviation is similar to the value that was present in the educational system. It is important to note that the average diameter

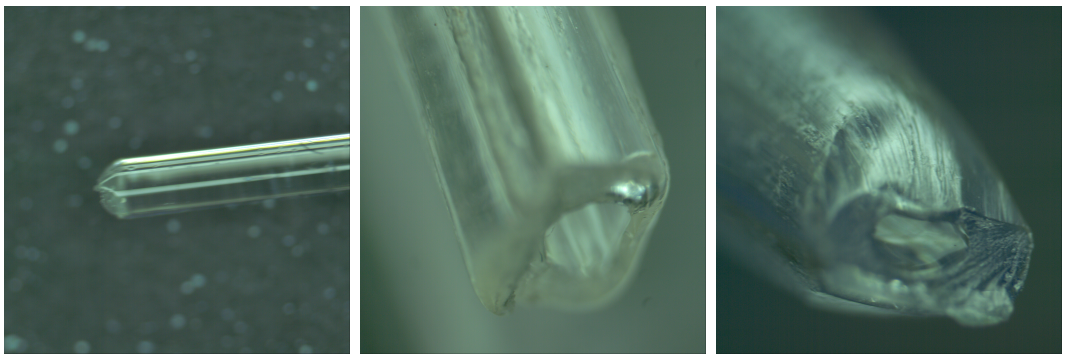

(a) Solid PMMA fiber (b) PC fiber with hole (c) PMMA fiber with hole

Figure 3-7: Solid and hollow fiber made from PMMA and PC

for this system was set to be about 3 times the target value for the educational system. Typically for the fiber drawing system, the smaller diameters show higher standard deviation due to higher tension in the fiber. It can be inferred that the advanced fiber system would have similar or better performance with less effort on control.

3.3.2 Single Material Solid and Hollow Polymer Fiber

After verifying that the advanced fiber system can produce a fiber with better standard deviation, experiments for using the system for different materials took place. Fig. 3-7 shows the different types of solid and hollow fibers that were made from the system. For solid fiber experiments, PC and PMMA preform materials were used. Fig. 3-7a shows the example of PMMA fiber with a diameter of $0.5mm$. The PC solid fiber was observed to be similar to Fig 3-7a. After successful fiber production in solid PC and PMMA fiber, fiber with a hole in the middle was produced. The preform that was used for the hollow fiber had a diameter of 0.25" with hole diameter 0.125". The resulting fiber was cut in, and the cross-sectional area view was captured. Fig. 3-7b shows the cross-section of the PC fiber with a hole. Fig. 3-7c shows the cross-section of the PMMA fiber with a hole. All the experiments discussed verified that the new system would be capable of producing neural probing fiber and cell scaffolding fiber.

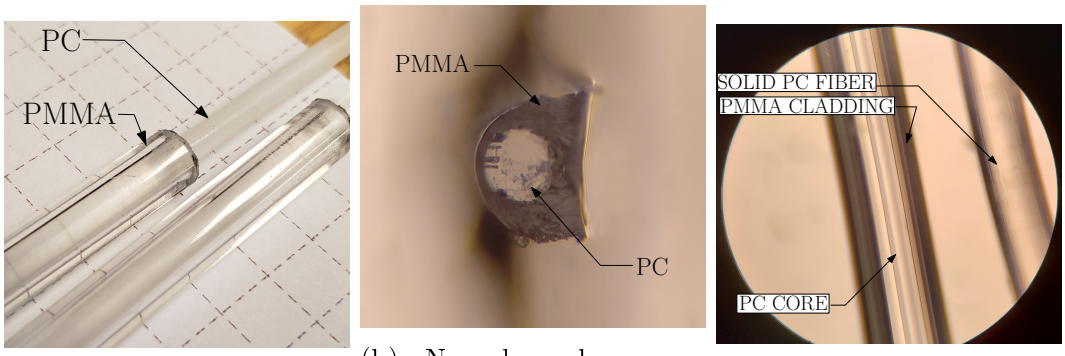

(a) Neural probe preform (b) Neural probe cross-section (c) Neural probe side view

Figure 3-8: Neural probe fiber produced from advanced fiber system

3.3.3 Neural Probe Fiber Production

The neural probing fiber was one of the main advanced that the system required to produce. The neural probe requires multiple prototypes to tune the optical parameter required for specific laser transmission. For this thesis, one example to show the capability of this system to produce the neural probing fiber is presented. Professor Seongjun Park of KAIST directed the detailed specification of the neural probing fiber. According to Professor Park, the neural probe had to have a PC core with PMMA cladding. The preform was made, as shown in Fig. 3-8a. The stock rod of PMMA with an outside diameter of 0.25" and hole diameter of 0.125" were purchased. The stock material was 6′ long, and it was cut to be a 12" each for ease of feeding to the machine. The PC core material was purchased as a 0.125" diameter rod. The PC core material was also cut into a foot each. The PC core material was then pushed into the PMMA material. Some sanding was required on the PC core material to slide the material into the cladding PMMA. Before drawing, the preform had to be placed into a vacuum oven for about 24 hours in about $90°C$. The vacuum oven will degas any microbubbles inside the preform. The neural probing fiber was drawn with a heater set to a temperature between $220°C$ to $250°C$. The laser micrometer was constantly monitored to meet the diameter specification of $100\mu m$ to $200\mu m$. The resulting fiber was within specifications. The produced fiber was inspected under a microscope, as shown in Fig. 3-8b and 3-8c. It was observed that PC core material

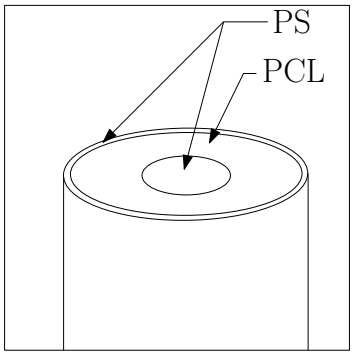

(a) Preform Composition

(b) Sheet of PCL

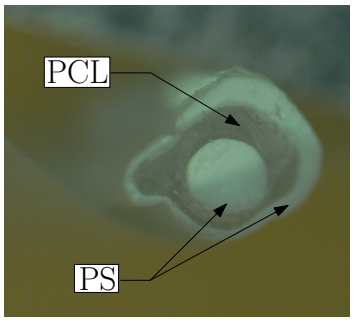

(c) Cell Scaffold Fiber

Figure 3-9: The cell scaffold fiber from advanced fiber system

was successfully surrounded by PMMA cladding material. The KAIST team has inspected the fiber samples and currently moving forward with animal testing.

3.3.4 Cell Scaffold Fiber Production

As discussed in the introduction, the cell scaffold fiber is one of the key fiber that needs to be prototyped on the fiber system in the lab environment with different parameters. The fiber preform was prepared similar to prior research article [72]. A new method to prepare the preform had to be developed to make smaller preform (0.25" diameter). As shown in Figure 3-9a, the schematic of the preform requires 2 cladding on a core material. The two different polystyrene(PS) rod and tube were purchased. The PS rod had a diameter of 0.125". The PS tube had an outside diameter of 0.25" and an inner diameter of 0.194". The PCL pallets were melted in vortex machine with anhydrous 99% chloroform. The PCL pallets were mixed to chloroform with a weight percent of 3%. For this experiment, $3.77g$ of the PCL pallets were mixed with $121.90g$ of chloroform. The mixture was covered with parafilm and mixed in a vortex for about an hour. The resulting solution was poured onto the aluminum baking pan of size $13"X9"$. The solution was quickly spread evenly on a baking pan by continuously tilting and rotating the pan. The PCL would then form a thin sheet, as shown in Fig. 3-9b. The PCL sheet is then rolled on the PS rod. After the PS rod is rolled with the PCL sheet, the rolled rod is pushed into the PS tube. The prepared preform was drawn into the fiber at the heating chamber

temperature set to $220°C$. The resulting fiber was within the diameter requirement of $200 - 500\mu m$. The resulting fiber is shown in Fig. 3-9c. The finished fiber will be submerged in cyclohexane overnight to melt away the PS layers [73]. This step is taking place in KAIST, where they will perform the growth of cells inside the scaffold fiber to verify that the fiber prototype is meeting the specification they need.

3.4 Generalized Design Approach for Fiber System

In this section, the generalized design approach for the desktop fiber system is presented. The design methods for fiber system using different sizes of preform material is shown. Also, this section will discuss multiple aspects of the fiber system that needs to be considered while designing a new system.

3.4.1 System Level Design

The design of the fiber system starts with the system overview design. In order to design the system, some of the requirements have to be introduced first. From the perspective of the biologists and neuroscientists, the fiber system's preform diameter is one of the most critical design parameters. The system design has to be changed based on the required preform and final diameter. For this section, the preform diameter is defined as D_{pre}. After deciding which diameter range of preform would be used for the system, the system structure can be designed.

The frame of the fiber system would be designed based on the sub-systems that would be attached. The sub-systems include the extruder system, laser micrometer system, and diameter control system. In order to leave the flexibility for modifying the design, a rail-based frame (such as 80/20) is recommended for structure. An example structure that was used for the advanced fiber system is shown in Fig. 3-10. The base was designed so that the structure is stable and does not fall sideways. The base width and length were designed to be around 60% to 70% of the system height. The designed structure was stable and had no vibration problems. The system mount had two pillars made of 80/20 framing structure. These rail-frame pillars were

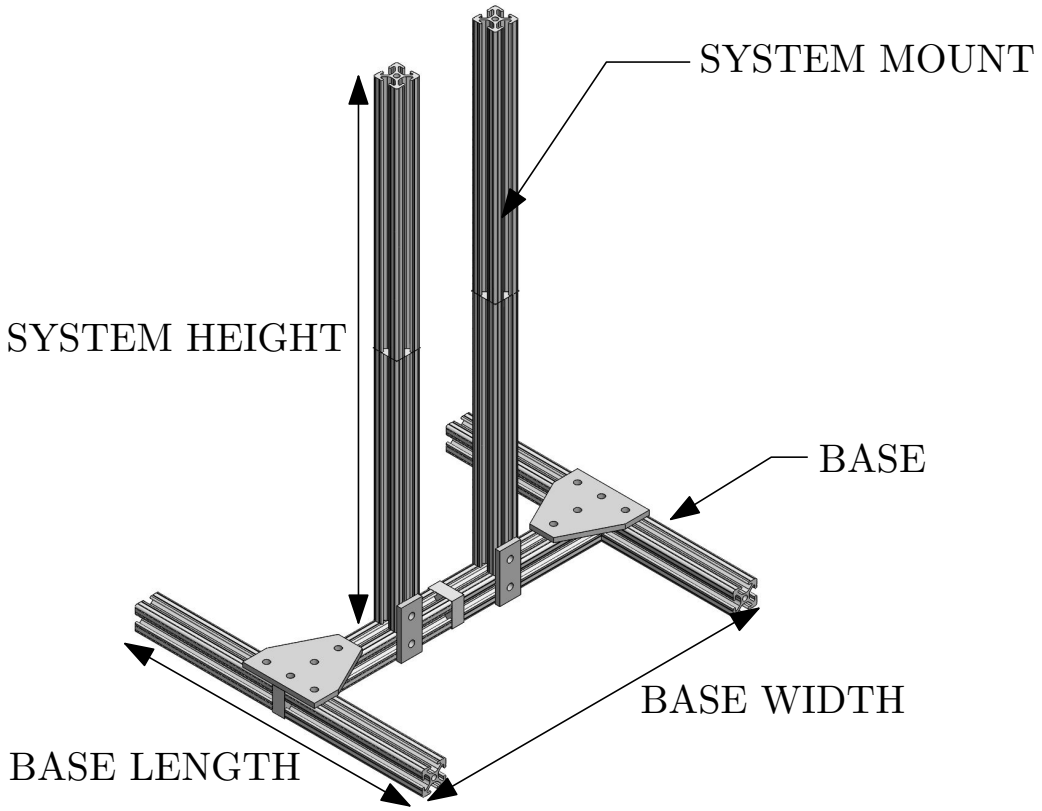

Figure 3-10: The general structure design

a critical component in the prototyping machine. Depending on the temperature of the heating chamber, some fiber would take longer to cool down than others. If the heating temperature is around $200°C$ to $300°C$, the total height of $50cm$ was more than enough to cool the fiber. However, having extra length allows the translation of the location of the sub-systems, which helps try different preforms in the future. After the base structure size is set, the other components of the system can be designed.

3.4.2 Extruder Design

The extruder system design will consider the details of the actuator system and heater system. For the heating chamber, two significant parameters can be changed. First is the diameter of the preform, as it was shown in Fig. 3-3, the preform is placed in the middle. The original heater design was intended for a preform diameter of 0.25". If larger preform were to be used, the diameter of the hold in the middle would have to

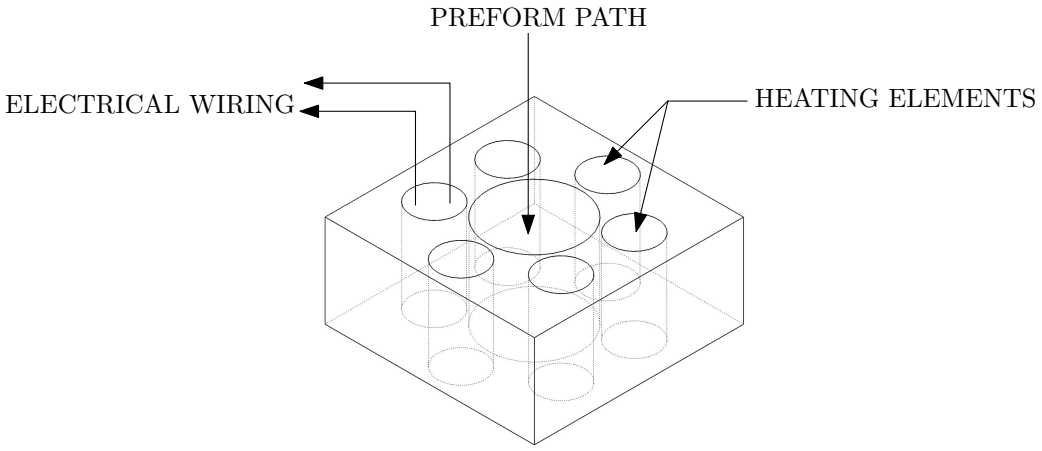

Figure 3-11: The alternative arrangement for heating elements

increase. As the diameter of the preform path increase, the heater needs to be placed further from the center. The heating element should be placed as close to the walls of the preform as possible to minimize the heat loss from the heaters. The arrangement of the heating elements can be increased by putting multiple heating elements, as introduced in Fig. 3-3. For the advanced fiber system in the thesis, only 2 heating elements were installed, although the design allowed for 4. From the experiments, it is best to keep the heating chamber as short as possible. Inside the heating chamber is conduction based heating. The longer path that preform has to travel with heat, the higher chance that disturbance may disturb the preform structure. The tolerance on the heating chamber's preform path is an important parameter as well. The conductive heating works best if the heating surface and the material has no air gap. However, if the preform path is smaller than the preform's diameter, the amount of force required to push the preform increases significantly. This diameter interference also will cause turbulence in the heating chamber, so the structure of the preform design cannot be guaranteed to stay in the fiber state.

The second major parameter for the heating chamber is the number of heating elements. The length of the heating chamber determines how long the preform has to stay in the heating chamber to reach the temperature for the drawing process. For the thesis, 300W was sufficient to make a preform diameter of 0.25" to reach around

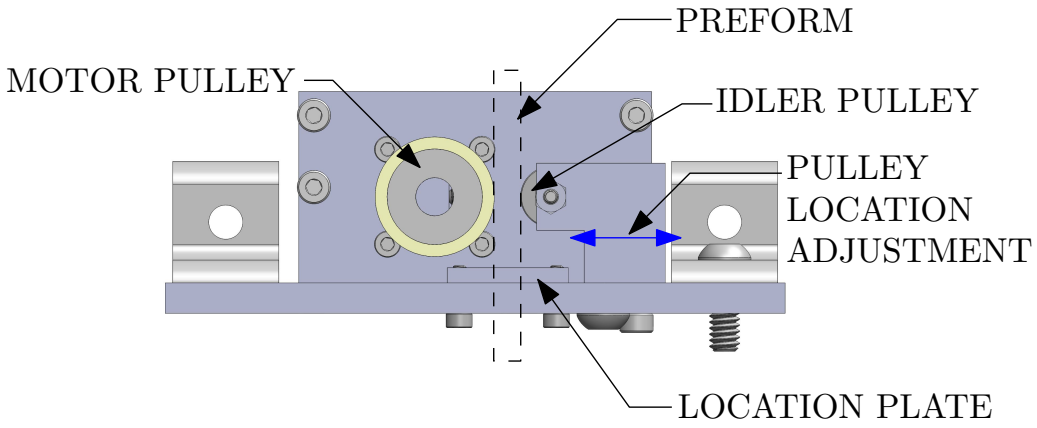

Figure 3-12: The general extruder actuation system design

$250°C$ without a problem. Besides, the heating chamber of length 1" was sufficient to heat the preform. If in the future, the preform needs to be heated to a higher temperature, additional heating elements can be inserted into the heating chamber. More holes can be drilled similar to an already existing design, or vertical holes can be placed surrounding the preform path, as shown in Fig. 3-11. If the heating elements are placed vertically, it is crucial to place the electrical leads of the heating elements to the face where the preform is fed. The electrical wiring placed on the exit of the heating chamber will interfere with the fiber output. This interference may allow some fiber production but eventually will either have the fiber attached to the heater wiring or operator failing to start the machine.

For the extruder actuator, compensation of the preform diameter has to be considered. Fig. 3-12 shows the design schematics of the extruder actuation system. As discussed in the mechanical design section, the two pulleys pinch the preform and push the preform into the heating chamber. For designing the actuator system, the preform diameter would change the system significantly. The two pulleys should leave at most the diameter of the preform as the spacing between the pulley wheels. The pulley wheels were chosen to be built from polyurethane. The polyurethane provides a generally high coefficient of friction with the most polymer material. However, it is important to note that there has to be a feature where the location of the idler pulley can be changed. The polyurethane is soft, and it requires to be squeezed on the preform to provide a strong feeding force. Typically, the design allowing the distance

between the two pulley range between $D_{pre} - 1mm$ and $D_{pre} + 1mm$ is a good design. The location plate is another feature to allow the preform diameter to be accepted. The location plate serves as a location reference, so the preform is not fed to the heating chamber with offset or tilt. For the thesis, this design provided satisfactory results. Nevertheless, for the future designs, having another locating plate on the top of the pulley assembly would constrain the preform better.

3.4.3 Diameter Control Design

For the diameter control design, the velocity of the product should be considered to choose the actuator. During the development of the advanced fiber system, two different types of motors were considered. First was the DC brushed motor with encoder, and the second was the stepper motor with a high gear ratio (for example, 1:100). The DC brushed motor provided the encoder reading and smooth output velocity. However, the DC brushed motor does not have the reasonable control of the velocity when the target velocity is extremely slow. In some fiber production, slow velocity on the diameter control is required. In that case, the use of stepper motor with high gear ratio output may be desired. The stepper motors have discretized rotational displacement, which may produce varying fiber diameter. However, with a sufficiently high gear ratio, the discretized motion is not visible. The stepper motor provides a slow production option for the fiber that cannot sustain high tension in the drawing process.

3.4.4 Summary of Parameters and Resulting Properties on Fiber System

The summary of the different parameters on the fiber system and how it influences the system is shown in Table 3.2. The heater capacity and its length can impact the entire system. With high heater capacity, the preform can be fed quicker. If the heater's length is short, the chance of turbulence inside the heating chamber is low. Besides, as the preform is fed quickly, the production speed should be fast to

Parameters	**Heater Capacity**	**Heater Length**	**Chance of Turbulence**	**Production Speed**
Feed Fast	High	Short	Low	Fast
Feed Slow	Low	Long	High	Slow
Feed Slow	Low	Short	Low	Slow
Feed Fast	High	Long	High	Fast

Table 3.2: The parameters for fiber system and its impact

produce fiber. In a case like this, the DC-bushed motor is recommended instead of the stepper motor for diameter control. If the heater capacity is low, the heater length has to increase to heat the preform to the target temperature. The longer the preform contact the walls of the heating chamber, the more likely the turbulence would occur. The production speed has to be slow to prevent turbulence. The third case is when the heater capacity is low, and the heater length is short. Then the preform should be fed at a slow rate to reach the target temperature. The turbulence is unlikely due to short contact of the preform and the heating chamber and the slow feeding speed. Nevertheless, this process is limited to a slow production rate as the feed speed is slow. The last case is when the heater is high-capacity, but the heater's length is long. Since the heater can heat the preform well, the feed rate can be fast. The production rate would be high, too, with a high feed rate. However, the process would have turbulence in the heating chamber. The long heating chamber and fast feed rate would contribute to the likeliness of the turbulence in the heating chamber. In conclusion, the first case would produce the optimal system for fiber.

Chapter 4

Desktop Fabric Manufacturing System

In this chapter, a novel fabric knitting manufacturing system is introduced. As discussed in the introduction, the knitting machine concept existed from the industrial revolution period. The first recorded patent describing the knitting machine was filed in 1889 [20]. Since the introduction of mass manufacturable knitted fabric, the concept of the knitting did not change much. The number of actuators and the types of actuators that were used to operate the machine evolved. There is a lack of innovation when we consider the fact that advanced fibers are being introduced. In this thesis, a new fabric knitting concept is introduced. The super-elastic Nitinol fiber that previously was knitted with extreme care and numerous preprocessing [61]. The new system described in this chapter removes the preprocessing steps required for the super-elastic Nitinol fiber to be knitted. This chapter will first introduce the conventional knitting machine method and how they are limited to be used for super-elastic fibers. The new process is then designed. The mechanical design to implement the process is discussed. The produced knitted fabric is different from any other previously developed fabric. As a result, the chapter concludes by introducing the new model derived from the experimental data and how it can predict the performance of the fabric.

4.1 The Process Investigation and Design

This section investigates the details on how the conventional knitting works and why it is limiting the super-elastic materials from being knitted. By investigating how the knits are formed with a conventional knitting machine, a new process can be designed. It would be easier to design the mechanical systems that would enable the process.

4.1.1 The Conventional Knitting Method

Conventional knitting provides a good rate of manufacturing and is a generally reliable process with flexible (such as cotton) fibers. The knitting methods utilize the needles with a latch, as shown in Fig. 1-6. Fig. 4-1 shows the conventional knitting process. The knitting machine holds onto an existing knit at the beginning, as shown in Fig. 4-1a. The needle would extend out, as shown in Fig. 4-1b. The latch on the needle would open as the previous knit tries to stay in position. As the needle reaches the maximum extension, the new fiber is fed onto the needle, as shown in Fig. 4-1c. The needle would start to reverse back to the original position, as shown in Fig. 4-1d. The previous knit would go under the latch and close the latch while the needle is being pulled in. The knit is complete as the needle returns to the original position, as shown in Fig. 4-1e. The needle can be empty at the beginning, and the process would be the same. The cam surface actuates the needles. The needles have pins attached to the body, which can allow the cam surface to push and pull the needles. The cam surface moves out the multiple needles in smooth sinusoidal wave motion, as shown in Fig. 4-1f. The cam would remove the complexity that would exist if the needles were to move one at the time. The cam also makes an efficient manufacturing process as multiple needles are moving together. Despite the benefits, the cam mechanism limits the knitting process from knitting super-elastic fibers.

The cam surface mechanism limits the knitting process to flexible fibers. The cam surface allows the needles to extend out, as shown in Fig. 4-1f. The peak of the needle extension will move along with the cam surface. This cam surface allows the multiple needles to grab the fiber as the knitting process proceeds. The example of fiber

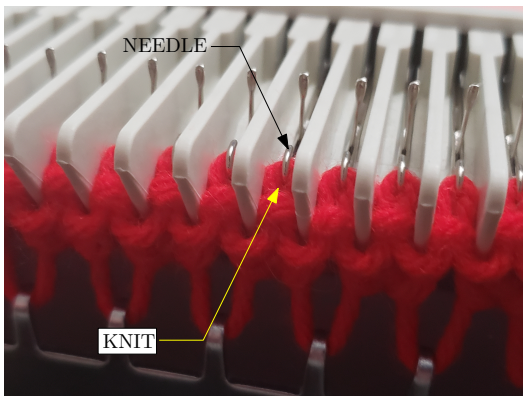

(a) The needle holding a previous knit before process starts

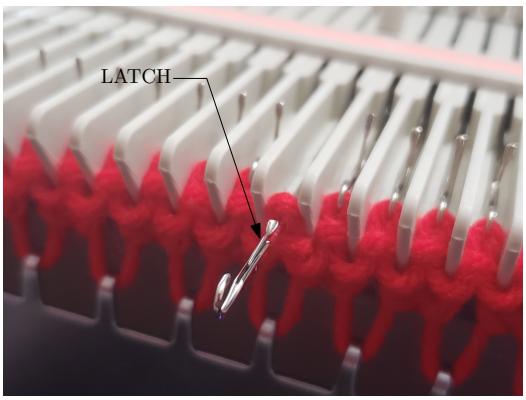

(b) The needle extending out of the previous knit

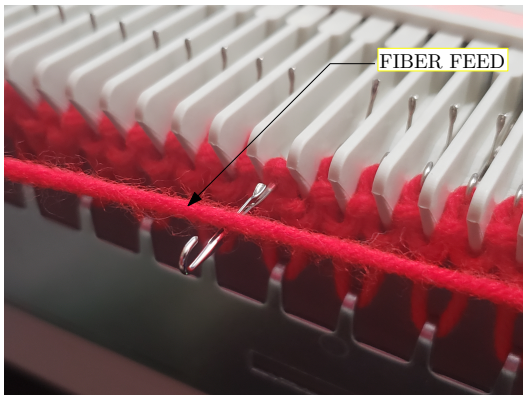

(c) The needle grabbing the fiber from feed

(d) The needle retracting while latch closing

(e) The needle completely retracted forming new knit

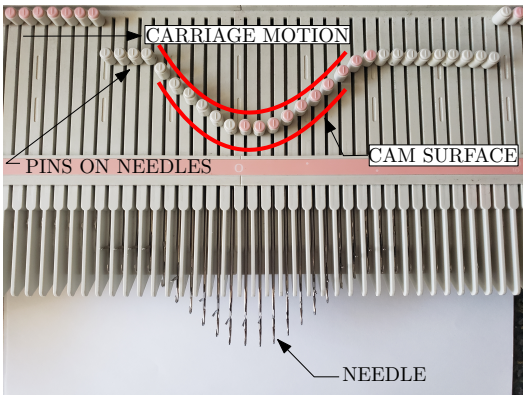

(f) The needles following cam surface

Figure 4-1: Investigating the conventional knitting process

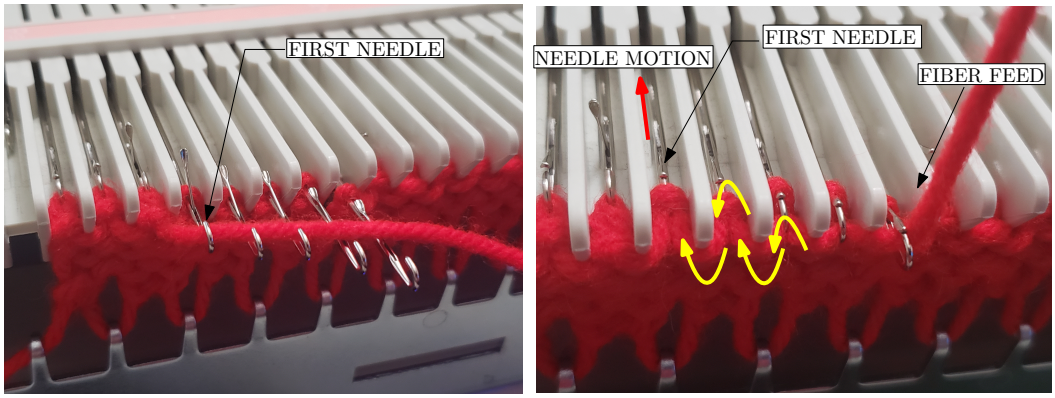

(a) The example of cam surface with needles grabbing fiber fed for new knits

(b) The problem with conventional cam surface actuation method in knitting

Figure 4-2: Investigating the conventional knitting problems

being grabbed by multiple needles is shown in Fig. 4-2a. The cam surface actuation provides a great rate of manufacturing but provides limitations when forming knits with rigid fibers. The many knits forming at once produce many points where the fiber has to be bent. As shown in Fig 4-2b, when multiple needles pull on a single fiber, the fiber will bend at multiple locations, as indicated in the figure. It was noted that the first needle to retract in Fig. 4-2b would pull the fiber that is being fed. This pulling motion would make the fiber to go through the bends shown with yellow arrows in Fig. 4-2b. It is important to note that the bending point on the fiber was not fixed. The entire fiber has to go through the bending path indicated with the yellow arrow. For soft fiber made from cotton or multiple strands of thin nylon, the cam surface would work well. For super-elastic or rigid fiber, it would require a significant force to make moving deformation along the entire length of the fiber.

In addition to the limitation on the large area deformation on the fiber, the lack of constraints prevents the conventional machine from knitting super-elastic fiber. The latches on the knitting needles are passive. The conventional knitting uses weights to allow the knit fabric to be pulled to provide tension on the fiber, so the fabric does not spring back out of the needles' latch. However, with super-elastic fiber, such tension is not sufficient with hanging weights. The fabric would spring back and escape the latches of the needle. This problem can be solved by providing additional constraints to the knit fabric as the process continues. Constant tension and controlling the

tension on the fabric during the manufacturing process would remove the limitation.

4.1.2 The New Process Design for Rigid Fiber Knitting

The conventional knitting machine method has limitations with the type of fiber it can knit. The process is limited to yarns or fiber that has characteristic similar to cotton or other polymer-based yarns that is flexible. For the fiber that is super-elastic, the existing knitting mechanism cannot knit to the fabric. In order the knit the fabric with fiber or yarn displaying extremely elastic properties, multiple new constraints have to be applied. In order to apply these new constraints, a new process, as described shown in Fig. 4-3 was invented.

Fig. 4-3 shows an overview of the new knitting process. The process was different from the conventional knitting method by using one needle at the time to form the knit. The targeted needle was extended out, as shown in Fig. 4-3a to form a new knit. After the needle was completely extended out, the latch would clear the existing knit, as shown in Fig. 4-3b. Also, as shown in Fig. 4-3b, the new fiber was grabbed by the needle. The needle then started to retract, as shown in Fig. 4-3c. The latch on the needle would be closed by the existing knit as the needle is further retracted, as shown in Fig. 4-3d. As the needle reached the original position, the new knit was formed, as shown in Fig. 4-3e. The knit forming process was similar to conventional methods. Additional process mechanisms need to be implemented to enable the knitting of the super-elastic material.

The tension bar mechanism is shown in Fig. 4-4 provides constant tension to the knitted super-elastic fabric. After the new row of knits was formed as a new process design described, without proper tensioning, the fiber would spring back and try to return to a straight fiber. Conventional knitting machines do not have a preventative measure to prevent the fiber from exiting the needle latches. After a row is finished, the tension bar would rotate while the entire row of needles moves forward. The resulting state is presented in Fig. 4-4b. The tension bar rotation and the extension of the needles had to match to ensure that knits were not stretched nor too loose to come out of the needle's latches. The process described above required extensive

(a) Target needle coming out

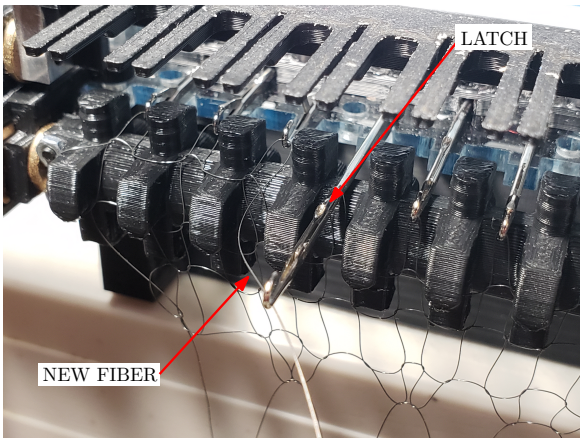

(b) Fiber being fed into the needle

(c) Needle being retracted forming a new knit

(d) The needle's latch closed

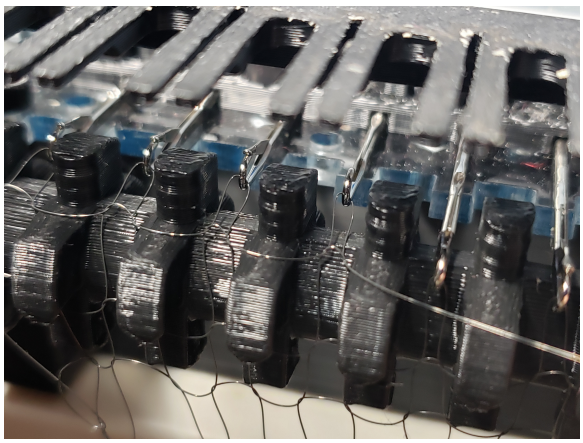

(e) New Formed Knit

Figure 4-3: The new process for knitting super-elastic rigid fiber

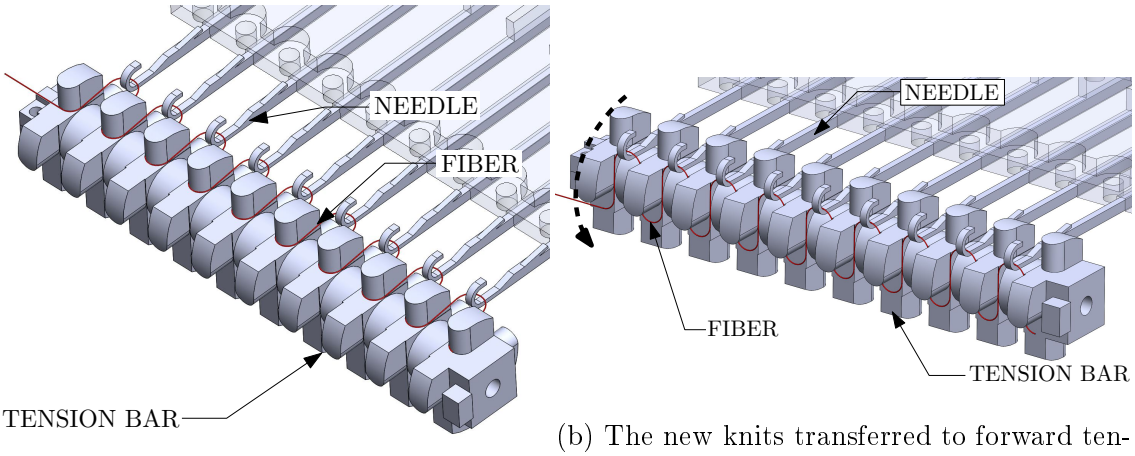

(a) The tension bar holding the newly formed knits

(b) The new knits transferred to forward tension bar

Figure 4-4: The tension bar rolling to transfer the knits to next row

mechanical design components to implement. The following section describes the mechanical systems to implement the process.

4.2 Mechanical Design

The entirely new knitting system was developed to implement the new knitting method described above. The designed system is shown in Fig. 4-5. The figure indicates the major subsystems that will be discussed in this section.

4.2.1 Stage Motion System

The stage motion system moves the stage to different target needles. Fig. 4-6, a stepper motor mounted to the linear stage, was connected to the main stage of the system. The linear stage was using a linear rail assembly with a ball screw coupled to the stepper motor's output. The main stage plate is colored as blue in the figure. The direction of travel is indicated with a dashed arrow in the figure. The main stage contains subsystems that interacted with the needles. The stage motion mechanism moved the mechanisms to correct target needles to enable single needle actuation.

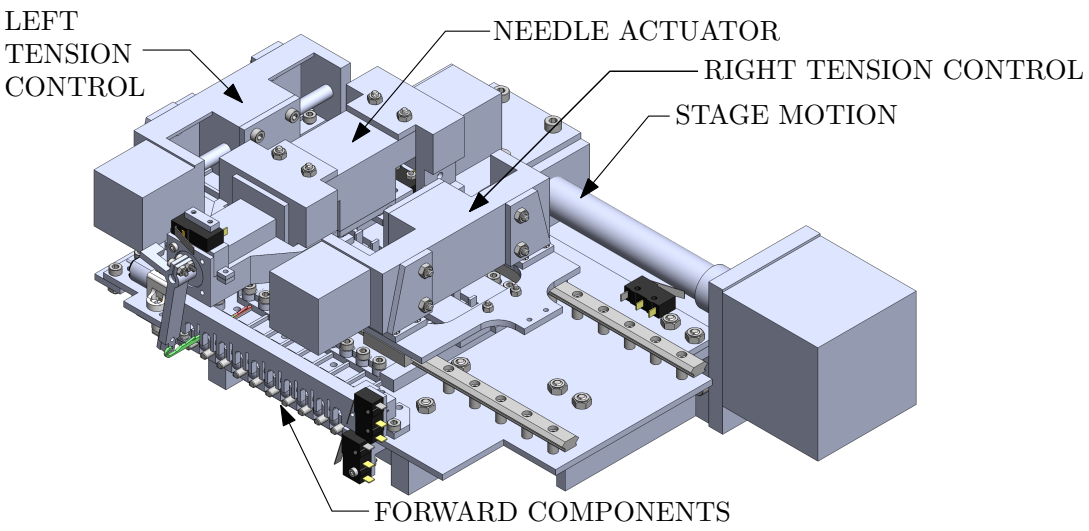

Figure 4-5: The super-elastic fabric knitting system

4.2.2 Needle Actuator System

The needle actuator system moved the needle in and out, forming a new knit. The needles were held on the base plate of the machine with a 3D printed part. The needle assembly with 3D printed needle holder is shown in Fig. 4-7a. For this machine, 9 needles were used, but for the future, extended numbers of the needles can be installed the same way. The holder is designed with transition tolerance to allow for the needles to slide easily. The needles had a handle or extruded piece attached to the top, as shown in Fig. 1-6. This handle comes out of the slots made on the holder, allowing it to become the actuator point for the actuators to interact. The Fig.4-7b shows how the actuator interacted with the needle. The linear stage with needle grab would be translated to the target needle handle by stage system. Then the needle's handle was in the position of the needle grab. The needle grab would move the needle in and out according to the linear stage's motion. For the knitting process, three positions are defined for the needles: forward, neutral, and reverse. The forward position is when the needle is extended out most to receive the new fiber. The example of the forward position is shown in Fig. 4-12. The neutral position of the needle is when the needle is holding the previous knits. The example of a neutral needle position is shown in Fig. 4-4b. After the needle formed a new knit, the needle pulled the new knit until

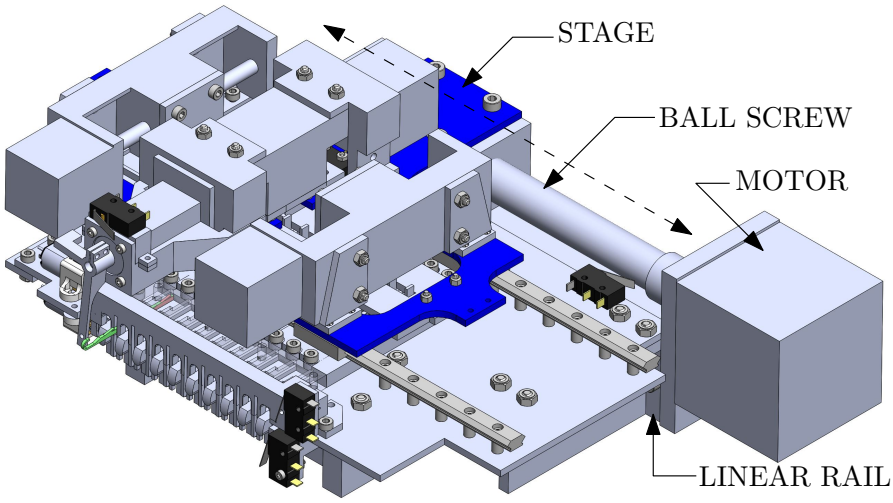

Figure 4-6: The stage motion system

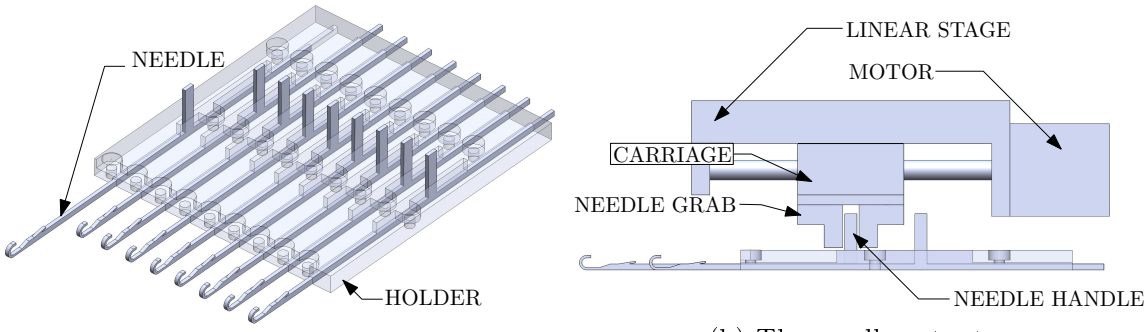

(a) The needle holder

(b) The needle actuator

Figure 4-7: The needle actuator system

the reverse position. The reverse position is shown in Fig. 4-4a. The reverse position would create tension on the new row of knitting. The tension constraint system and front components worked together to keep this tension.

4.2.3 Tension Constraint System

The tension constraint system worked with the tension bar described in section 4.1.2. The main function of the tension constraint system was to actuate all the needles together and hold them together to maintain tension in the fabric when knitting took place. The simplified schematics of the system is presented in Fig. 4-8. The red and blue parts are called tension plates. The tension plates allowed the needle handles

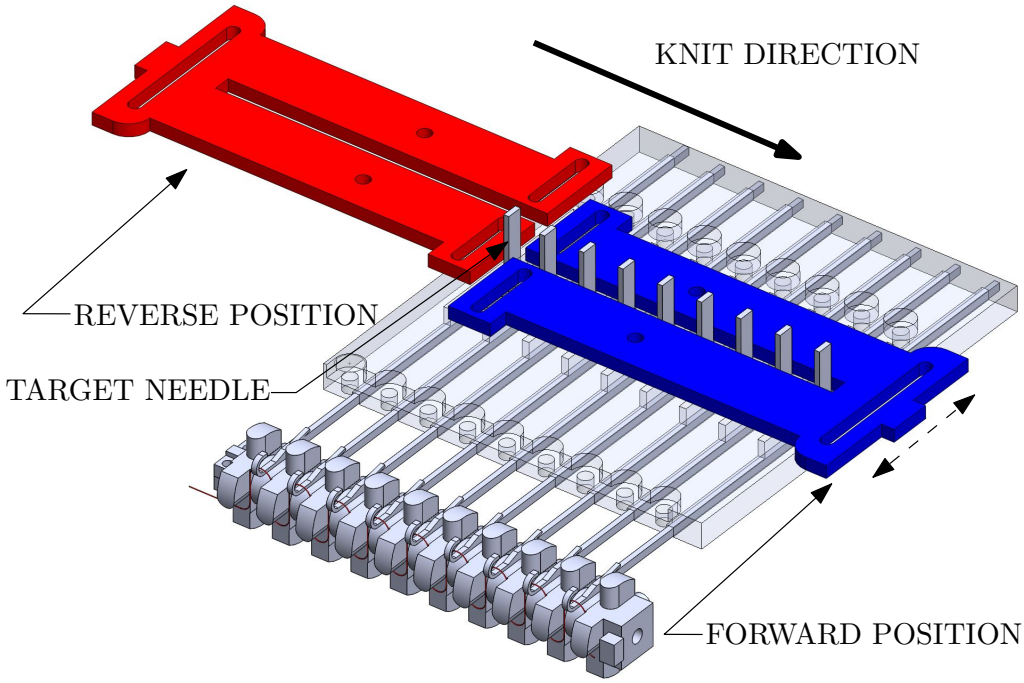

Figure 4-8: The tension constraint system schematics

to slide into the slot in the middle through stage motion. The tension plate kept the needles in a fixed position, so the tension or elastic spring back force from the fiber did not shift the needles. The plates were also used to perform the knit row transfer by moving the entire row of needles together while the tension bar is rolling.

The implementation of the tension plate is shown in Fig. 4-9a. The tension plates moved in linear motion with the stepper motor actuator shown in Fig. 4-9a. Similar to Fig. 4-8, The Fig. 4-9 shows the general knitting progressing to the right as indicated as knit direction. When the knitting was progressing in the right direction, the left tension plate was in the reverse direction while the right tension plate was in the forward direction. The targetted needle was allowed to move forward or reverse but was constrained by the needle actuator. The knitting process proceeded with the needle moving forward to grab a new fiber and returned to the reverse position of the tension plate. This motion allowed the knits to be formed with constant tension, as shown in Fig. 4-4a. The knitting process continued to the next needle. The transition between reverse position knits on the left and forward position knits on the

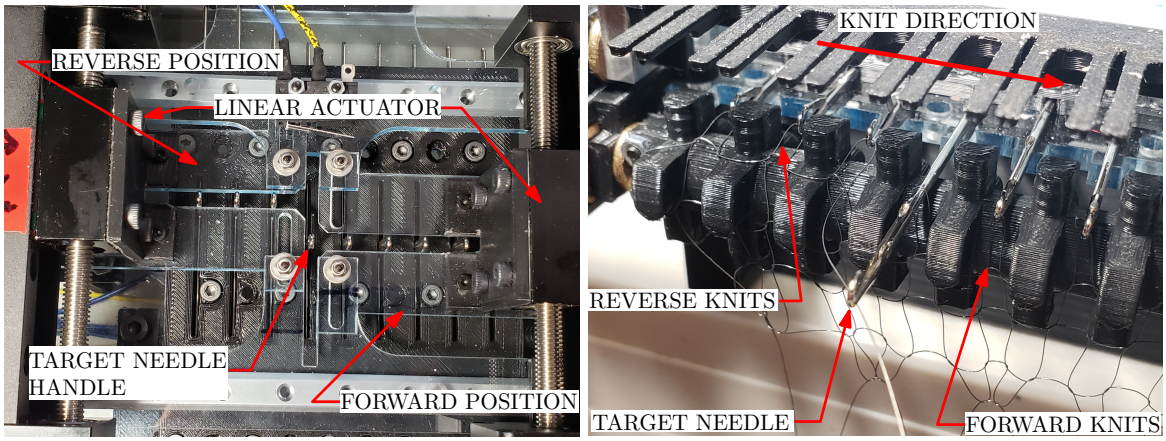

(a) The implemented tension constraint mechanism

(b) The knit forming positions with tension constraint mechanism

Figure 4-9: The needle actuator system

tension bar is shown in Fig. 4-9b. The components explained until now enables the super-elastic fiber knitting. However, additional accessories are attached to make the process more robust.

4.2.4 Front Components

The front components include multiple parts that make up the system that interacted directly with the fiber. The front components are shown in Fig. 4-10. The front components include a tension bar, guard, and nozzle. Each of the front components has distinct functions.

The guard is shown in Fig. 4-11. The main function of the guard was to keep the knits fixed when the needle was moving to the forward position. The DC motor drove the guard with an encoder attached, as shown in Fig. 4-11. The limit switch was attached to the other end of the guard to home the guard during initialization. The closed state of the guard is shown in Fig. 4-12. Fig. 4-12 is showing the cross-section of the guard while holding the fiber knit. When the needle is moving to a forward position to grab a new fiber, the guard came down to prevent the existing knit to follow the needle out. This ensured that the existing knit would clear out of the latch. After the needle grabbed the new fiber, the guard would open while the needle was

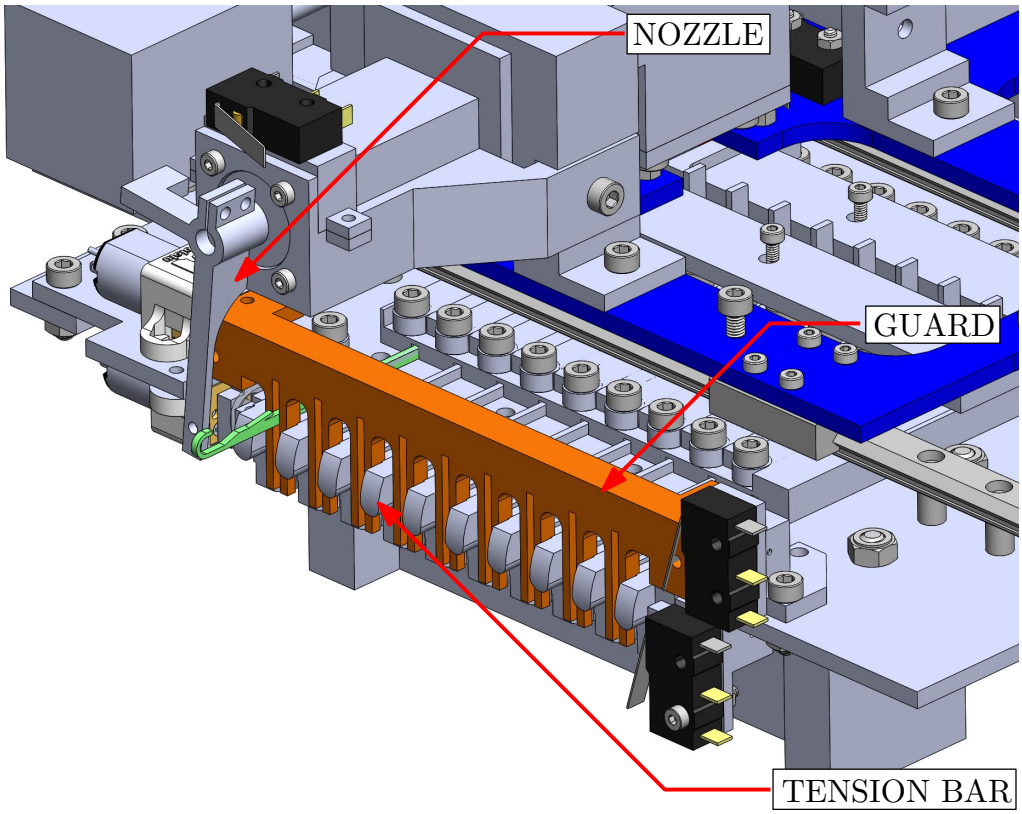

Figure 4-10: The front components on knitting system

retracting. The latch on the needle was closed by the previous knit that cleared the needle. The latch motion is shown as a dashed arrow in Fig. 4-12.

The tension bar enabled the constant tension knitting method. The tension bar, combined with the needle's position, allowed the knits to be always tensioned. The two main states of the tension bar were shown in Fig. 4-4a and 4-4b. The tension bar had the same actuator and sensor layout as the guard. The DC motor drove the tension bar, as shown in Fig. 4-11. The limit switch on the right side of the figure allowed homing of the tension bar. The motor and homing method applied to the tension bar allowed the tension bar to move exactly 90° every new row of knitting.

Finally, the nozzle fed the new fiber for knitting. The nozzle worked with two sets of positions for each direction the knitting was progressing. The nozzle system and the example of the two positions are shown in Fig. 4-13. When the stage was moving, the nozzle was set in the low position. After the stage reached the next needle, the nozzle was set to the high position. This position ensured that the fiber was placed on

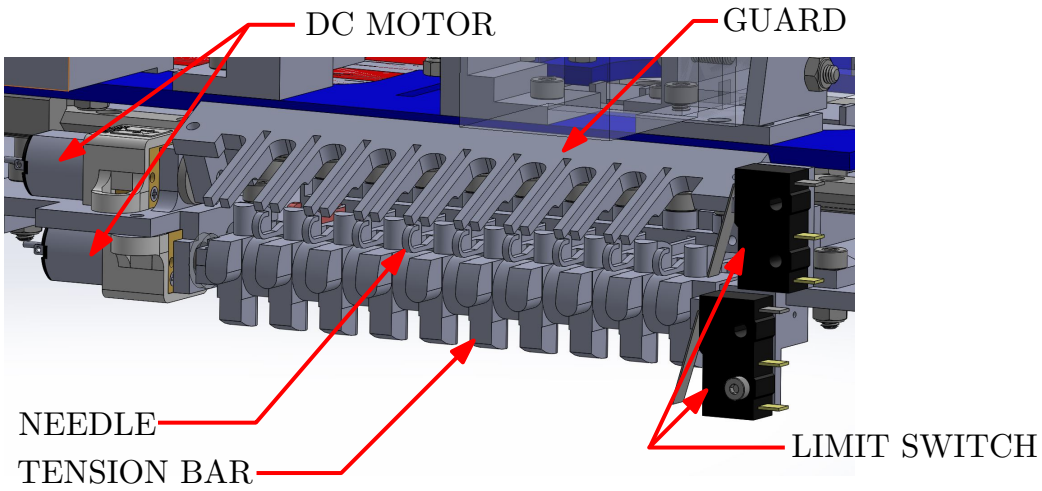

Figure 4-11: The guard and tension bar

top of the needle in the hook. The needle would then come to the forward position. The nozzle moved to the low position to place the new fiber. Finally, the needle went to reverse position, forming a new knit. It should also be noted that the nozzle direction led the knitting motion. For example, if the knitting direction was to the left, the nozzle was set to move high and low position on the left as well. The nozzle system can be an optional accessory if the operator is manually feeding the fiber. The manual operation may be helpful during the initial fabric production to test the fiber.

4.3 Modeling and Experimental Verifications of the Fabric

After implementing the mechanical designs, few sample fabrics were produced for experiments. The experiments focused on acquiring the stress and strain curve of the fabric. After the data were acquired, a model was developed to predict the performance of the fabric. This model was then verified with one additional fabric that was produced.

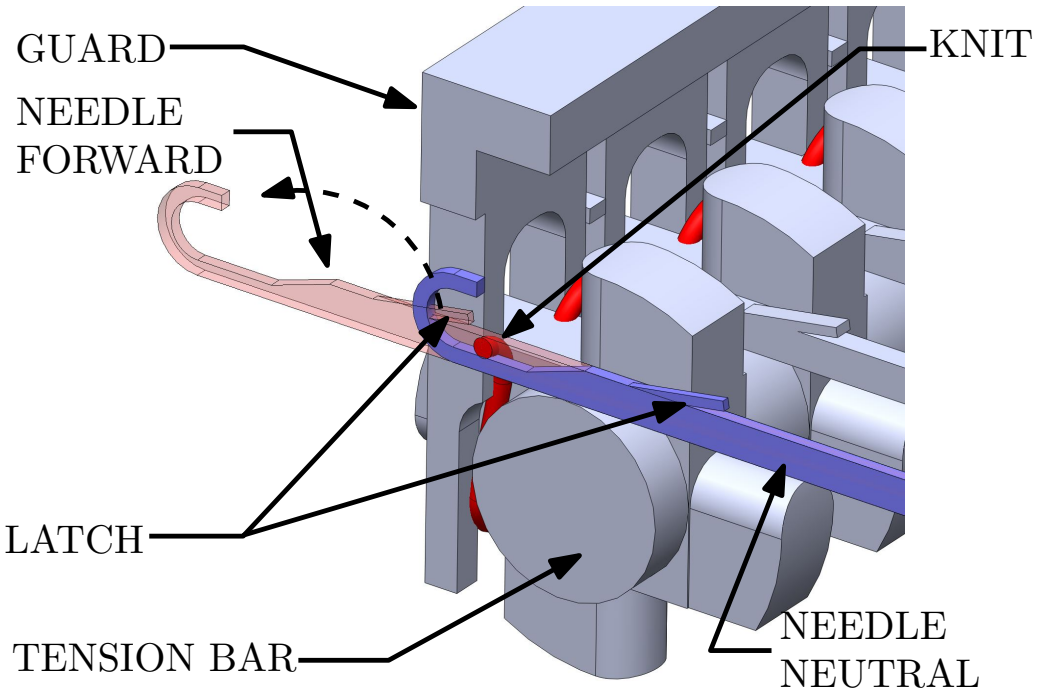

Figure 4-12: The guard and tension bar

4.3.1 Fabrication of Nitinol Fabric

The overall schematic of the Nitinol fabric made for the experiments is shown in Fig. 4-14. The fabric had 9 knits in a row and 9 rows in total. This fabric design utilized the entire row of the designed system. In addition to the 9 rows, for the beginning of the knit process, the odd number knitting row was placed. The odd number of knitting is shown in Fig. 4-15. The odd number knitting skipped a needle for each knitted needle. This knit method allowed the fully knitted row to hold the shape as the knit progress. The fixtures were made, as shown in Fig. 4-16. This fixture helps to maintain the knit fabric shape and ease the machine to release the fabric successfully. The fixtures had 3D printed frame that was straight to keep the fabric from curling near the edges. The fixtures also used key rings and key hooks to make an easy connection to the edge row of the fabric. The same fixture was used to perform stress and strain experiments. As a result, 3 different fabrics were fabricated using 3 different diameters of Nitinol Fiber. The diameters of the fibers that were used: 0.003", 0.006" and 0.008".

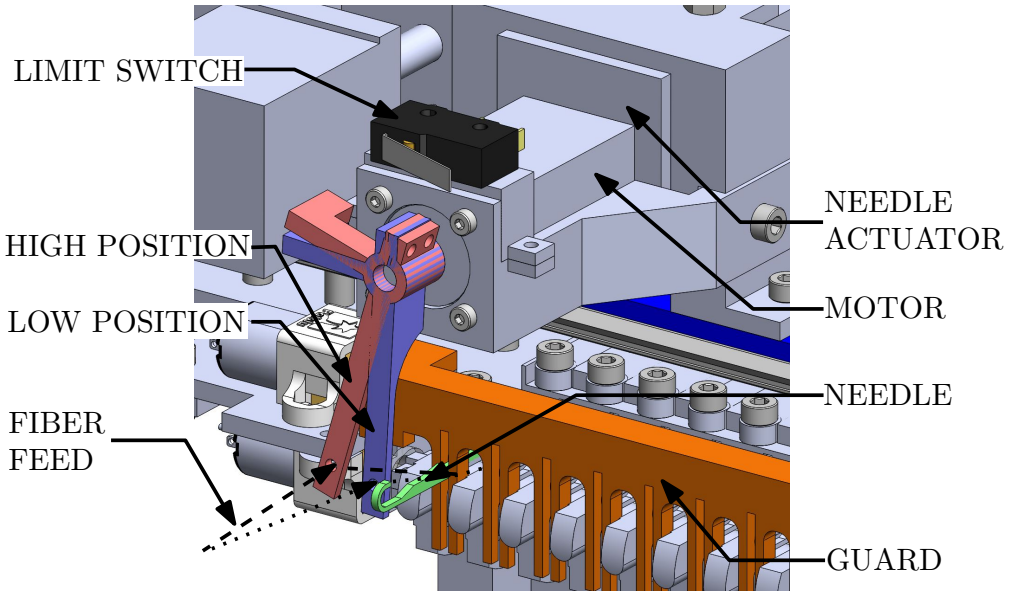

Figure 4-13: The nozzle system with different position

4.3.2 Experimental Setup to Measure Stress and Strain

A special setup was required to acquire the stress and length curve of the knitted Nitinol fabric. The original plan for this thesis was to utilize the Instron machine to automatically measure the stresses and corresponding strain values of the knitted fabric. Due to the recent COVID-19 situation, campus access was limited. As a result, the author had to come up with a more traditional way to perform stress and strain experiments. The experimental setup is shown in Fig. 4-16. The 3D printed fixture was used to hold the fabric. The fabric was placed on the grid surface to measure the distance the fabric stretched. The digital weight scale was placed to pull one side of the fixture. The other side fixture was held by hand. A plastic chair with a hole in the middle was placed on top of the entire experimental setup. This hole allowed the camera to be positioned to record video of the distance that fabric stretched and the reading on the digital weight scale. The experiments proceeded slowly by hand, pulling until either the fabric fails or the operator cannot physically produce more force to pull the fabric. The experiments were designed to perform the pulling test twice. Unfortunately, the 0.003" fabric broke upon the first trial. The recorded video was then processed in MATLAB. The recorded video was analyzed frame by frame,

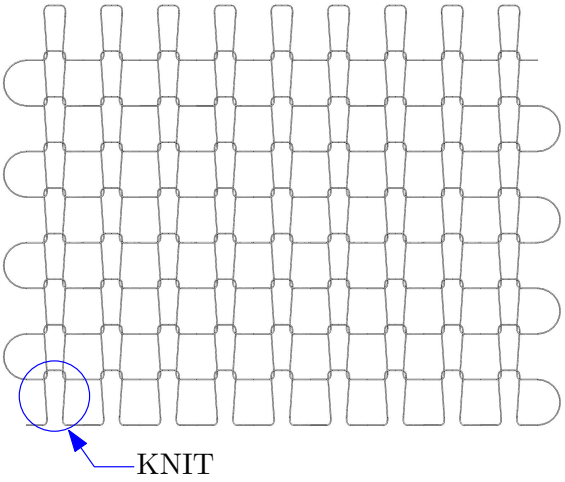

Figure 4-14: The schematic of the fabric produced for experiments

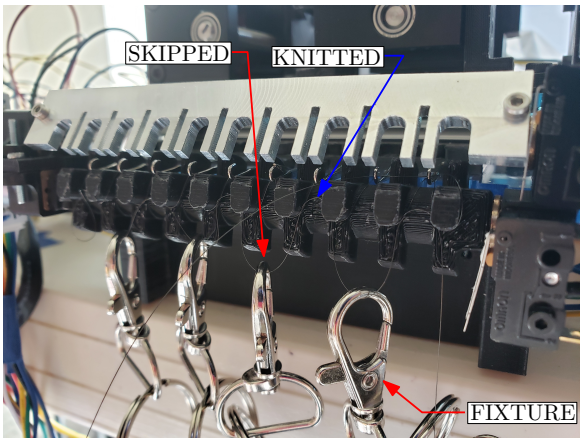

Figure 4-15: The odd number knit for first row of knitting process

and the image was extracted for every time the digital scale changed the value. The image processing toolbox in MATLAB was used to find the distance between the two fixtures in each frame. The measured results are shown in section 4.3.3.

4.3.3 Results and Analysis of Fabric Experiments

The measured length of the fabric and the corresponding load that was applied is shown in Fig. 4-17. The individual results of the experimental results are included in Appendix B. The results showed that thinner diameter fabrics tend to stretch to a longer length. It is also important to note that for 0.003" and 0.006" fabric, the repeated experiments do not show much difference. A small deviation may be coming

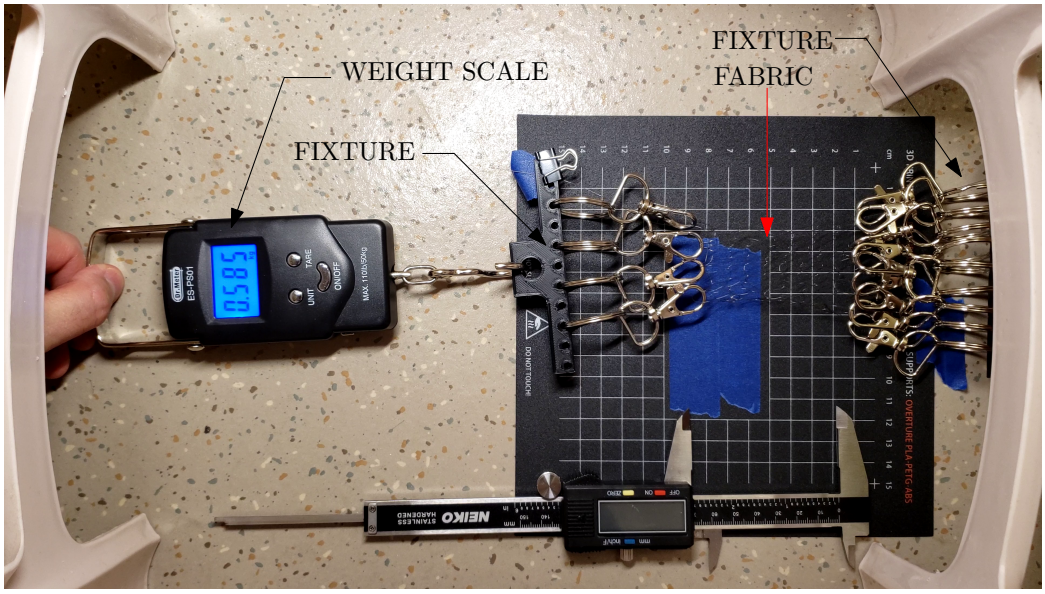

Figure 4-16: The experimental setup to measure the stress and length curve of the fabric

from the offset in initial length measurement or measurement error. The measured load data were converted to stress values. The stress is related to the cross-section area of the fabric. Since the knitted fabric does not have a constant cross-sectional area, it was estimated to be a cross-sectional area of the fiber multiplied by 18. The 18 came from 9 knits in a row, and each knits having 2 vertical strands of fiber. The resulting stress and length plot is shown in Fig. 4-18. The stress of 0.003" fabric was too high compared to the other fiber data—the graph in Fig. 4-18 was cropped to $50MPa$ to make the trends more visible.

The important trend that was observed from the length and stress data was that all the different diameter fabric showed the same but shifted curve. The data were shifted in length (x-axis) to make all the data to start at length approximately 0. The resulting plot is shown in Fig. 4-19. The optimal shifting distance was determined using the MATLAB's curve fit function. Firstly, the reference was set with the original unloaded length of the 0.003" fabric. All the fabric length was offset with the initial length of the 0.003" fabric, which was $47.69mm$. The other diameter fabric was shifted in length until the best r^2 value was achieved with the exponential model with 2 terms. The shift resolution was set to be $1mm$ to ease the computational

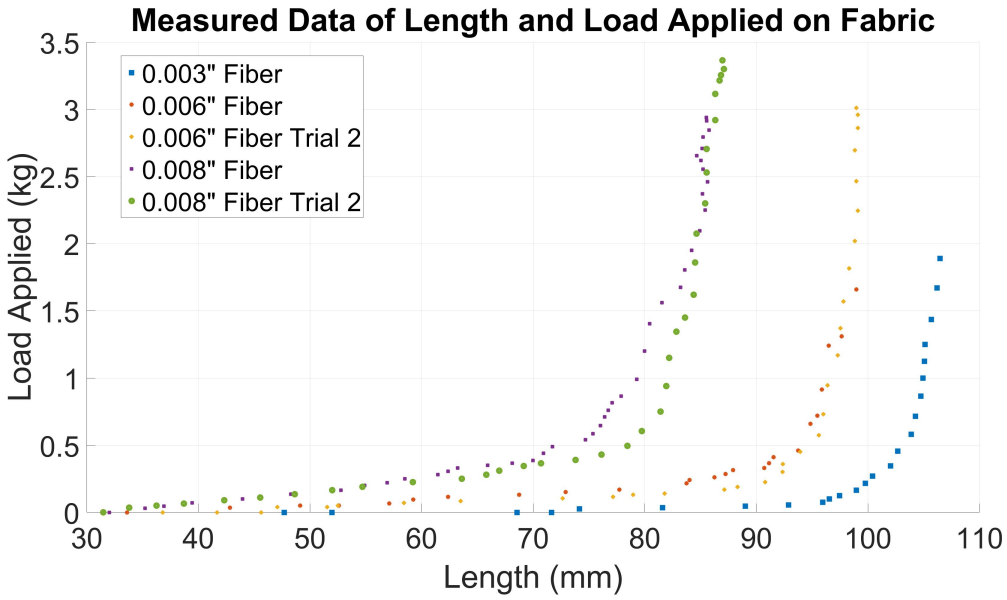

Figure 4-17: The experimental result of different fabric showing length and load applied

time. The 5 experiments yield a curve equation:

$$\sigma = 0.004355 \cdot e^{0.4145 \cdot l} + 6.412 \cdot 10^5 \cdot e^{0.05819 \cdot l} \tag{4.1}$$

Where the σ represents the stress applied to the fabric, and l represents the length of the fabric. The r^2 value for this model was 0.965. The equation 4.1 could be used to predict the performance of the fabric with different diameters.

Analysis of how the knits were formed revealed the relationship between the fabric fabrication parameter and the performance parameter. The fabric can be modeled as series and parallel springs, as shown in Fig. 4-21. There are 9 rows of spring and 9 columns of the spring. If we assume that each of the springs was the same, we can estimate that each of the spring would get $\frac{1}{9} \cdot F_{applied}$. The series spring assumption also suggests that all the springs in the column would move the same displacement under tension. In order to estimate how much displacement each knit can move, the knit forming geometry was investigated. The tension bar and needle's reverse position geometry details are shown in Fig. 4-22. The initial loop height was around $10mm$. The tension bar allowed the spacing of each knit to be $9.35mm$. The length

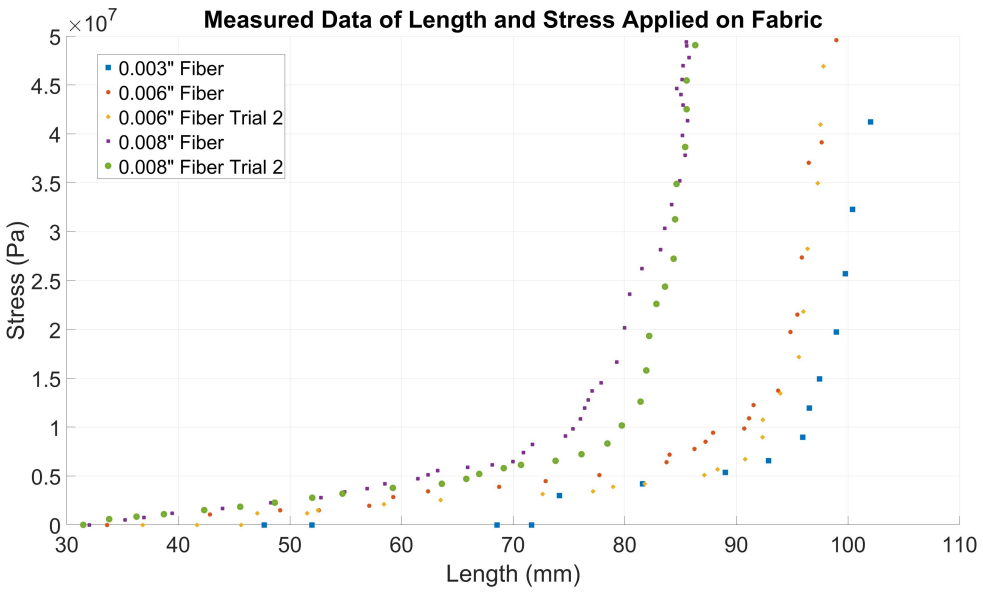

Figure 4-18: The fabric experimental results showing length and the stress applied

of fiber that occupies between the knits was approximately $9.35mm$. As a result, the initial tensile motion of the fabric, each knit, would convert half of the $9.35mm$ to its height. The 9 rows of knits would allow the fabric to actuate around $42.075mm$ in total. The SolidWorks simulation was used, as shown in Fig. 4-23 to validate the fabric actuation limit. The initial set up of the simulation is shown in Fig. 4-23a. The fiber was simulated to be half the length of $20mm + 9.35mm$ because the symmetry boundary condition was used. The simulation diameter was set to be 0.006". The roller boundary condition was applied on the other end of the fiber. The example of the simulation results is shown in Fig. 4-23b. The maximum displacement occurred at the location the force was applied. The summarized maximum displacement values for different load conditions are shown in Table 4.1. The results showed that each loop converges to a maximum displacement value of around $13.25mm$. The displacement at $0.1N$ was measured to be $8.699mm$. The difference in displacement multiplied by 9 equals $40.959mm$. The value is similar to the geometrical estimate of the fabric displacement. As a result, we can estimate that the fabric would perform as weak spring until it reaches displacement value around $40mm$, and afterward, the fabric would behave as stronger spring with tensile elongation being dominant.

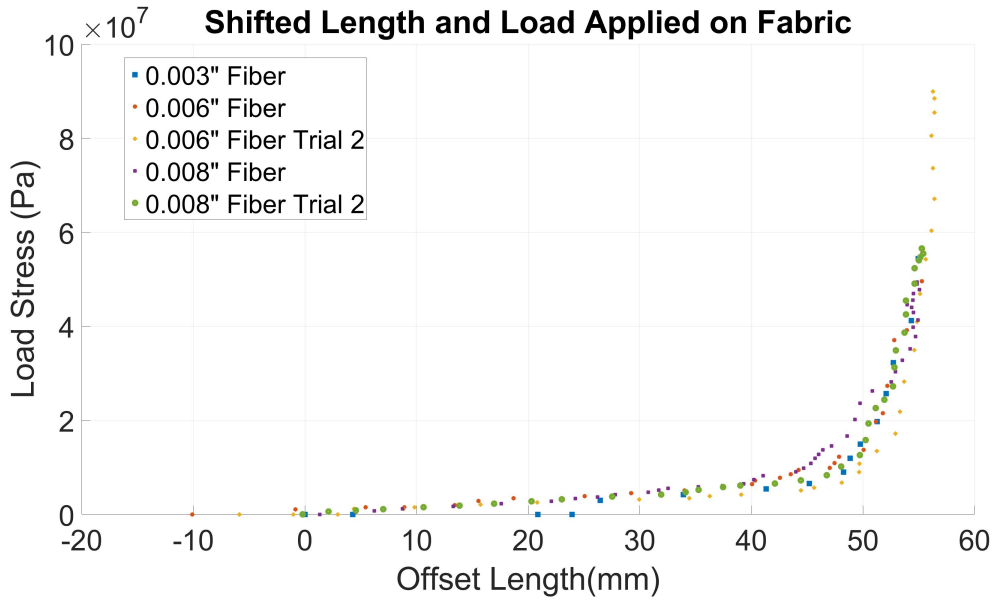

Figure 4-19: The fabric experimental results showing offset length and the stress applied

The two different phases in fabric performance were present in Fig. 4-20. Fig. 4-20 is zoomed in to remove data points with extremely high stress. As the experiments were done manually, some experimental data had a larger range of load applied compared to others. In the offset length figure, it was clearly observed that up until length of $40mm$, the stress increases linearly with a small slope, while after about $50mm$, the stress increases linearly with a new higher slope. This slope change corresponds with the above paragraph's derivation of geometrical limit around $40mm$. In order to acquire a smooth transitioning model, the exponential curve with two terms was selected for the base model. It can be estimated that as long as the tension bar geometry and needle's negative positions do not change, the produced fabric would follow the model. A new fabric would be fabricated to validate the model.

4.3.4 Verification of Performance Model of the Super-elastic Nitinol Fabric

The model developed in the previous section was verified with a new validation fabric. New fabric was made from the fiber with a diameter of 0.008". The number of knits

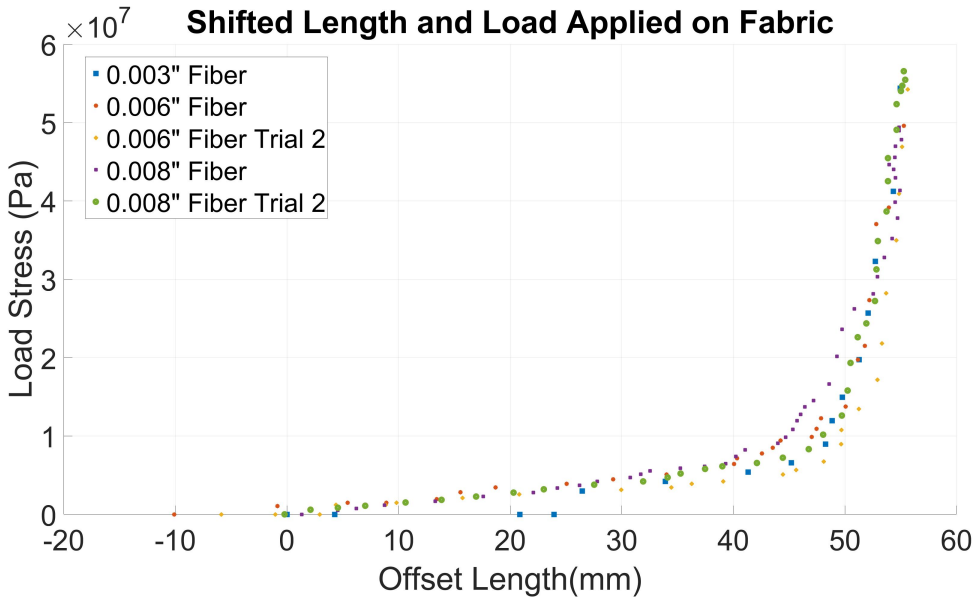

Figure 4-20: The fabric experimental results showing offset length and the limited values of stress applied

in a row and the number of rows were kept the same as other experimental fabric. The initial length of the fabric was measured to be approximately $39.5mm$. The model's length can be added to this initial value to get the relationship between the length and the load applied value. The model predicted the relationship, and the experimental measurement is shown in Fig. 4-24. It was observed that the model did not fit well with the measured values. However, it was also observed that by offsetting the length, the results would match better to the model. The error can be calculated by calculating the corresponding load value for the measured length using the model equation. The error can be calculated using the equation:

$$\%Error = |\frac{L_m - L_p}{L_p}| \cdot 100 \tag{4.2}$$

The L_m represents the load measured during the experiments. The L_p represents the load predicted using the model. Using the Equation 4.2, the average error with the model was 90.21%. Since the percent error was not satisfactory, the length offset was applied again to the measured value. The offset to set the initial length of the fabric to be $35mm$ is shown in Fig. 4-25. The results match very well with the model.

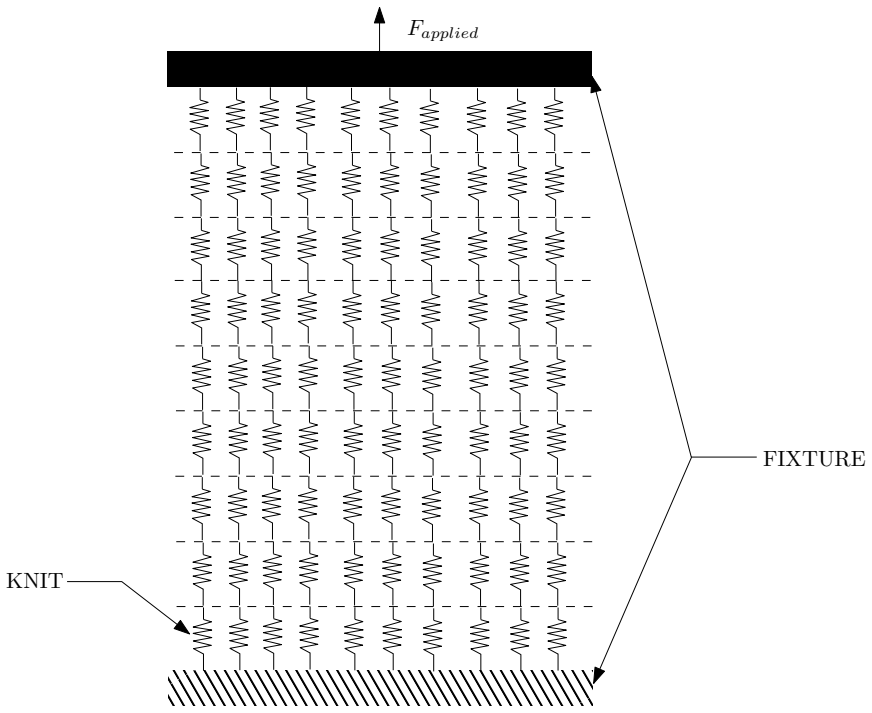

Figure 4-21: The spring model of the fabric

The percent error calculated with Equation 4.2 was 20.09%. The majority of the error comes near the length 0. Since there two points from the measured data that had 0 as the length, the percent error value would be 100%. However, by offsetting the length, the improvement was significant. This model mismatch was likely to be caused by the inaccurate measurement in the experiment. The digital scale may not be high resolution enough to sense the initial tension, which set the initial length of the fabric at slightly longer than it was. Further testing with precision equipment is recommended.

4.4 General Design Approach for Super-Elastic Knitting System

From the fabrication of the prototype knitting system in this thesis, multiple aspects of the machine can be improved for future versions. This section presents the generalized approach in designing the super-elastic fiber knitting system. Based on the fabric's

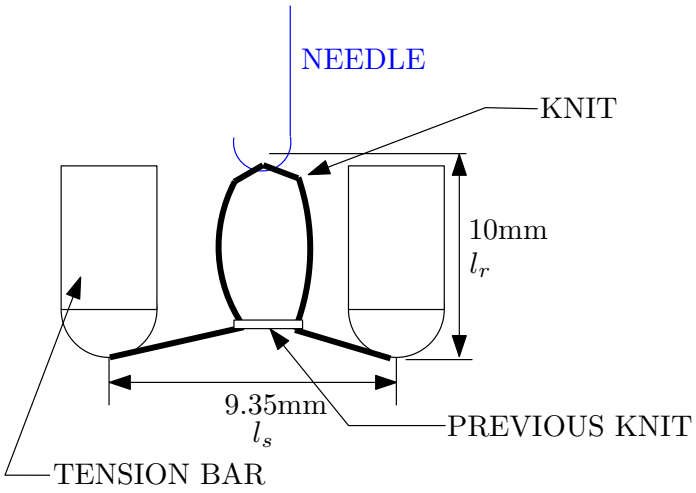

Figure 4-22: The knit fabrication geometry

Force Applied (N)	Maximum Displacement (mm)
1	13.23
0.9	13.15
0.8	13.03
0.7	12.90
0.6	12.75
0.5	12.54
0.4	12.23
0.3	11.75
0.2	10.90
0.1	8.70
0	0

Table 4.1: The summary of load and maximum displacement of fiber bending simulation from SolidWorks Simulations

performance needs, the design parameters can be derived to meet the performance requirements. Each subsection discusses the component that influences the fabric's performance or property. The subsections discuss how the design parameter influences the fabric property and estimate the relationship.

4.4.1 Needle System Design

The needle system design influences the knit shape. As discussed in the previous sections, the needle has 3 main positions. The knitting needle's geometry defines the forward and neutral position. As shown in Fig. 4-26, the length l_e defines the

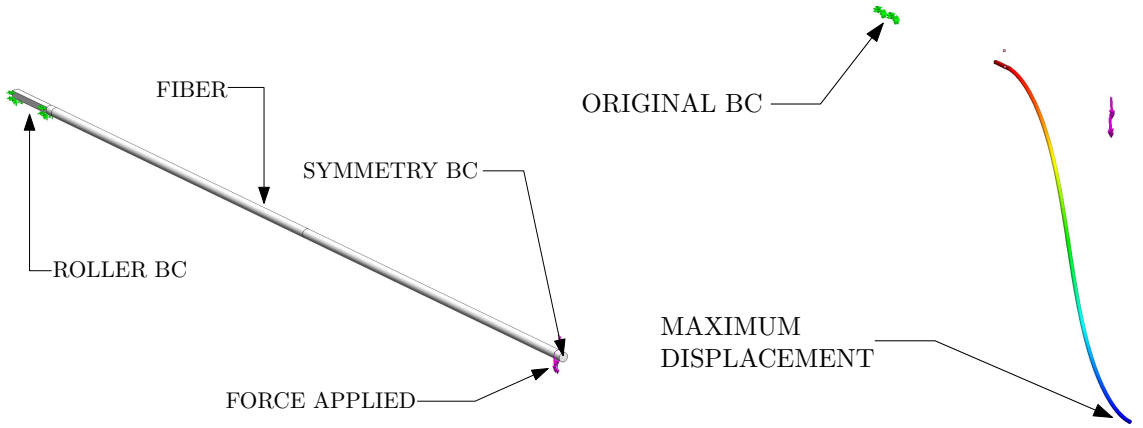

(a) The SolidWorks simulation setup

(b) An example of SolidWorks simulation result on a fiber knit

Figure 4-23: The needle actuator system

extension length. The extension length is equal to the distance from the tip of the hook to the latch opening. The extension length is also the distance between the needle's positive position to the neutral position. As a result, when designing the needle holder, as shown in Fig. 4-7a, the possible travel forward has to allow at least l_e of motion. The designer can determine the negative travel limit. The negative pull distance decides the loop's height for each knit. As defined in Fig. 4-22, the l_r is reverse length. The l_r is equivalent to the distance of travel between the neutral position to the reverse position of the needle. The change in l_r would mainly change the resting length of the fabric. However, the definition of l_r combined with the spacing of the needles would influence the fabric as well.

The spacing of the needle also influences the fabric's property significantly. From Fig. 4-22, the l_s was defined. The l_s is the spacing between the needles. The tension bar is placed in the middle of the two needles, so the tension bar teeth are placed with the same spacing as the needle spacing. As discussed in Section 4.3.3, the l_s determined the extension limit of the fabric before the slope of the length and load curve transition to a different mode. The approximate mode transition of the fabric is estimated as:

$$l_{transition} = \frac{l_s}{2} \cdot R \tag{4.3}$$

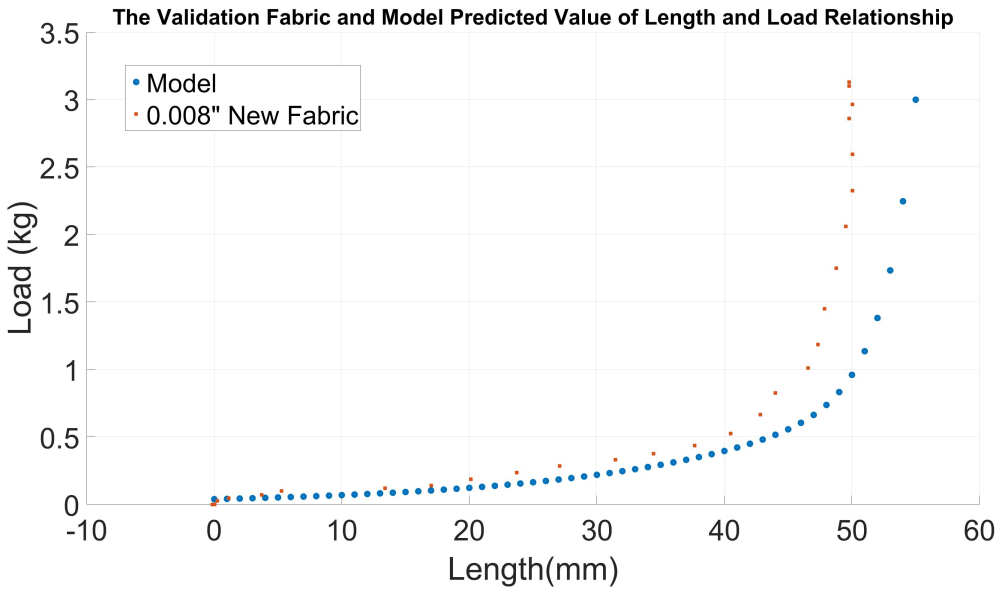

Figure 4-24: The comparison between model predicted performance and measured performance

Where $l_{transition}$ is the length that fabric can extend until the mode changes. R is defined as the number of rows of the knits in the fabric. The needle spacing is likely to be fixed once a machine is designed. The needle holder fixes the needle spacing throughout the entire process. It can be summarized that simple modifications of the fabric performance parameter would depend on the change in the l_r value.

4.4.2 Tension Bar Design

The tension bar design is dependent on the needle's travel limits. The first design aspect of the tension bar is the cross-sectional geometry. The cross-section of the tension bar and the needle's neutral and reverse location is shown in Fig. 4-27. The key design constraint is that the tension bar geometry has to match the l_r when the needle is at neutral and reverse. If the two lengths do not match at the corresponding needle position, the knit will either escape the needle due to low tension or tension bar will not rotate because the tension is too high. The location of the tension bar is also dependent on the needle limits and the defined l_r.

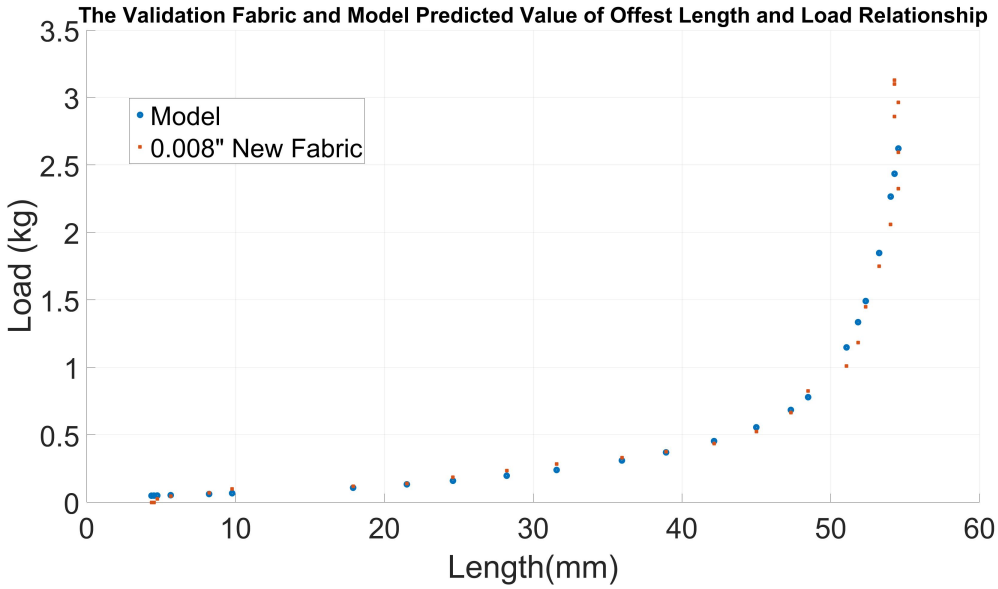

Figure 4-25: The comparison between model predicted performance and offset of measured performance

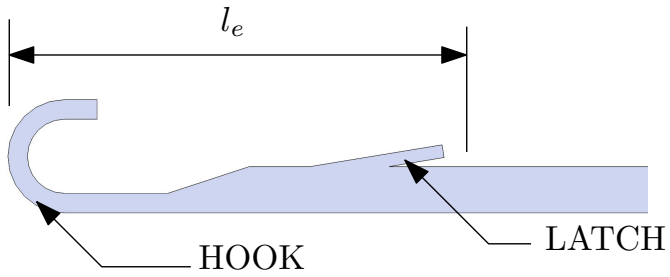

Figure 4-26: The geometry of needle

4.4.3 Summary of Parameters and Resulting Properties of the Fabric System

The fabric system has two main parameters that can be controlled, and they influence the resulting fabric property. The parameters and their influences on the fabric are shown in Table 4.2. The needle spacing (l_s) does not influence the resting length of the fabric. The needle spacing does change the maximum displacement that fabric can extend to before the mode changes. As discussed in the 4.4.1, the further apart the needles are the maximum displacement of the fabric before the mode change increases. The needle pulls length (l_r) is the second parameter that impacts the fabric

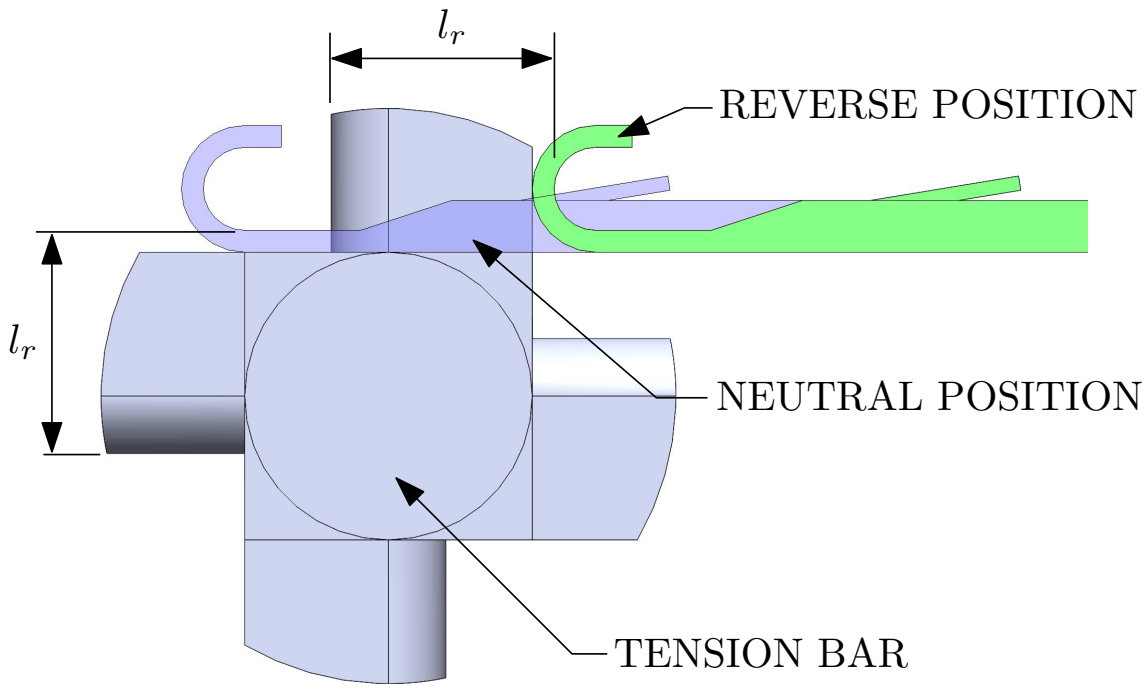

Figure 4-27: The tension bar cross-section showing design example

Parameters	**Fabric Rest Length**	**Fabric Maximum Displacement**
Close Needle Spacing (l_s)	Not effected	Short
Far Needle Spacing (l_s)	Not effected	Long
Short Pull Length (l_r)	Short	Not Effected/Short
Long Pull Length (l_r)	Long	Not Effected/Long

Table 4.2: The parameters for fabric system and its impact

performance. The longer l_r provides taller knit. This taller knit makes the initial fabric length to be longer. This parameter may influence the maximum displacement of the fabric. If the fabric made from long l_r is pulled in the width direction, the same effect as having large l_s occurs. The loop height (l_r) decreases and (l_s) is increases. This conversion may not be easily done when the fiber's diameter is large, or the fiber has high stiffness. Generally, the pull length would not influence the maximum fabric displacement.

Chapter 5

Conclusion

5.1 Contributions

This thesis contributed to three major sectors of the scientific community. The first is the education community. As mentioned in the introduction, the educational fiber system was deployed to multiple classes and successfully provided rich data to allow the students to learn data analytics and process control. The second is the biological and neuroscience community. The advanced fiber manufacturing system successfully produced different types of fibers that are commonly produced for the biological and neuroscience community. The system would allow the researchers to develop new prototypes with lower costs quickly. The third is the advanced fabric research community. The new fabric fabrication method introduced in this thesis can be used to produce new types of fabric for new applications. The Nitinol knitted fabric with a unique 2 phase performance can be used for many applications that require considerable strain and large spring back. Further research in all three communities would allow this research to carry more impact.

5.2 Conclusion

This thesis introduced three new mechatronics system related to fiber and fabric manufacturing in desktop scale. The educational fiber manufacturing system showed

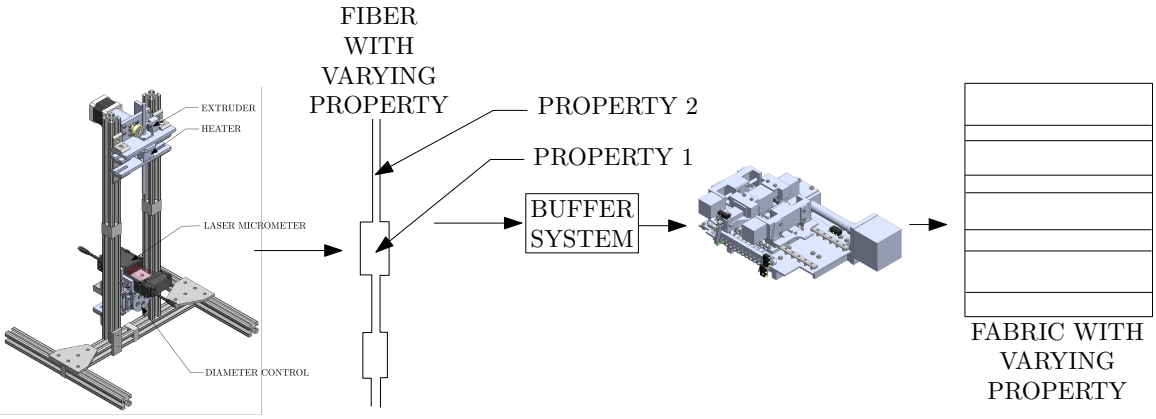

Figure 5-1: The coupled system example

that the system could achieve a fiber diameter standard deviation of $0.0274mm$. The system was also able to demonstrate an educational aspect of identifying the problems on the system with data and implementing controllers to fix the data. The advanced fiber manufacturing system showed that the fiber manufacturing system's desktop version could be used to produce fiber for biological and neuroscience applications. The fiber system demonstrated that it could produce a solid fiber with different polymer material, fiber with a hole, neural probing fiber, and cell scaffold fiber. The fabric system demonstrated the knitting of super-elastic Nitinol fiber without pre-processing. The new knitting method was invented, and the mechanical system was designed to implement the method. In addition, the new fabric's stress and length relationship were derived from data. The relationship was also validated with a validation sample.

5.3 Future Work

There are multiple future works to continue from this thesis. Mainly there would be improvements and combining the work of fiber and fabric systems. There would be projects to continue the educational effort using the fiber machine and to convert the fabric machine as a combined educational system as well. This section will discuss future projects that would be of interest to continue from this thesis.

For the fiber system, a wider range of educational and control design content can

be developed. Especially with the coupled system of fiber and fabric manufacturing system, an exciting inventory and scheduling topics would rise. Shirley Lu (MIT SM 2020) wrote a Master's thesis on the development of the necessary inventory buffer system that is installed between the fiber system and the fabric manufacturing system. Her system would solve the mismatch problem between the continuous rate of production on the fiber machine and the discretized fabric production rate. The example of implementation of the buffer system is shown in Fig. 5-1. As shown in the figure, the fiber system can vary the fiber property along with the fiber. The property variation can be the diameter or different material. The effort would be taken by both the buffer system and the knitting system to place the fiber with specific property to the correct location of the fabric. The resulting fiber would have added complexity, which would yield more properties than the input property just from the fiber. For example, with the varying fiber diameter in fiber level, the fiber's property is only influenced by bending and axial loading. However, placing the fiber in fabric, more properties are influenced. The fabric can be designed to be different in pulling and bending in both width and length direction. This research topic would require reliable modeling and control for each individual component and an extensive predictive modeling approach to estimate each input's result. This research would also require extensive simulation as troubleshooting 3 coupled systems without simulation would be a time-consuming job. This project is expected to yield novel control methods, novel fabric material, and the development of efficient simulations.

The KAIST team led by Professor Seongjun Park will work on animal testing of the fibers for the advanced fiber manufacturing system. Professor Park has received a sample of fibers from the advanced fiber manufacturing system. The samples include the neural probe and the cell scaffolding. Professor Park's team would post-process the fiber for use in animals and growing cells. He plans to use the neural probe for implementing and testing laser transmission in the mouse's brain. He also plans to test the quality of the cell scaffolding fiber from the advanced fiber machine by growing cells inside the fiber. Eventually, Professor Park's team will build the fiber system at KAIST. By utilizing the thesis's generalized design approach methods, his

team can design and tune the system as they need.

The super-elastic fabric knitting system will require additional effort in characterizing and modeling the fabric and applying the system on various applications. For modeling effort, more collaboration with theoretical and applied structural mechanics research team is planned. Attempt to derive an analytical model on the super-elastic fiber would be taken in the future, and more data acquisition to validate the model would be necessary. In the thesis, the fabric stress and strain properties were measured in the direction of the knit. For future research, characterizing the fabric performance in the perpendicular direction to the knit direction would be investigated as well. In order for the modeling research to continue, the fixture would have to be improved. The fixture should be designed to add minimum variation to the fabric itself yet hold the fabric in the correct way. The new fixture would be used to hold the fabric perpendicular to the knit direction as well. With the proper modeling of the fabric performance, further applications of the fabric can be investigated.

As a result, exploring the possible application space with the combination of the super-elastic fabric with different materials would be investigated. The conventional knitting machine and developed knitting system can change the fiber in the middle of the fabric operation to create a fabric with different fiber. For conventional knitting, this technique is commonly used to change the color of the fabric. For the new fabric system, there may be a challenge in joining the different materials of fiber when the transition of material occurs. This method is different, then the system in Fig. 5-1 because some fabric material cannot be drawn. The knits can be created by changing the feeding fiber. However, the method to join the two ends when the transition of fiber happens has to be investigated. The free ends of fiber in the fabric poses a possible knit loss and complete failure of the knit before loading happens. After the joining process, the property of the fabric with super-elastic material can be investigated. The fabric with super-elastic fiber and commonly used fiber such as nylon can generate a functional cover to the robotic joints. These functional cover can be used to initially act as bearing until the fabric mode changes to act as a brake or limiter. The fabric would have exciting property as it can allow for multiple degrees of

motion instead of a bearing with only 1 degree of freedom. The fabric's applications in robotic actuation space are promising.

Appendix A

Fiber Experimental Results

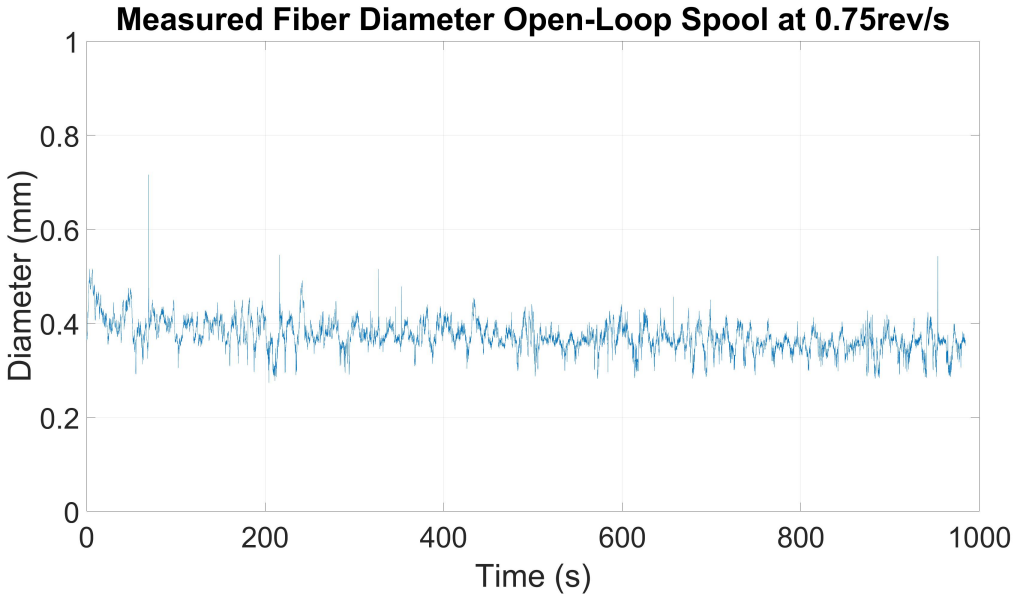

Figure A-1: Open-Loop fiber diameter measurement for spool velocity of 0.75rev/s

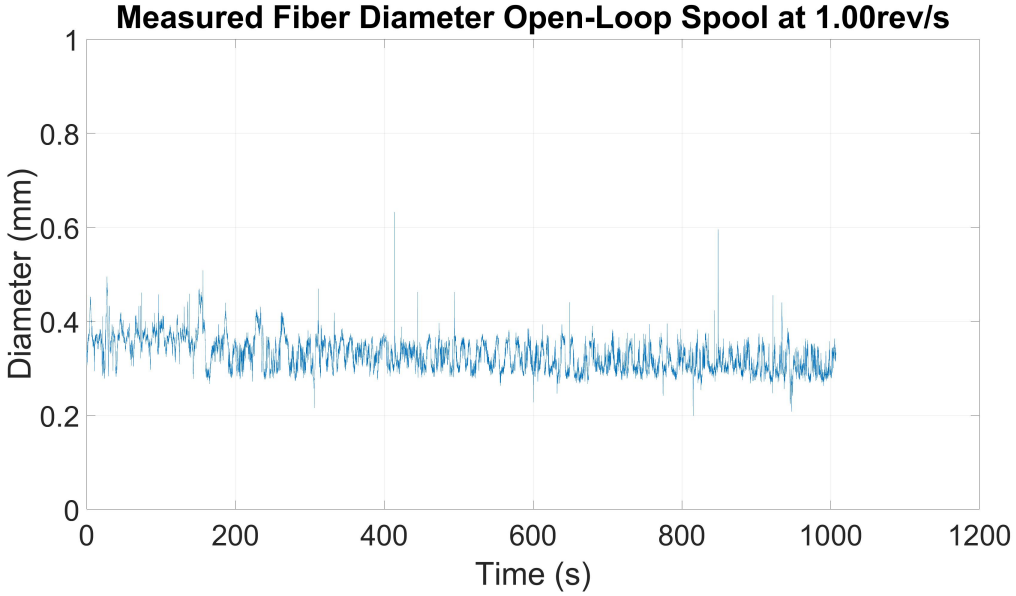

Figure A-2: Open-Loop fiber diameter measurement for spool velocity of 1.00rev/s

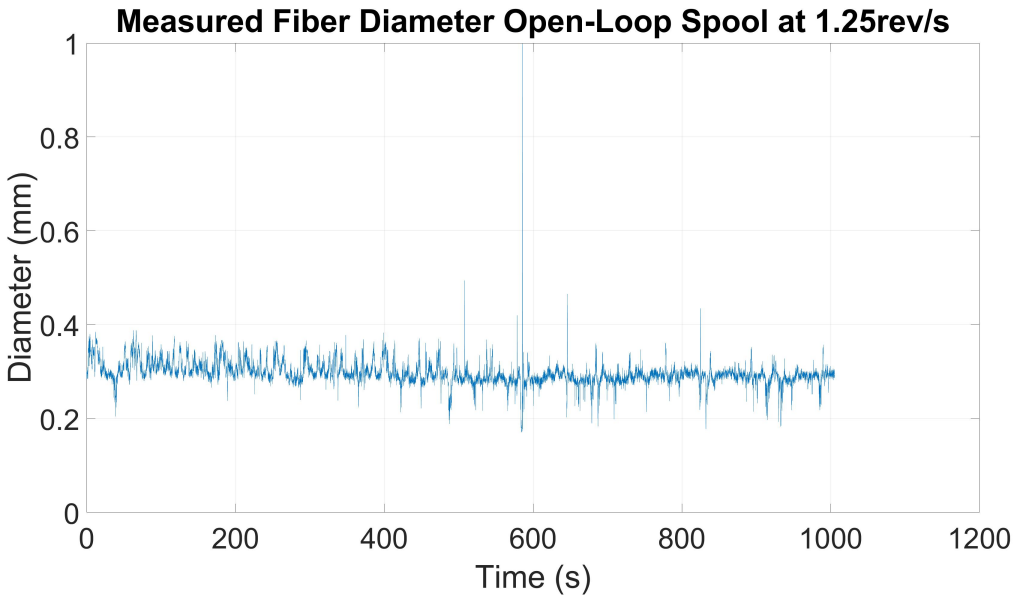

Figure A-3: Open-Loop fiber diameter measurement for spool velocity of 1.25rev/s

Appendix B

Fabric Experimental Results

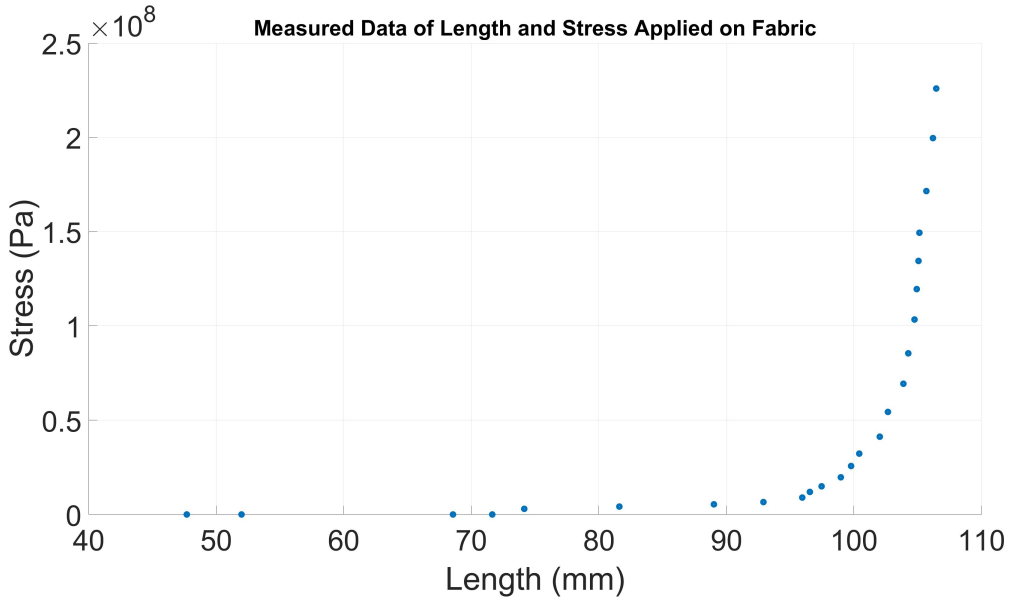

Figure B-1: Measured length and load result of the fabric made from 0.003" diameter Nitinol fiber

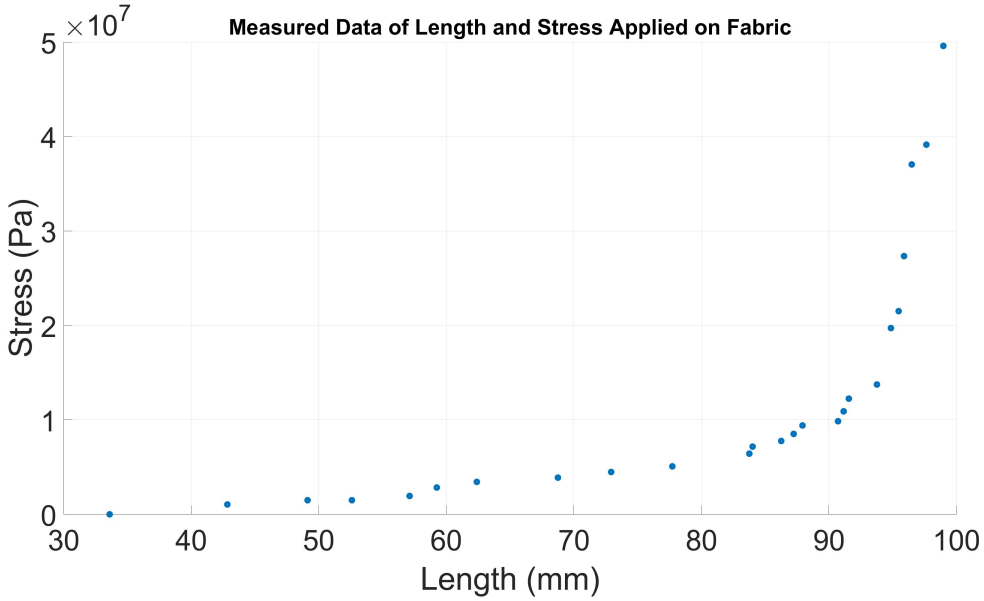

Figure B-2: Measured length and load result of the fabric made from 0.006" diameter Nitinol fiber

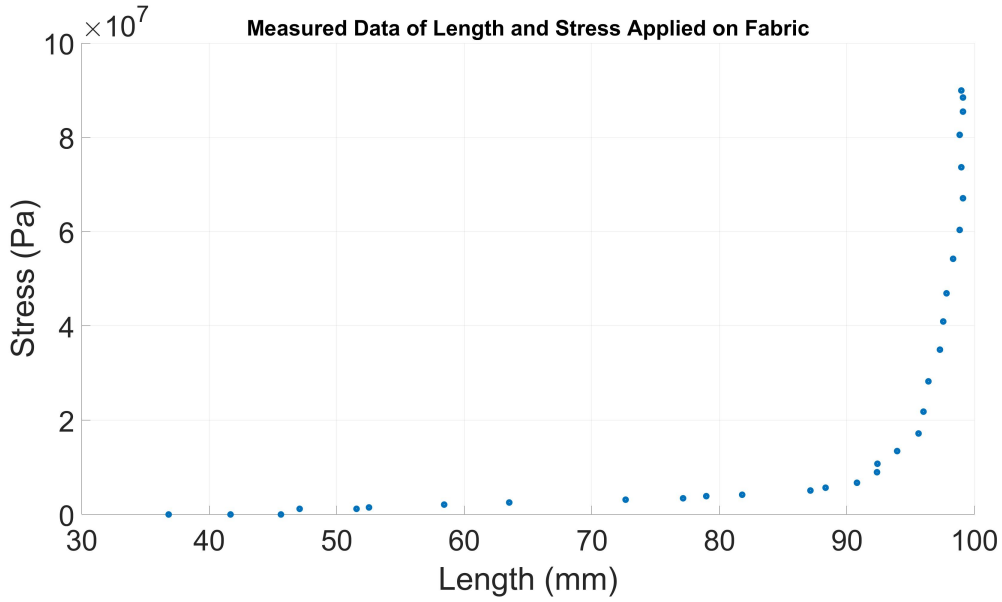

Figure B-3: Second trial of measured length and load result of the fabric made from 0.006" diameter Nitinol fiber

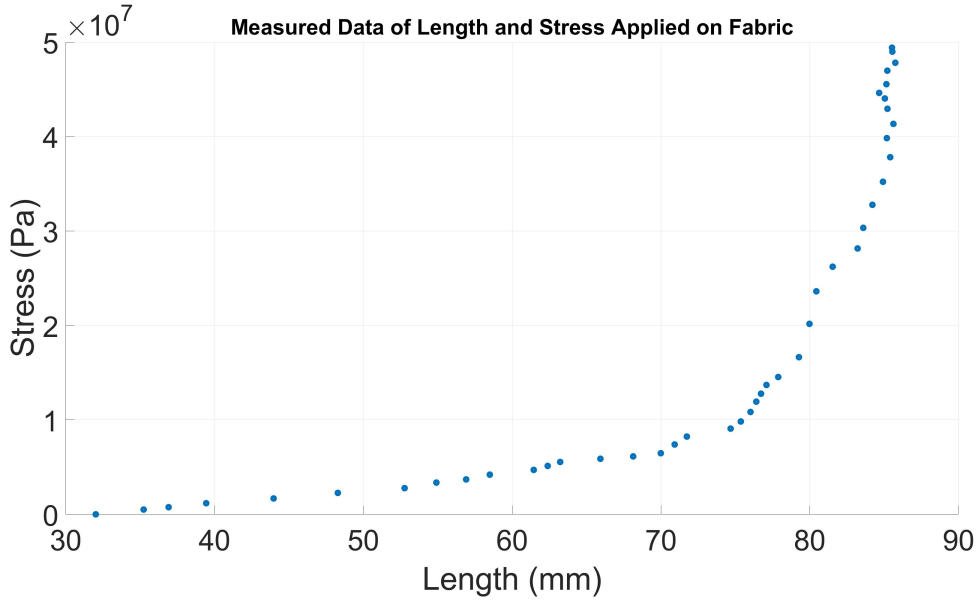

Figure B-4: Measured length and load result of the fabric made from 0.008" diameter Nitinol fiber

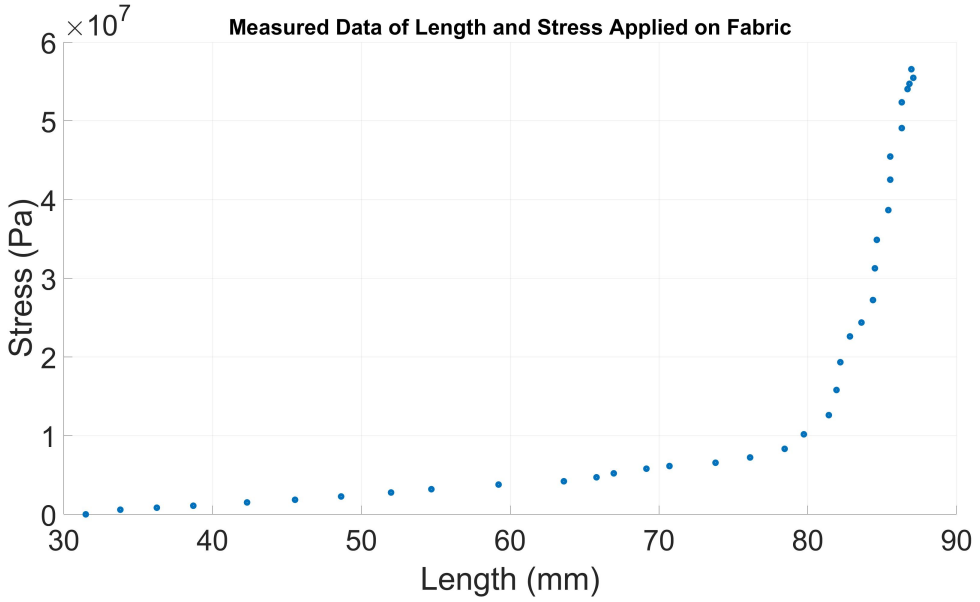

Figure B-5: Second trial of measured length and load result of the fabric made from 0.008" diameter Nitinol fiber

Bibliography

[1] Thorlabs, "Specialty optical fiber manufacturing." [Online]. Available: https://www.thorlabs.com/images/TabImages/Fiber_Capabilities_Tower_A1-780.jpg

[2] U. C. Paek and R. B. Runk, "Physical behavior of the neck-down region during furnace drawing of silica fibers," *Journal of Applied Physics*, vol. 49, no. 8, pp. 4417–4422, 1978. [Online]. Available: https://doi.org/10.1063/1.325495

[3] A. L. Yarin, "Stationary configuration of fibers formed under nonisothermal conditions," *Journal of Applied Mechanics and Technical Physics*, vol. 23, no. 6, pp. 865–870, Nov 1982. [Online]. Available: https://doi.org/10.1007/BF00911045

[4] S. R. Choudhury, Y. Jaluria, and S. H.-K. Lee, "A computational method for generating the free-surface neck-down profile for glass flow in optical fiber drawing," *Numerical Heat Transfer Part A: Applications*, vol. 35, no. 1, pp. 1–24, 1999.

[5] S. Lee and Y. Jaluria, "Simulation of the transport processes in the neck-down region of a furnace drawn optical fiber," *International Journal of Heat and Mass Transfer*, vol. 40, no. 4, pp. 843 – 856, 1997. [Online]. Available: http://www.sciencedirect.com/science/article/pii/0017931096001652

[6] S. R. Choudhury and Y. Jaluria, "Practical aspects in the drawing of an optical fiber," *Journal of Materials Research*, vol. 13, no. 2, p. 483–493, 1998.

[7] A. Mawardi and R. Pitchumani, "Optical fiber drawing process model using an analytical neck-down profile," *IEEE Photonics Journal*, 2010.

[8] Z. Yin and Y. Jaluria, "Neck down and thermally induced defects in high-speed optical fiber drawing," *ASME Journal of Heat Transfer*, 2000.

[9] ——, "Thermal transport and flow in high-speed optical fiber drawing," *ASME Journal of Heat Transfer*, vol. 120, 1998.

[10] A. Mawardi and R. Pitchumani, "Numerical simulations of an optical fiber drawing process under uncertainty," *J. Lightwave Technol.*, vol. 26, no. 5, pp. 580–587, Mar 2008. [Online]. Available: http://jlt.osa.org/abstract.cfm?URI=jlt-26-5-580

[11] S. H. Law, G. W. Barton, and T. N. Phan, "The causes and nature of diameter variations along optical fiber," pp. 5650 – 5650 – 12, 2005. [Online]. Available: https://doi.org/10.1117/12.581789

[12] A. Mulpur and C. Thompson, "Modal diameter control of linear isothermal optical fibers," in *Proceedings of IEEE International Conference on Control and Applications*, Sep. 1993, pp. 433–438 vol.1.

[13] ——, "Nonlinear control of optical fiber diameter variations," *IEEE Transactions on Control Systems Technology*, vol. 4, no. 2, pp. 152–162, March 1996.

[14] S. Tchikanda and K.-M. Lee, "State space modeling for optical fiber drawing process," in *Proceedings of the 2002 American Control Conference (IEEE Cat. No.CH37301)*, vol. 6, May 2002, pp. 4954–4959 vol.6.

[15] S. Tchikanda, K.-M. Lee, and Z. Zhou, "A state space model for modern feedback control of optical fiber drawing process," in *Proceedings 2003 IEEE/ASME International Conference on Advanced Intelligent Mechatronics (AIM 2003)*, vol. 2, July 2003, pp. 856–861 vol.2.

[16] Z. Wei, K.-M. Lee, S. W. Tchikanda, Z. Zhou, and S.-P. Hong, "Free surface flow in high speed fiber drawing with large-diameter glass preforms," *ASME Journal of Heat Transfer*, vol. 126, 2004.

[17] Z. Wei, K.-M. Lee, and Z. Zhou, "A reduced order model for robust control of optical fiber drawing," vol. 73, 01 2004.

[18] NC State College of Textiles, "Filament yarns and texturing," *Textile Fundamentals NC State Wilson College of Textiles*, 2008.

[19] ——, "Weaving fundamentals and design," *Textile Fundamentals NC State Wilson College of Textiles*, 2008.

[20] R. W. Scott, "Art of narrowing knitted webs," US US Patent 410,858, 1889.

[21] Y. Lu, K. Morris, and S. Frechette, "Current standards landscape for smart manufacturing systems," 2016.

[22] J. Davis, T. Edgar, J. Porter, J. Bernaden, and M. Sarli, "Smart manufacturing, manufacturing intelligence and demand-dynamic performance," *Comput. Chem. Eng.*, vol. 47, pp. 145–156, 2012.

[23] F. Tao, Q. Qi, A. Liu, and A. Kusiak, "Data-driven smart manufacturing," *J. Manuf. Syst.*, vol. 48, pp. 157–169, 2018.

[24] K.-D. Thoben, S. Wiesner, and T. Wuest, "Industrie 4.0' and smart manufacturing-a review of research issues and application examples human robot collaboration in cyber physical production systems view project empirische untersuchung aktueller und zukünftiger nutzungsgrade mobiler computersystem," *Artic. Int. J. Autom. Technology*, vol. 11, no. 1, 2017.

[25] H. S. Kang, J. Y. Lee, S. Choi, H. Kim, J. H. Park, J. Y. Son, B. H. Kim, and S. D. Noh, "Smart manufacturing: Past research, present findings, and future directions," *International Journal of Precision Engineering and Manufacturing - Green Technology*, vol. 3, no. 1, pp. 111–128, 2016.

[26] S. Kim, D. D. Kim, and B. Anthony, "Dynamic control of a fiber manufacturingprocess using deep reinforcement learning (under review)," *IEEE/ASME Transactions on Mechatronics*, 2020.

[27] MIT Professional Education, "Smart manufacturing program boosts productivity in factories," *MIT News*, 2018.

[28] ——, "Smart manufacturing: Moving from static to dynamic manufacturing operations." [Online]. Available: https://professional.mit.edu/course-catalog/smart-manufacturing-moving-static-dynamic-manufacturing-operations

[29] B. Anthony and R. D. Braatz, "2.874/10.354/10.554 process data analytics." MIT, 2019.

[30] D. Silver, A. Huang, C. J. Maddison, A. Guez, L. Sifre, G. van den Driessche, J. Schrittwieser, I. Antonoglou, V. Panneershelvam, M. Lanctot, S. Dieleman, D. Grewe, J. Nham, N. Kalchbrenner, I. Sutskever, T. Lillicrap, M. Leach, K. Kavukcuoglu, T. Graepel, and D. Hassabis, "Mastering the game of go with deep neural networks and tree search," *Nature*, vol. 529, p. 484, Jan. 2016. [Online]. Available: https://doi.org/10.1038/nature16961

[31] V. Mnih, K. Kavukcuoglu, D. Silver, A. Graves, I. Antonoglou, D. Wierstra, and M. A. Riedmiller, "Playing atari with deep reinforcement learning," *CoRR*, vol. abs/1312.5602, 2013. [Online]. Available: http://arxiv.org/abs/1312.5602

[32] T. P. Lillicrap, J. J. Hunt, A. e. Pritzel, N. Heess, T. Erez, Y. Tassa, D. Silver, and D. Wierstra, "Continuous control with deep reinforcement learning," *arXiv e-prints*, p. arXiv:1509.02971, Sep 2015.

[33] S. P. K. Spielberg, R. B. Gopaluni, and P. D. Loewen, "Deep reinforcement learning approaches for process control," in *2017 6th International Symposium on Advanced Control of Industrial Processes (AdCONIP)*, May 2017, pp. 201–206.

[34] R. Cui, C. Yang, Y. Li, and S. Sharma, "Adaptive neural network control of auvs with control input nonlinearities using reinforcement learning," *IEEE Transactions on Systems, Man, and Cybernetics: Systems*, vol. 47, no. 6, pp. 1019–1029, June 2017.

[35] S. Gu, E. Holly, T. Lillicrap, and S. Levine, "Deep reinforcement learning for robotic manipulation with asynchronous off-policy updates," in *2017 IEEE International Conference on Robotics and Automation (ICRA)*, May 2017, pp. 3389–3396.

[36] T. Inoue, G. D. Magistris, A. Munawar, T. Yokoya, and R. Tachibana, "Deep reinforcement learning for high precision assembly tasks," *CoRR*, vol. abs/1708.04033, 2017. [Online]. Available: http://arxiv.org/abs/1708.04033

[37] S. C. Xue, R. I. Tanner, G. W. Barton, R. Lwin, M. C. J. Large, and L. Poladian, "Fabrication of microstructured optical fibers-part ii: Numerical modeling of steady-state draw process," *J. Lightwave Technol.*, vol. 23, no. 7, p. 2255, Jul 2005. [Online]. Available: http://jlt.osa.org/abstract.cfm?URI=jlt-23-7-2255

[38] J. Yang, "Numerical modeling of hollow opticalfiber drawing process," Ph.D. dissertation, Rutgers, 2008.

[39] S. C. Xue, M. C. J. Large, G. W. Barton, R. I. Tanner, L. Poladian, and R. Lwin, "Role of material properties and drawing conditions in the fabrication of microstructured optical fibers," *J. Lightwave Technol.*, vol. 24, no. 2, p. 853, Feb 2006. [Online]. Available: http://jlt.osa.org/abstract.cfm?URI=jlt-24-2-853

[40] A. F. Abouraddy, M. Bayindir, G. Benoit, S. D. Hart, K. Kuriki, N. Orf, O. Shapira, F. Sorin, B. Temelkuran, and Y. Fink, "Towards multimaterial multifunctional fibres that see, hear, sense and communicate," *Nature Materials*, vol. 6, p. 336, May 2007. [Online]. Available: https://doi.org/10.1038/nmat1889

[41] M. Bayindir, A. F. Abouraddy, F. Sorin, J. Viens, J. D. Joannopoulos, and Y. Fink, "Novel optoelectronic fibers codrawn from conducting, semiconducting and insulating materials," in *(CLEO). Conference on Lasers and Electro-Optics, 2005.*, vol. 3, 2005, pp. 1686–1687 Vol. 3.

[42] O. Shapira, K. Kuriki, N. D. Orf, A. F. Abouraddy, G. Benoit, J. F. Viens, A. Rodriguez, M. Ibanescu, J. D. Joannopoulos, Y. Fink, and M. M. Brewster, "Surface-emitting fiber lasers," *Opt. Express*, vol. 14, no. 9, pp. 3929–3935, May 2006. [Online]. Available: http://www.opticsexpress.org/abstract.cfm?URI=oe-14-9-3929

[43] M. Bayindir, A. Abouraddy, J. Arnold, J. Joannopoulos, and Y. Fink, "Thermal-sensing fiber devices by multimaterial codrawing," *Advanced Materials*, vol. 18, no. 7, pp. 845–849, 2006. [Online]. Available: https://onlinelibrary.wiley.com/doi/abs/10.1002/adma.200502106

[44] C. Lu, S. Park, T. J. Richner, A. Derry, I. Brown, C. Hou, S. Rao, J. Kang, C. T. Moritz, Y. Fink, and P. Anikeeva, "Flexible and stretchable nanowire-coated fibers for optoelectronic probing of spinal cord circuits," *Science Advances*, vol. 3, no. 3, 2017. [Online]. Available: https://advances.sciencemag.org/content/3/3/e1600955

[45] S. Park, G. Loke, Y. Fink, and P. Anikeeva, "Flexible fiber-based optoelectronics for neural interfaces," *Chem Soc Rev*, 2019.

[46] A. Canales, S. Park, A. Kilias, and P. Anikeeva, "Multifunctional fibers as tools for neuroscience and neuroengineering," *Accounts of Chemical Research*, vol. 51, no. 4, pp. 829–838, 2018, pMID: 29561583. [Online]. Available: https://doi.org/10.1021/acs.accounts.7b00558

[47] S. Park, Y. Guo, X. Jia, H. K. Choe, B. Grena, J. Kang, J. Park, C. Lu, A. Canales, R. Chen, Y. S. Yim, G. B. Choi, Y. Fink, and P. Anikeeva, "One-step optogenetics with multifunctional flexible polymer fibers," *Nature Neuroscience*, 2017.

[48] R. A. Koppes, S. Park, T. Hood, X. Jia, N. A. Poorheravi], A. H. Achyuta, Y. Fink, and P. Anikeeva, "Thermally drawn fibers as nerve guidance scaffolds," *Biomaterials*, vol. 81, pp. 27 – 35, 2016. [Online]. Available: http://www.sciencedirect.com/science/article/pii/S0142961215009734

[49] D. Shahriari, G. Loke, I. Tafel, S. Park, P.-H. Chiang, Y. Fink, and P. Anikeeva, "Scalable fabrication of porous microchannel nerve guidance scaffolds with complex geometries," *Advanced Materials*, vol. 31, no. 30, p. 1902021, 2019. [Online]. Available: https://onlinelibrary.wiley.com/doi/abs/10.1002/adma.201902021

[50] D. D. Kim, S. Park, S. Kim, and B. Anthony, "The conversation for the need of low cost prototype fiber system for biological and neurological applications," 2019.

[51] W. J. Buehler, J. V. Gilfrich, and R. C. Wiley, "Effect of low-temperature phase changes on the mechanical properties of alloys near composition tini," *Journal of Applied Physics*, vol. 34, no. 5, pp. 1475–1477, 1963. [Online]. Available: https://doi.org/10.1063/1.1729603

[52] F. E. Wang, W. J. Buehler, and S. J. Pickart, "Crystal structure and a unique "martensitic" transition of tini," *Journal of Applied Physics*, vol. 36, no. 10, pp. 3232–3239, 1965. [Online]. Available: https://doi.org/10.1063/1.1702955

[53] Memry Corporation, "Introduction to nitinol," 2017.

[54] J. Abel, J. Luntz, and D. Brei, "Hierarchical architecture of active knits," *SMART MATERIALS AND STRUCTURES*, 2013.

[55] K. Eschen and J. Abel, "Effect of geometric design parameters on contractile smaknitted actuator performance," in *Proceedings of the ASME 2017 Conference on Smart Materials, Adaptive Structures and Intelligent Systems*, 2017.

[56] K. Eschen, J. Abel, R. Granberry, and B. Holschuh, "Active-contracting variable-stiffness fabricsfor self-fitting wearables," in *Proceedings of the ASME 2018 Conference on Smart Materials, Adaptive Structures and Intelligent Systems*, 2018.

[57] K. Eschen and J. Abel, "Performance and prediction of large deformation contractile shape memory alloy knitted actuators," *Smart Materials and Structures*, 2019.

[58] R. Granberry, B. Holschuh, and J. Abel, "Experimental investigation of the mechanisms and performance of active auxetic and shearing textiles," in *Proceedings of the ASME 2019 Conference on Smart Materials, Adaptive Structures and Intelligent Systems*, 2019.

[59] R. Granberry, K. Eschen, B. Holschuh, and J. Abel, "Functionally graded knitted actuators with niti-basedshape memory alloys for topographically self-fittingwearables," *Advanced Materials Technologies*, 2019.

[60] A. Šalej Lah, P. Fajfar, G. Kugler, and T. Rijavec, "A niti alloy weft knitted fabric for smart firefighting clothing," *Smart Materials and Structures*, 2019.

[61] H. Koon, J. Laven, and J. Abel, "Manufacture of ultra-dense knitted superelastic structures," in *Proceedings of the ASME 2018 Conference on Smart Materials, Adaptive Structures and Intelligent Systems*, 2018.

[62] D. D. Kim and B. Anthony, "Design and fabrication of desktop fiber manufacturing kit for education," in *Dynamic Systems and Control Conference*, 2017.

[63] Adafruit, "Platinum rtd sensor - pt100 technical details." [Online]. Available: https://www.adafruit.com/product/3290

[64] I. Hwang, J. Kim, and S. Hur, "Accuracy review on long wired rtd instrumentation circuits," *International Symposium on Future I and C for Nuclear Power Plants*, 2017.

[65] Keyence, *CCD Thrubeam Type Laser Sensor IG Series Instruction Manual*, Keyence, 1-3-14, Higashi-Nakajima, Higashi-Yodogawa-ku, Osaka, 533-8555, Japan, 2010.

[66] D. D. Kim, S. Kim, and B. Anthony, "Development of desktop fiber manufacturing system for smart manufacturing education (submitted)," *ASTM Smart and Sustainable Manufacturing*, 2019.

[67] Texas Instruments, "Drv8825 stepper motor controller ic," Jul. 2014. [Online]. Available: https://www.ti.com/lit/ds/symlink/drv8825.pdf

[68] V. Pandey and V. K. Giri, "High frequency noise removal from ecg using moving average filters," in *2016 International Conference on Emerging Trends in Electrical Electronics Sustainable Energy Systems (ICETEESES)*, 2016, pp. 191–195.

[69] Omega, "Hi-density cartridge heaters with 321 stainless steel sheath." [Online]. Available: https://www.omega.com/en-us/industrial-heaters/cartridge-heaters/hdc00001-series/p/HDC00005

[70] Omega, "Cn142 controller user's guide." [Online]. Available: https://assets.omega.com/manuals/process-control-and-monitoring-devices/controllers/pid-controllers/M5302.pdf

[71] Pololu, "Tic t249 usb multi-interface stepper motor controller." [Online]. Available: https://www.pololu.com/product/3138

[72] Z. Cui, B. Nelson, Y. Peng, K. Li, S. Pilla, W.-J. Li, L.-S. Turng, and C. Shen, "Fabrication and characterization of injection molded poly (epsilon-caprolactone) and poly (epsilon-caprolactone)/hydroxyapatite scaffolds for tissue engineering," *Materials Science and Engineering: C*, vol. 32, no. 6, pp. 1674 – 1681, 2012. [Online]. Available: http://www.sciencedirect.com/science/article/pii/S092849311200183X

[73] D. Shahriari, G. Loke, I. Tafel, S. Park, P.-H. Chiang, Y. Fink, and P. Anikeeva, "Scalable fabrication of porous microchannel nerve guidance scaffolds with complex geometries," *Advanced Materials*, vol. 31, no. 30, p. 1902021, 2019. [Online]. Available: https://onlinelibrary.wiley.com/doi/abs/10.1002/adma.201902021